YEAR END TECHNICAL REPORT

September 17, 2013 to May 17, 2014

Rapid Deployment of Engineered Solutions for Environmental

Date submitted:

June 30, 2014

Principal Investigator:

Leonel E. Lagos, Ph.D., PMP®

Florida International University Collaborators:

Yelena Katsenovich, Ph.D.
Ravi Gudavalli, Ph.D.
Claudia Cardona, DOE Fellow
Robert Lapierre, DOE Fellow
Paola Sepulveda, DOE Fellow
Joel McGill, DOE Fellow
Hansell Gonzalez, DOE Fellow
Valentina Padilla, DOE Fellow
Christian Pino, DOE Fellow

Submitted to:

U.S. Department of Energy
Office of Environmental Management
Under Cooperative Agreement # DE-EM0000598

FIU | Applied Research Center
FLORIDA INTERNATIONAL UNIVERSITY

Addendum:

This document represents one (1) of five (5) reports that comprise the Year End Reports for the period of September 17, 2013 to May 17, 2014 prepared by the Applied Research Center at Florida International University for the U.S. Department of Energy Office of Environmental Management (DOE-EM) under Cooperative Agreement No. DE-EM0000598.

The complete set of FIU's Year End Reports for this reporting period includes the following documents and are available at the DOE Research website for the Cooperative Agreement between the U.S. Department of Energy Office of Environmental Management and the Applied Research Center at Florida International University (http://doeresearch.fiu.edu):

Project 1: Chemical Process Alternatives for Radioactive Waste
Document number: FIU-ARC-2014-800000393-04b-233

Project 2: Rapid Deployment of Engineered Solutions for Environmental Problems
Document number: FIU-ARC-2014-800000438-04b-223

Project 3: Remediation and Treatment Technology Development and Support
Document number: FIU-ARC-2014-800000439-04b-225

Project 4: Waste and D&D Engineering and Technology Development
Document number: FIU-ARC-2014-800000440-04b-220

Project 5: DOE-FIU Science & Technology Workforce Development Initiative
Document number: FIU-ARC-2014-800000394-04b-079

Each document will be submitted to OSTI separately under the respective project title and document number as shown above.

TABLE OF CONTENTS

LIST OF FIGURES

LIST OF TABLES

EXECUTIVE SUMMARY

During FIU Year 4, two subtasks related to the Hanford Site were carried out under Task 1 of Project 2. Subtask 1.1 conducted literature search on several solubility measurement approaches necessary to determine uranium mobility in the post-treated soil and initiated isopiestic measurements that most closely mimic the unsaturated vadose zone environment. For this subtask, FIU-ARC completed a literature review, fabricated an isopiestic chamber equipped with a pressure transducer connected to the acquisition system and initiated preliminary testing to evaluate the experimental procedures. Experimental studies also continued for mineralogical and morphological characterization of NH_3-treated U(VI)-bearing solids precipitated from the solution mixture containing major pore water cations and ions that could be present in pore water from mineral phase dissolution. For this subtask, FIU explored alternative sample preparation methods that help to increase an atomic percentage of U(VI) in the composition of solid phases for more accurate identification of known U phases via X-ray diffraction. This research is still on-going and might require preparation of new samples to continue identification of solid phases. Currently, two graduate students are involved in this research, including DOE Fellow Robert Lapierre, working towards a master's thesis and DOE Fellow Claudia Cardona, a Ph.D. candidate, working towards her Ph.D. dissertation.

Subtask 1.2 completed a series of experiments to qualitatively and quantitatively characterize changes on the bacteria surface after uranium exposure and evaluate the effect of bicarbonate ions on U(VI) toxicity of a less uranium tolerant *Arthrobacter oxydans* strain, G968, by analyzing changes in adhesion forces and cell dimensions via profile plots. In addition, supplementing AFM analysis, cell viability was assessed by the Live/Dead BacLight Bacterial Viability Kit (Molecular Probes) to quantitatively illustrate how bacterial cells are affected when exposed to uranium in the presence of varying concentrations of bicarbonate ions. The results of this research were included in the DOE Fellow Paola Sepulveda's thesis who graduated in the spring of 2014.

During FIU Year 4, two new subtasks related to the Savannah River Site (SRS) were added under Task 2. SRS was one of the major producers of plutonium for the U.S. nuclear program during the Cold War. Since then, it has become a hazardous waste management facility responsible for nuclear storage and remediation of contaminated soil and groundwater from radionuclides. Intended and accidental leakages of acidic waste solutions from the F/H-Area facilities created a contaminated groundwater plume with an acidic pH between 3-5.5, polluted with a variety of radionuclides and chemicals. Subtask 2.1 provided FIU's support for groundwater remediation at the SRS F/H Area. Thus far, experiments were performed on the designed experimental matrix that involved 3.5 mM colloidal silica, 10 ppm humic acid, and natural sediments collected from the F/H Area, to simulate the uranium removal process from the solution in the pH range from 3 to 8. Uranium analyses were done on filtered and unfiltered samples to account for uranium adsorbed to the colloidal Si or HA particles. Analysis by means of ICP-OES provided information on Si and Fe in the solution. DOE Fellow Hansell Gonzalez, a PhD student, is supporting this task.

Task 2.2, Monitoring of U(VI) bioreduction after ARCADIS demonstration at F-Area, was focusing on microcosm experiments to replicate the treatment performed by ARCADIS at SRS and investigating the mineralogical changes that occur in the soil due to the addition of molasses.

The study aimed to determine whether forms of reduced iron such as siderite and pyrite would arise in the reducing zone and if any mineralogical changes occurred in sediments during the re-oxidation period when treated sediments were exposed to air. Once completed, these experiments would help to explain the types of reactions that might occur after turning the aquifer from an aerobic to an anaerobic environment.

Detailed task descriptions and deliverables and milestones can be found in the Project Technical Plan (Appendix 1).

INTRODUCTION

Past practices of waste disposal operations allowed radioactive waste discharges to retention basins, trenches, or cribs where the waste percolated into the soil. These leakages influenced the vadose zone sediments by creating a potential source for groundwater contamination and risk to receptors, those who will use these groundwater resources down gradient, through water uptake from contaminated wells or discharge to surface water. Uranium (VI) is a key contaminant of concern at 18 U.S. Department of Energy (DOE) facilities within the United States. In neutral or basic pH conditions, uranium undergoes hydrolysis in aqueous solutions and can readily complex with a wide variety of ligands. Common ligands in the environment that form a diverse suite of aqueous uranyl complexes include: hydroxyl, phosphate, carbonate, silicate and organic substances. These complexation reactions often result in the formation of mobile aqueous species or precipitation of U-bearing minerals. Soil properties, groundwater and pore water characteristics have a tremendous effect on uranium speciation and the formation of mineral phases. Surveys of the Hanford Site contaminated areas suggested that carbonate and hydrogen carbonate are the major ions in the groundwater composition and in pore water saturated with Ca and Mg-carbonates. In a bicarbonate-rich environment, carbonate anions are an important complexing agent for U(VI), forming highly soluble and stable uranyl dicarbonate $UO_2(CO_3)_2^{2-}$ and uranyl tricarbonate $UO_2(CO_3)_3^{4-}$ complexes, which become the predominant aqueous species at pH 7.0-8.0. There is a growing concern that elevated uranium concentrations could slowly migrate downward, creating a risk of higher U concentrations reaching the groundwater and then entering the Columbia River along the shoreline.

Environmental factors, such as pore water ion composition, have tremendous effect on both uranium and its mineral phases. Additional research is necessary to understand the effect of these factors on the behavior of U(VI) in vadose zone sediments before implementation of the ammonia gas injections technology.

Based on the results of this investigation, Project 2 has accomplished the following in 2013-2014:

- Completed a progress report on characterization of new samples prepared to minimize nitratine impact (April 2014).
- Completed a progress report on atomic force microscopy assessment of bacterial cells exposed to U(VI) (April 2014).
- Completed a progress report on the results for batch experiments using colloidal silica, humic acid, sediments and U(VI) (March 2014).
- Completed a progress report on microcosm studies prepared with SRS sediments (February 2014).
- A manuscript was published in the Environmental Chemistry Journal. Gudavalli, R.P., Katsenovich, Y., Wellman, D., Lagos, L., and B. Tansel, 2013. Quantification of kinetic rate law parameters for the dissolution of sodium meta-autunite as a function of aqueous bicarbonate concentration, Environmental Chemistry, 10, 6, p.475-485 http://dx.doi.org/10.1071/EN13117.
- A manuscript was published in the Chemical Geology journal. Gudavalli, R.P., Katsenovich, Y., Wellman, D., Idarraga, M., Lagos, L., and B. Tansel, 2013, Comparison of the kinetic rate law parameters for the dissolution of natural and synthetic autunite in

the presence of bicarbonate ions. Chemical Geology, 351, p. 299-309.

- Two manuscripts were prepared for the submission to the peer review journals: The Effect of Bicarbonate on the Microbial Dissolution of Autunite Mineral in the Presence of a Low U(VI)-Tolerant Strain, Arthrobacter oxydans G968 and A Study of Cell Viability on DOE Hanford Soil Isolates: Effect of U(VI) and Bicarbonate.
- DOE Fellow Paola Sepulveda graduated with an MS degree in biomedical engineering and DOE Fellow Valentina Padilla with an MS degree in environmental engineering.
- Presented results of research at the Waste Management 2014 (WM2014) Conference (March 2014).
  - Rate of Uranium Release from Calcium Meta-Autunite: Effect of Bicarbonate Solutions on the Dissolution (14218). Ravi Gudavalli, Yelena Katsenovich, Leonel Lagos, Dawn Wellman (Oral presentation).
  - The Effect of Ca Ions on the Removal of U(VI) via In-Situ Ammonia Gas Injection at the Hanford Site 200 Area (14434). Yelena Katsenovich, Claudia Cardona, Leonel Lagos (Oral presentation).
  - A Study of Cell Viability on DOE Hanford Soil Isolates: Effect of U (VI) and Bicarbonate (Student poster), Paola Sepulveda (DOE Fellow).
  - The effect of Si and humic acid on U(VI) removal from the SRS F/H area groundwater (Student poster), Joel McGill (DOE Fellow), Yelena Katsenovich.
  - Microcosm study on mineralogical changes of post molasses injection with SRS F-area sediments (Student poster), Valentina Padilla (DOE Fellow).
  - Characterization of the uranium-bearing products of novel remediation technology (Student poster). Robert Lapierre (DOE Fellow), Yelena Katsenovich.

TASK 1.1: SEQUESTERING URANIUM AT THE HANFORD 200 AREA BY IN SITU SUBSURFACE PH MANIPULATION USING AMMONIA (NH3) GAS INJECTION

INTRODUCTION

One of the goals of the remediation efforts at the Hanford Site 200 Area is to predict the behavior and fate of vadose zone uranium contaminants, which are considered as a potential source of contamination for the underlying groundwater system. The technology under consideration to sequester U(VI) is a manipulation of soil pH via ammonia gas injection to the uranium-contaminated soil. The soil pH manipulation causes uranium co-precipitation during mineralogical changes and the formation of uranium-bearing precipitates in the treated vadose zone soil. The injection of reactive gases such as NH_3 can reduce the potential for radionuclide mobility in the subsurface without water addition causing undesired downward contaminant migration. The formation of a relatively insoluble mineral complex that contains uranium is very valuable for the environment because immobile contamination will spread less in the subsurface. However, there is a need for a better understanding of the stability of the U-bearing precipitates created in the soil as a result of remedial actions. This information would help to accurately predict the mobility of U(VI) in the post-treated vadose zone soil.

This report discusses literature approaches for solubility measurements necessary to determine uranium mobility in the post-treated soil. Emphasis is given to the isopiestic method that most closely mimics the vadose zone environment. The report also evaluates the experimental procedures of the solubility experiments and presents initial data to validate the accuracy of measurements taken from isopiestic apparatus.

DETERMINATION OF SOLUBILITY

Solubility is dependent on many factors present in the environment and it relies on attributes of both the solvent and the solute. The traditional method to determine solubility is to measure the amount of solute that can be dissolved in a solvent until the system reaches equilibrium. By determining the solubility of a compound, Gibbs free energy of formation and other important thermodynamic constants such as enthalpy and entropy can be calculated. Additionally, the solubility of a compound determines its mobility in the subsurface to a great extent and the potential for its diffusion into the groundwater. This is especially important when dealing with environmental contaminants such as uranium or other radionuclides.

There exist several techniques to measure solubility. To mimic solubility of solid phases in the saturated environment, it is best to conduct solubility tests in batch reactors and measure the amount of solute that will dissolve in a given amount of solvent. However, quantifying mineral solubility under unsaturated conditions using this traditional approach will result in an inaccurate value. Quantification of mineral solubility for vadose zone environments needs to consider the isopiestic method which allows for a more accurate determination of the relevant solubility data. The water activity and osmotic coefficient determined via the isopiestic method will provide a better understanding of the solubility behavior U-bearing precipitates in vadose zone environments. One of the first steps to take when performing solubility experiments is to characterize samples taken from the environment or synthetically synthesized.

SAMPLE PREPARATION

If the solvent of interest is soil pore water, then it should be prepared to comprise most of the ions that the real pore water contains. This can be done by taking samples of sediments from the environment under consideration and then spinning them in an ultracentrifugation process. This involves removing sediments, homogenizing them, and then centrifuging for 8 hours at 500 rcf. The procedures yields pore water, which can then be analyzed to determine the ion composition and its aqueous speciation (MINTEQA2 code) (Liu et al., 2004). If the experiments are to be carried out with soil, then the soil should reflect the consistency and make-up of the environment that is being studied. In the experiments carried out by Kohler et al. (2003) using illite, samples for the dissolution were prepared by grinding, sieving and washing in an acidic sodium acetate solution to remove carbonate impurities. They also pre-dissolved the mineral before the solubility experiment. Some of the samples were pre-dissolved in 0.01 M HCl and others in 0.01 M NaOH solutions (Kohler et al., 2003).

Gorman-Lewis et al. (2009) implemented solubility experiments in a batch reactor using synthetic uranyl phosphate minerals. Liu et al. (2004) conducted solubility experiments for uranyl compounds using an electrolyte mixture, prepared on sodium nitrate/bicarbonate solution at an ionic strength of 0.05, which was synthesized from $NaNO_3$, $NaHCO_3$, NaOH, and/or HNO_3. Some solutions were also made with calcite and $Ca(ClO4)_2$ and then allowed to equilibrate for 12 months. Both electrolyte solutions were exposed to the air to attain carbon dioxide equilibrium. They also prepared their solute by washing it in electrolyte solutions but not air dying, so that it remains as U^{6+}.

After preparing the solutes, Gorman et al. (2009) boiled them in water, air-dried and then analyzed the particles. Perez et al. (2000) kept the solid phase mineral in a glass Parr bomb with water for about 18 days in order to improve the crystallinity. When testing soddyite's solubility, Giammar et al. (2002) allowed the flask to reach equilibrium with CO_2 before and after adding the soddyite; however, during the experiment, the flasks were capped. Rai et al. (2005) prepared their solvent by deaerating deionized water and storing it in an argon atmosphere. They also pretreated the plutonium to be tested by ozonating it before the experiment as well as equilibrating the precipitate in the mother solution for four days and then centrifuging and washing in pH 10 deionized water (with 0.005 M NaOCl). These steps helped to maintain plutonium in a hexavalent state.

Analysis of solute

Another necessary step in solubility experiments is to do characterization studies of the solute before and after testing to ensure that it has not transformed into the secondary solid phase. In case of the formation of secondary phases, the solubility constant cannot be used to calculate thermodynamic constants, unless the secondary and initial phases are both in equilibrium. To determine what compounds are present before and after the experiment, X-ray diffraction analysis, spectroscopy, or chemical analysis should be implemented. Kohler et al. (2003) analyzed the solute (illite) prior to the experiment in order to ensure its purity through the use of X-ray diffraction and SEM/EDS for the composition. Kohler et al. (2003) also employed the Molybdate Blue method established by Koroleff in 1976, and used a Perkin-Elmer ELAN 6000 ICP-MS to analyze the concentrations of various elements (Si, Al and Mg) of the solute

dissolved into the solvent. In addition, they used the BET method to calculate the particles' surface area (Kohler et al., 2003).

Gorman-Lewis et al. (2009) analyzed the solute (uranyl hydrogen phosphate, uranyl orthophosphate, and autunite) throughout the solubility experiment using ICP-OES. This instrument determines the concentrations of dissolved elements (uranium, phosphate, calcium, and oxygen) of the solute in the solution. They also analyzed and characterized the solute before the experiment as well as after experiments by sampling 10 mg of residue at the end of the experiment to ensure that it had not undergone a change. Giammar et al. (2002) conducted X-ray diffraction analysis and used a scanning electron microscope to analyze the solute, soddyite, composition throughout the experiment. Perez et al. (2000) implemented X-ray powder diffraction, scanning electron microscopy, and ICP-MS for chemical characterization and Fourier Infrared spectroscopy to characterize the uranophane mineral.

Rai et al. (2004) carried out extensive analysis to calculate uranium, plutonium and phosphorous concentrations via ICP-MS to test the samples taken throughout the experiment. In addition, a Wallace liquid scintillation counter was used to count alpha activity to determine the activity of the plutonium in the solution. The oxidation state of plutonium was found using a computer-interfaced Cary-14 ultraviolet-visible-near-infrared (UV-VIS-NIR) X-ray absorption near edge spectroscopy. The JADE 3.0-PDF cards were used as a reference for the X-ray diffraction pattern found experimentally.

Variables of the solubility process

To carry out the experiment, factors such as temperature, pH, water activity and carbonate concentration should be controlled. These variables can greatly affect the solubility of a substance. Gorman Lewis et al. (2009) used a pH meter in their experiments to continuously monitor the vessels pH. In order to keep the pH constant, they used HNO_3 and/or NaOH or KOH as buffers when carrying out solubility experiments with uranyl hydrogen phosphate, uranyl orthophosphate, and autunite. It is optimal to choose a buffer whose ionic strength has been calculated to match the ionic strength of the experiments.

Giammar et al. (2002) also implemented solubility experiments using a uranium mineral soddyite in a batch reactor. Since they were investigating the dissolution of soddyite, certain experimental steps were taken to ensure it didn't react when joined with the solvent. The pH level of the experiment was chosen at a value at which there is limited formation of other uranyl complexes. In this case, they determined that the minimal formation of uranyl carbonate species occurred at pH 6. The pH was initially set using NaOH and the type of buffer used was the one with a very low affinity for metal complexation [5 mM 2-(n-morpholino) ethanesulfonic acid (MES) buffer]. These are important considerations because they all reduce the risk of secondary reactions which would make the solubility experiment invalid.

When Liu et al. (2004) investigated the dissolution of various uranium complexes such as metashoepite, becquerelite, metaautunites and chernikovite, they used $NaNO_3$, $NaHCO_3$, NaOH, or HNO_3 to set the pH at different values. Ilton et al. (2006) set the pH for their Na-boltwoodite solubility experiments using carbonate free 0.1 M NaOH. Rai et al. (2005) used HCl and NaOH to adjust the pH to test uranium and plutonium phosphates, when there was 0.001 and 0.01 M phosphate. But when the phosphate was variable between 0.001 and 1.0 M, they used H_3PO_4 and

NaH_2PO_4 to set the hydrogen ion concentration at a constant value ($pC_{H+} = 3.5$) using GMIN code and Pitzer parameters. At high ionic strengths, measured pH was not able to accurately express the hydrogen ion concentration or the activity occurring in the solution.

$$pC_{H+} = pH_{obs} + A \quad \text{Eq 1}$$

Where A is the conversion depending on the composition of the solution. Felmy et al. (2005) also used this conversion equation when determining the solubility of $NaUO_2PO_4$*xH_2O. For their $NaNO_3$ solvent solution, A was -0.037 for 0.5 M $NaNO_3$ and 0.315 for 3.0 M $NaNO_3$, found using a titration method.

It has been found that impurities can affect a compound's solubility. This is because the impurity may bind to the compound's surface and thus reduce the surface area that is in contact with the solvent. An example of the effect of impurities is silica's reduced solubility in the presence of aluminum (Iler et al., 1979). To remove carbonate impurities, Kohler et al. (2003) washed the solute (illite) in an acidic solution. In the case of uranium oxides, it has been found that as bicarbonate concentrations increase so does the uranium compound's solubility. Higher concentrations of other complexants can also increase the rate of dissolution of compounds.

Ilton et al. (2006) investigated Na-boltwoodite's solubility with varying concentrations of bicarbonate. The concentrations were chosen based on conditions at the Hanford site: 0, 0.1, 0.3, 0.6, 1.2, 3.5, 6, 12, 20, 30 and 50 mM $NaHCO_3$. They found that increasing carbonate and pH levels caused a significant increase in the Na-boltwoodite solubility as well as in all uranium silicates. They also purified their samples prior to the experiment by washing them in boiling water and then vacuum drying them.

It has been observed by Perez et al. (2000) that the rate expression is proportional to carbonate concentrations for uranophane dissolution and, for uranyl oxyhydroxide dissolution in bicarbonate solution, the rate order was 0.65 in ratio with the total carbonate concentration (Steward and Mones, 1997). Lie et al. (2004) recorded a ratio of 15:(17-20) for the increase in magnitude of the dissolution rate to the increase in bicarbonate activity. The steps controlling the uranium dissolution in the presence of carbonate was electron transfer, coordination of carbonate species on its surface, and the detachment of uranium-carbonate species from the surface. *(Further details on the effect of carbonate concentrations are provided in the section titled, "Factors affecting solubility".)*

Another factor Kohler et al. (2003) took into consideration was particle surface area. They measured the surface area of the mineral particles of illite since particle surface area is a factor that can influence solubility. This was done through argon absorption following the B.E.T. method and they found the surface area to be about 130 m^2/g for the illite particles. Ilton et al. also measured the surface area of their particles of Na-boltwoodite using the BET method. They calculated a surface area of about 30.78 m^2/g.

Other steps to minimize reactions occurring to the solute include limiting exposure time to oxygen which could cause redox reactions. In a solubility experiment by Liu et al. (2004), the authors did not allowed their mineral species to be exposed to the air for long periods of time so that their mineral would not be oxidized. Ilton et al. (2006) confined the solution to an argon atmosphere. In the experiments conducted by Gorman-Lewis et al. (2009), the pH of the solvent,

in this case pore water, was held constant. The pH was set by considering the various elements in the solvent. Through a trial and error method, the pH was set at the value which yielded a near zero saturation index of calcite, mimicking the conditions of the natural pore water. The solution containing calcite was combined with an electrolyte solution and filtered to eliminate solid calcite particles (Liu et al., 2004).

Furthermore, in order to determine activity coefficients in an experiment, the water activity must be known and controlled throughout the entire experiment. Berberich et al. (2003) reported that salt hydrates well as water activity buffers in ionic liquids and organic solvents. In their experiments, they monitored the water activity using humidity sensors, which were equilibrated using dry nitrogen, deionized water and salt solutions (LiCl, K_2CO_3, and NaCl). To control the water activity of the ionic liquid 1-butyl-3-methylimidazolium hexafluorophosphate, Berberich et al. (2003) combined 10 g of it with less than 0.1% wt water to 20 mL of 0.2 g/mL of the higher salt hydrate (salt hydrates used: NaI, Na_2HPO_4, NaAc, $CuSO_4$, $Na_4P_2O_7$, Na_2HPO_4, and Na_2HPO_4). This container was then kept at a constant temperature and shaken. Periodically, samples were extracted and removed and the water content was measured. A salt hydrate pair can control the water activity as long as there is at least a small amount undissolved in the system. Pre -equilibration of an ionic liquid over a saturated salt solution is another method to control water activity but it takes longer to reach equilibrium and is only applicable to initial measurements.

Christian et al. (1963) employed a solute isopiestic equilibration technique that involved distributing by vapor contact a volatile solute (water) between a phase of known water activity and the organic solution. The experimental isopiestic chamber with the solution was equilibrated at the known constant water activity. A beaker containing a solution or solid of known relative humidity was placed on the bottom of the chamber, which was sealed airtight throughout the equilibration process. The half-life for equilibration was calculated as:

$$t_{1/2} = \frac{0.693}{k(\frac{p_s^C}{C_s^D})} \quad \text{Eq 2}$$

Where C_s^D represents the final concentration of solute in the solution corresponding to the equilibrium partial pressure p_s^C (Christian et al., 1963).

Blanco et al. (2006) also employed an isopiestic technique. They prepared their solutions by weight and then the cups were placed in a steel block kept in a bath at a constant temperature. The whole apparatus was placed in a modified glass vacuum desiccator, which was equilibrated to a constant pressure by pumping air out (4.5 kPa). Throughout their equilibration experiment, they weighed the cups periodically; from this, they were able to determine the molality of the solutions. When the solutions in all the samples had the same molality, they concluded that the system had reached equilibrium. They used potentiometric titration with silver nitrate for anion analysis and potentiometric titration with NaTPB for cation analysis.

Park et al. (1998) used a 140 mL four- necked isopiestic apparatus. Using a necked flask reduces the time it takes for the heat to transfer to reach equilibrium compared to a conventional isopiestic apparatus. The system was set at a constant pressure by vacuuming out air; vacuuming also removes any dissolved gases in the sample solutions. The isopiestic apparatus was placed in a water bath with a temperature controller to maintain a constant temperature. The molality of

the solutions was determined from their measured weight and the following equation was used to calculate the activity of the water:

$$a_w = \exp\left[\frac{\mu - \mu^0}{RT}\right] \quad \text{Eq3}$$

Where a_w is the activity of the solvent, μ is the chemical potential of the solvent, μ^0 is the standard state chemical potential of the solvent, R is the gas constant and T is the absolute temperature.

Blanco et al. (2006) took this type of isopiestic apparatus one step further by implementing one with 12 legs. The volume of their apparatus was 2400 mL and to all 12 legs were attached 25 mL flasks in which the solutions were kept. The entire apparatus was vacuumed until the pressure was around 4.5 kPa and the cups were weighed at intervals varying from 8 days to 2 weeks until the system reached equilibrium. The apparatus was submerged in a bath at a constant temperature (298.15±0.1) K, in which it circulated about its central axis via a rotating motor. This temperature controlled bath was enclosed in a larger air thermostat. Of the 12 cups, they filled two with NaCl reference solutions, nine with the KCl solutions whose solvent activity was being calculated, and one cup was used as a reservoir for water. Buoyancy corrections were applied and they calculated the solvent's activity using the same equation given by Park et al. (2004). To calculate the water activity, Amado and Blanco (2004) used the following formula:

$$ln a_w = -0.001 v_s m_s M_w \Phi_{ref} \quad \text{Eq 4}$$

Where a_w is the water activity, v_s is the salt stoichiometric coefficient, m_s is the salt molality, M_w is the solvent's molecular weight, and Φ_{ref} is the practical osmotic coefficient of the reference salt solution.

Lin et al., (1996) used a nine legged isopiestic apparatus. The 10 cm^3 flask was evacuated of air before the process slowly reached equilibrium. In the nine flasks, three were filled with a standard KCl solution (isopiestic reference), two with NaCl solution and four with the solutions whose water activities were being determined. For a polymer/salt system, they filled 2 flasks with $MgSO_4$ or $(NH_4)_2SO_4$, three contained KCl solutions, one contained pure polymer, and three contained polymer/salt mixtures. Then it was sealed and placed in a constant temperature bath consisting of two tanks. The outer tank was used to prevent temperature fluctuation and the inner tank equilibrated the sample. The isopiestic apparatus was rotated around in the temperature bath at an angle and the nine attached flasks also rotated about the central axis. Each sample flask was weighed to determine the molality. Prior to removing the sample flasks for weighing, dry preheated air was pumped into the cell to prevent condensation (Lin et al., 1996).

Solubility experiments in batch reactors

Gorman-Lewis et al. (2009) conducted two types of batch solubility measurements, under saturated and supersaturated conditions. For the under saturated experiments, they added 350 mg of the solid phase of the solute (autunite) to 125 cm^3 of pure water used as a solvent. The supersaturated experiments consisted of adding 350 mg of the mineral to a solution, which already contained stoichiometric concentrations of the elements found in the solute. In the case of the solubility experiments with autunite, the solution contained stoichiometric concentrations of U, P, and Ca from additions of UO_2 $(NO_3)_2$, $NH_4H_2PO_4$, and Ca $(NO_3)_2$. If any of the final

concentrations of the starting values decreased, then the experiment was classified as supersaturated. Each reaction vessel was then sealed and agitated for a period of time.

Giammar et al. (2002) experimented to determine the solubility of soddyite. For the mineral synthesis, 0.1 M UO_2 $(CH_3COO)_2$ *$2H_2O$ and 0.1 M Na_2SiO_3*$5H_2O$ were combined in a 23-mL Parr bomb. This was heated to 110 Celsius for ten days. The precipitated solids were filtered with a 0.2 micrometer membrane, washed with boiled deionized water and then diluted with 20 mL of water. The mass concentration of soddyite was determined by pre-weighing the filter and solids and then the solution.

Ilton et al. (2006) conducted solubility experiments in batch reactors over a 7 day period. They combined 0.25 g of the prepared Na-boltwoodite to 100 mL of solution. Additional $NaNO_3$ was added to keep sodium concentrations at a constant 50 mM. They tested the solubility at a variety of bicarbonate concentrations, representative of the pore water at the Hanford Site to determine what its effect on Na-boltwoodite would be (0, 0.1, 0.3, 0.6, 1.2, 3.5, 6, 12, 20 , 30 and 50 mM $NaHCO_3$ was used). Some of the samples they tested were preleached with 50 mM bicarbonate solution over a 24 hour period to dissolve any contaminants and then were tested in solution with 1.2, 6 and 50 mM bicarbonate. This pretreatment enabled them to evaluate the effect of contamination that a uranium and Si deficient phase would have on the Na-boltwoodite's solubility.

Perez et al. (2000) tested the solubility of uranophane by placing 0.5 g of the mineral in 100 mL of solution in a batch reactor. Samples taken throughout the experiment were filtered through 0.20 micrometer membranes so that only the uranium that had actually been dissolved would be counted. The dissolution rate was calculated by determining the uranium concentration with a SCINTREX UA-3 uranium analyzer and determining calcium and silicon concentrations with an ICP-AAS analyzer. Also, a small amount of concentrated nitric acid solution was used to prevent the samples from precipitating or absorbing.

Rai et al. (2005) conducted solubility experiments of uranium and plutonium phosphates in argon atmosphere chambers. 20 mg of the mineral ($(UO_2)_3(PO_4)_2 \cdot 4H_2O(s)$) was added to 40 mL of an aqueous phosphate solution of 0.001 M-1.0 M. For plutonium phosphate solubility tests, 5 mg of the solid was added to 30 mL of an aqueous phosphate solution of 0.1-1.0 M and 0.0001-0.1 M.

Elless and Lee, (1998) tested uranium solubility of carbonate-rich uranium contaminated soil by combining 200 g of air-dried soil (with particles less than 4 mm) in 2.5 L deionized water. The water was prepared by being allowed to equilibrate with CO_2 before mixing with the soil. For the first 10 days, the samples were shaken manually three times a day. It is ideal when testing a mineral's solubility to analyze the solution periodically and measure its dissolution over time. This is because the dissolution rate may change over time. Elless and Lee, 1998 took samples after 1, 3, 7, 14, 21, 28, 70 and 300 days from the initial mixing. The samples were set to rest and after an hour, a 50 mL aliquot was taken from each sample. These aliquots were vacuum-filtered (0.45 micrometer pore holes). These samples were analyzed for pH, cations and anions, total uranium and alkalinity. At the end of the experiment after 300 days, 200 mL of the extracted solution, after being filtered, was mixed with 2 g of an anionic exchange resin (DOWEX1-X8, 50 to 100 mesh). This was shaken for 20 hours and then centrifuged before being analyzed for uranium using ICP-mass spectrometry.

Ilton et al. (2006) carried out two different batch reactor experiments: (i) experiment with sampling that occurred after the full 7 days of the test concluded, and (ii) kinetic experiments in which frequent samples were taken. They mixed both batch reactors continuously and from the kinetic experiments drew 4-mL samples to be acidified with nitric acid and then analyzed. They tracked the pH and determined the dissolution rate of Na-boltwoodite by measuring silicon and uranium concentrations. The authors found that dissolution rates initially were quite rapid but then decreased over time; this is a trend which many uranium minerals follow.

Kohler et al. (2003) found that illite's dissolution rate slowed immensely over time. To track the dissolution rate, they extracted 20-mL samples and shook the bottles prior to an extraction. These samples were centrifuged (10 min. at 3000 rpm) and then the supernatant was filtered (0.2 micrometer filter). Filtration is an important step in solubility experiments because it helps to eliminate colloids. The particles small enough to be able to pass through the membrane are defined as dissolved. But, some particles smaller than the filtration holes could still be caught and the retention of these small colloids could cause an underestimation of dissolution rates. Kohler et al. (2003) used 0.2 micrometer filters when testing illite solubility; Gorman-Lewis et al. (2009) used 0.1 micrometer filters for uranium compound solutions and Rai et al. (2005) used 40 Angstrom filters for plutonium, uranium phosphate solutions. Rai et al. pretreated their filters to prevent absorption or pH changes by acidifying and storing it. They shook the sealed solutions throughout the experiment and to take samples, they centrifuged the suspensions and then decanted the supernatant. The supernatant was filtered through the acidified filters prior to analysis.

Gorman-Lewis et al. (2009) periodically extracted aliquots from the vessels and, after being filtered, diluted and acidified prior to ICP-OES. This analysis determines the dissolved concentrations of the various elements (uranium, phosphate, oxygen, and calcium) found in the solute (autunite). Ten (10) mg of residue was also collected at the end of the experiment for XRD analysis.

As with the other experiments after adding the soddyite mineral, Giammar et al. (2002) took samples by filtering 5 mL of suspension, collecting the last 1 mL of the filtered sample and diluting 0.5 mL of it to 5 mL with 1% HNO_3. These were then filtered and analyzed. The filter paper was mounted on glass slides and dried to be analyzed later with XRD and SEM. To measure the uranium concentrations, Giammar et al. diluted 0.5 mL of the unfiltered aliquot to 10 mL with 10% HNO_3.

Liu et al. (2004) conducted solubility experiments of uranium in the sediment samples in the Teflon centrifuge tubes at a sediment/solution ratio of 200 g/L. The tubes were shaken constantly and samples were taken after 65, 149 and 197 days. Prior to extracting samples, the tubes were centrifuged at 5000 rcf for 20min. The 0.2 mL aliquot of supernatant were removed and then acidified (0.1 mol/L HNO3) and diluted before being evaluated via kinetic phosphorescence analyzer for uranium (detection limit=4.9 ng/L for U^{6+}, standard and samples prepared in 0.1 mol/L HNO_3). Control samples containing a known concentration (500 & 100 microgram/L U^{6+}) of the mineral were used for comparison (Liu et al., 2004).

The mineral solubility experiments varied in the time it took to reach a steady state. Gorman-Lewis et al. (2009) found that their uranyl complexes reached equilibrium in water after 6-12 days. The under saturated experiment took longer than the supersaturated experiment.

Meanwhile, Kohler et al. (2003) ran their experiment for 100 days before the illite reached equilibrium in the solvent. In addition, some of the samples tested by Liu et al. never reached steady state even after 200 days of reaction. Their explanation was that, in that instance, uranyl diffusion in micro fractures was causing a slow dissolution.

Calculations from solubility data

Gorman-Lewis et al. (2009) defined the fraction able to pass through the 0.1 micrometer filter as dissolved. They plotted the log of mole per kg vs. time for the dissolved concentrations of uranium, phosphate and calcium in order to determine the solubility of autunite. Using the Debye-Huckel equation, they were able to calculate the activity coefficients for each trial at given variations of temperature and pH. Gorman-Lewis et al. (2009) used the extended Debye-Huckel formula to calculate activity coefficient, ɣ as:

$$\log(\gamma)=\frac{-Az_i^2\sqrt{I}}{1+aB\sqrt{I}}+\mathrm{bI} \qquad \text{Eq 5}$$

Where A and B are constants with given values of 0.5105 and 0.3285 $kg^{\frac{1}{2}}mole^{-1/2}$ respectively (based on Helgeson et al. (1981)). A=$\frac{1.8248E6*p^{1/2}}{(\varepsilon T)^{1/2}}$ and B=$\frac{50.29E8*p^{1/2}}{(\varepsilon T)^{1/2}}$, p is the density in g cm^-3, Ɛ is the dielectric constant of water and T is temperature in Kelvins. The I is the ionic strength (in molality (m) units of concentration):

$$I=\frac{1}{2}\Sigma\, m_i z_i^2 \qquad \text{Eq 6}$$

Where m_i is the molality of a specific ion and z_i^2, is the ionic charge of the ith ion in the solution. The summation is taken over all ions; *a* and *b* are 5.22 and 0.062 that stand for values of RbNO3 electrolyte, which was the closest approximation for the uranyl experimental solution used. *b* is an empirical parameter characteristic of the electrolyte and *a* is dependent on the "effective diameter" of the ion in the solution.

Once the activity coefficient is determined, the solubility can be calculated as:

$$a_\mathrm{i}=\gamma_\mathrm{i}\cdot M_\mathrm{i} \qquad \text{Eq 7}$$

Where a_i is activity; M is the molar concentration of ions and γ is the activity coefficient, calculated from the Debye-Huckel equation.

The solubility constant is the product of the activity of all of the ions in the solute:

$$K_{sp}=(\gamma\cdot M)*\left(\gamma_2\cdot M_2\right)\ldots \qquad \text{Eq 8}$$

Where, γ is the activity coefficient and M is the concentration of that ion.

Gorman-Lewis et al. (2009) were able to determine that the log of the solubility constant for autunite was -48.36, -13.17 for uranyl hydrogen phosphate and -49.36 for uranyl orthophosphate.

Ilton et al. used the Pitzer ion-interaction model and Davies equation to calculate the solubility constant. If *a*B* is equated to one (1) and *b* is set to $0.2\mathrm{A}z_i^2$, then the expression used by Gorman

et al. (2009) is reduced to the Davies equation. The Davies equation calculates the log of the activity when the ionic strength is less than 0.5 M.

$$log\gamma_i = -Az_i^2[\frac{\sqrt{I}}{(1+\sqrt{I})-0.2I})] \quad \text{Eq 9}$$

They calculated the solubility constant to be the average log of 5.85.

Liu et al. (2004) calculated the solubility constant of uranophane and Na-boltwoodite using a formula with the activities of each aqueous species. For uranophane:

$$K_{sp} = a_{UO_2^2}^2 + a_{Ca^2} + a_{H4SiO4}^2\, a_{H^+}^{-6} \quad \text{Eq 10}$$

And for Na-boltwoodite:

$$K_{sp} = a_{UO_2^2}^2 + a_{Na} + a_{H4SiO4}^2\, a_{H^+}^{-3} \quad \text{Eq 11}$$

Where a_i is the activity of aqueous species *i*, that was calculated using the analytical data for each sample. From this equation they determined K_{sp} for uranophane as 11.58 and 6.15 for Na-boltwoodite.

Perez et al. (1999) investigated the solubility of uranophane in bicarbonate solutions and they were able to calculate the dissolution rate from the uranium concentration, which was plotted as a function of time (mol dm^{-3} per hour). The initial dissolution rate was calculated by determining the least squares fitting of the uranium concentrations at the beginning of the experiment. This initial rate (mole m^{-3} s^{-1}) was normalized to the solution volume and total solid surface area in the reactor. This normalized dissolution rate is presented as the dissolution rate for uranophane (mol s^{-1} m^{-2}). The solubility constant was calculated using the following formula, which involves the activity constants of calcium, uranyl, silicon and water:

$$K_s = a_{calcium} * a_{uranyl}^2 * a_{silicon}^2 * a_{proton}^{-6} \quad \text{Eq 12}$$

Furthermore, at high bicarbonate concentrations (greater than 5E-3 mol/dm^3) when the $UO_2(CO_3)_3^{4-}$ complex is the dominant aqueous species, the calculated equilibrium constant for the dissolution reaction can be defined as:

$$K = a_{calcium} * a_{uranyl\ complex}^2 * a_{silicon}^2 * a_{bicarbonate}^{-6} \quad \text{Eq 13}$$

Assuming congruent dissolution, they were able to calculate the equilibrium constant using the experimental uranium concentration values and HARPHRQ code. The authors checked these values by measuring the calcium and silicon concentrations taken from samples extracted throughout the experiment. The log of the solubility constant for uranophane in bicarbonate solution was calculated to be about 11.7 (Perez et al., 1999).

Rai et al. (2004) worked backwards by first predicting the Gibbs free energy of formation of their uranium phosphate mineral based on the Guillaumont et al. model (but excluding UO_2PO_4). By using this constant, they were able to calculate the log of the solubility constant as -49.08. Giammar et al. also used already published formation constants to calculate their solubility constant. They calculated the equilibrium of their system using the program MINEQL+ and the

Davies (1962) equation in order to determine the ionic strength corrections. They used thermodynamic constants of dissolved uranyl species from Grenthe et al. (1992) and the formation constant of $UO_2(OH)_2$ (aq) from Silva (1992) and the formation constant of $UO_2H_3SiO_4$ from Satoh and Choppin (1992). They calculated the equilibrium by considering various hydrolysis, carbonate complexation and silicate complexation with uranyl cation reactions. The equilibrium of soddyite solubility was defined as:

$$K_s = \frac{\left(UO_2^{2+}\right)^2 (SiO_2)}{(H^+)^4} \quad \text{Eq14}$$

Factors affecting solubility

Phase and molecular structure

The phase that a compound is in also affects its solubility since each phase has unique properties and behaves differently. The attractive forces between gas molecules are very low and this allows them to spread out and become completely miscible with another gas. Liquids have more prevalent attractive forces between their molecules and so in order to be soluble, the solvent in which they are dissolved must have molecular forces strong enough to dissociate the solute molecules. When in the solid phase, the solvent must overcome the lattice strength and attractive forces between the molecules of each particle. In addition, within the general category of the physical phase of a compound, there are different species which might be present. A compound in the solid form could be amorphous or crystallized. This difference alone will have an effect on its solubility. For example, solid silica compounds can take a crystallized or amorphous molecular structure; while both have the same elemental make-up, the amorphous phase of silica has a higher solubility (Iler, 1979). This tends to hold true in all cases, with the amorphous phase being more soluble than the crystalline phase. Amorphous phase compounds are more soluble because their bonds are more easily dissociated since they don't have the strong crystal lattice of a crystalline solid.

Solubility also varies between different crystalline formations that a given compound can form (Gorman-Lewis et al., 2007). Silica can take the solid crystal form of quartz or cristobalite. Both are crystalline molecules but cristobalite has a lower density because of its more open structure and it also has a more negative enthalpy of solution (Holm et al., 1967; Iler et al., 1979). These factors all contribute to cristobalite having a higher solubility than quartz (Iler et al., 1979). Different crystalline structures tend to be stable at different thermodynamic conditions, so one will occur more prevalently given the conditions than another. One crystalline structure might be more soluble than another given the strength of its crystal lattice. If the crystal lattice is not as strong in one particle type as in another, then it will dissolve more readily.

Particle size

The size of the solute particle also plays a role in the solute's solubility. As the particle size decreases, solubility will increase. This is due to the increasing surface energy that smaller particles have. The solvent can surround more solute surface area if the particles are smaller. Thus, it will be able to dissolve them easier (Iler et al., 1979; Gorman-Lewis et al., 2007).

pH

pH also affects solubility because, in order for a solution to reach a saturated state, it must be at an equilibrium. This dynamic equilibrium can be affected by changing the concentration of hydrogen or hydroxide ions. Hydroxide compounds are affected by pH changes because they are directly influenced by changes in hydroxide concentrations. If the pH is lowered, this means that the hydroxide concentration is lower and so the solubility will increase to try and produce more hydroxide ions. This follows Le Chatelier's Principle. pH also greatly affects the solubility of salts of a weak acid. This is because, if we add more hydrogen ions, effectively lowering the pH, the chemical reaction of dissolution of the salt will shift to the right and solubility will increase. However, pH does not affect the solubility of salts of a strong acid. Beyond these generalizations, pH can have a more complex influence on the solubility of other compounds. For example, at a pH greater than 9, the solubility of silica greatly increases; silica becomes soluble and more mobile. When at a pH above 10.7, amorphous silica will dissolve completely (Iler et al., 1979). The pattern that illite's solubility follows is also typical for the solubility of most aluminum silicates and complex mulit-oxides. There is also a rate law describing the dissolution rate of oxide minerals as a function of pH.

$$\text{Rate} = k * a_{H+}^{n} \qquad \text{Eq 15}$$

Where a is proton activity and is raised to the nth power. There also exists a more general and complex form of the dissolution rate equation, which incorporates the reactive surface of the mineral, temperature, activities of the protons and species, function of the ionic strength and function of the saturation state (Dolejs et al., 2010).

If solubility experiments are to be done without varying pH, then a constant pH must be determined at which to carry out the experiments. This value can be set by mirroring the environmental conditions under consideration. If there is an element that has reached equilibrium in the solvent, then the desired pH can be calculated by finding the pH at which, for example, calcite reaches equilibrium within the ground water. The pH is altered until the saturation index of calcite nears zero. This, then, is the pH value that the solubility experiments should be carried out at.

Temperature

Generally, as temperature increases, the solubility of liquids and solids increases. But for gases, it is the opposite and the solubility decreases with increasing temperature (Jones et al., 2012). Temperature has such an effect on solubility because, according to Le' Chatelier's principle, if a reaction is endothermic or exothermic, we can predict in what direction it will proceed if heat is added or taken away (erudite.com, 2012). The solubility of minerals tends to increase with increasing temperature when below 300-500 Celsius. An alumino-silcate illite becomes increasingly more soluble at higher temperatures (Kohler et al., 2003). Calcium containing minerals' solubility increases as well with increasing temperature but then begins to decrease when the temperature is higher than 350-450 Celsius. Minerals such as quartz and corundum have solubilities which level off around 500 Celsius. In addition, some minerals follow very different trends; for example, portlandite's solubility decreases with increasing temperature (Dolejs et al., 2010). It has also been found that many carbonate minerals, such as calcium carbonate, have decreasing solubility with increasing temperature.

Temperature also plays a large role in determining what phase of the compound will occur and the phase in turn affects the solubility. Temperature can affect whether a compound is crystalline or amorphous; and if it is crystalline, the temperature influences what species of crystal is formed. Pressure also helps to form the shape of the particle. For example, silica can take many different molecular formations. Above 900 Celsius, silica takes the form of cristobalite. While at atmospheric pressure when the temperature is 573 up to around 867 Celsius, silica can exist stably as quartz. If the pressure is also altered we find that from 400-500 Celsius at 0.8-1.3 kilobars, silica exists as Keatite (Iler et al., 1979).

Carbonate concentrations

In many sediment layers, carbonate species are a very prevalent compound and so carbonate concentrations must be taken into consideration when carrying out solubility experiments on minerals. Carbonate minerals themselves tend to increase in solubility with decreasing temperature. Their solubility also increases with increasing atmospheric pressure and also sees an increase in solubility when CO_2 partial pressures increase or in general as saturation levels of the solvent decrease. Interestingly, the dissolution of calcium carbonate lowers the partial pressure of CO_2.

It has been found in many minerals such as uranium complexes that their solubility increases with increasing bicarbonate concentrations (Ilton et al., 2006). In minerals containing uranium, high levels of bicarbonate cause uranyl complexation with carbonate ions and this increases the mineral's solubility (Elless and Lee, 1998). In Ilton et al.'s (2006) solubility experiment with Na-boltwoodite in bicarbonate solution, the incongruent dissolution of Si and U was determined. In opposition, Perez et al. (2000) concluded that uranophane dissolves congruently in bicarbonate solutions, but perhaps they didn't take frequent enough samples. Ilton et al. (2006) also noted that incongruent dissolution could be followed by periods of congruent dissolution. This could also be due to impurities. Giammar et al. (2002) noted that a 1-2% mole impurity could cause an excess uranium concentration such as that recorded by Ilton et al. (2006).

Ilton et al. (2006) in the experiments pretreated the Na-boltwoodite with 50 mM bicarbonate and found that, at 1.2 mM and 6 mM bicarbonate, the uranium's kinetic behavior changed and its concentration became much less than silicon. Silicon's concentration was unaffected by the pretreatment and it behaved as it had previously. Furthermore, at 1.2 mM bicarbonate, the ratio of uranium (aq) to silicon (aq) declined over time. Ilton et al. (2006) concluded that a uranium-rich, silicon-poor precipitate was forming. At 50 mM bicarbonate, the steady states of uranium and silicon were both lower than the untreated test results at the same bicarbonate concentration. Unlike the untreated tests, uranium and silicon both reached steady states in 1.2 and 6 mM bicarbonate solution. So, perhaps there was an impurity present that once dissolved away in the pretreatment method led to more congruent dissolution results.

Also, high bicarbonate concentrations can actually reduce the precipitation of a secondary phase and this was observed by Perez et al. (2000). Increases in bicarbonate concentrations also increases pH (Ilton et al., 2006). This increase in pH can also affect solubility because solubility tends to be dependent on pH levels. A study by Steward and Mones (1997) found that carbonate may have a greater effect on the dissolution rates of uranium hydroxides than pH when the solution is at a basic range (8-10). This is important for mineral dissolution because the environment usually occurs at more alkaline conditions.

PROCEDURES OF ISOPIESTIC EXPERIMENTS

In the environment, solubility influences the behavior and fate of many contaminates, both naturally occurring and technogenic in origin. The importance of quantitative measurements of solubility resulted in numerous reviews of specific techniques to measure solubility. Solubility determinations by the isopiestic method, which is considered to be one of the most accurate methods for solubility determinations, can be applied to precipitates created after ammonia gas injections to sequester uranium in the vadose zone. The basic features of the method include isothermal equilibration of samples of known masses and known initial concentrations through a common vapor phase. The solvent will distill isothermally from one crucible to another until each solution reaches the same chemical potential. All of the solutions at equal vapor pressure or isopiestic equilibrium have the same solvent activities. By equilibration, the samples with a standard of known solvent activities under the conditions of the experiment as a function of molality, the solvent activity of other solution can be determined (Rard, 1985). The composition of all the solutions placed in the same vessel is changed during equilibration to reach a common vapor pressure at constant temperature. This method permits the monitoring of concentration changes by weighing the samples at equilibrium and must be known to about 0.001 *m*. The balance used in the experiments should have a precision no less than 1×10^{-5} g. The apparatus to conduct experiments consists of a vacuum desiccator or closed chamber kept at a constant temperature. The apparatus used in the experiments is also equipped with a high accuracy pressure transducer with a range of 0-30 psia (Omega Engineering, Inc.) that will provide a measurement of water vapor pressure and allow for monitoring as the system approaches equilibrium. Rard and Platford (2000) gave a very detailed general description of the isopiestic method with an emphasis on experimental aspects.

Stock solutions were prepared by weight using distilled and deionized water from a Barnstead NANOpure water purification system or plasma grade water. Pure "ultra dry" grade chemicals or high purity salts obtained from Alfa Aesar, Puratronic, 99.999% (metal basis) were used. Preparation of the reference solutions will include breaking the glass ampoules and transferring their contents rapidly to polyethylene bottles containing weighed amounts of water. Since the heats of dissolution of the anhydrous salts are significant, the stock bottles with water need to be cooled using dry ice well below freezing in order to prevent excessive temperature increases (Gruszkiewicz and Simonson, 2005). The high purity salts, Puratronic, 99.999% (metal basis), were oven-dried at 110^{o}C for 3 hours and then stored in a tightly sealed container to prevent contact with moisture for the reference solution preparation.

Isopiestic cups should be made from an excellent thermal conductor and be chemically inert to the experimental solutions. If chemically inert metals cups with lower thermal conductivities are used, a few extra days are needed to compensate for the equilibration period (Rard, 1985). The materials usually used for cups include tantalum, platinum, copper, and nickel (Rard, 1985; Velazquez-Rivera et al., 2006; Mason and Gardner, 1936). Our experiments use 15-mL nickel cups; to avoid evaporation losses, tightly fitted light nickel lids will be immediately added after the chamber is open. Nickel crucibles with standards and experimental solutions will rest in holes drilled part way through the aluminum block that has a good thermal conductivity that will maintain a uniform temperature distribution (Figure 1). The vessel is being kept in the environmental chamber to control the stable temperature (Figure 2).

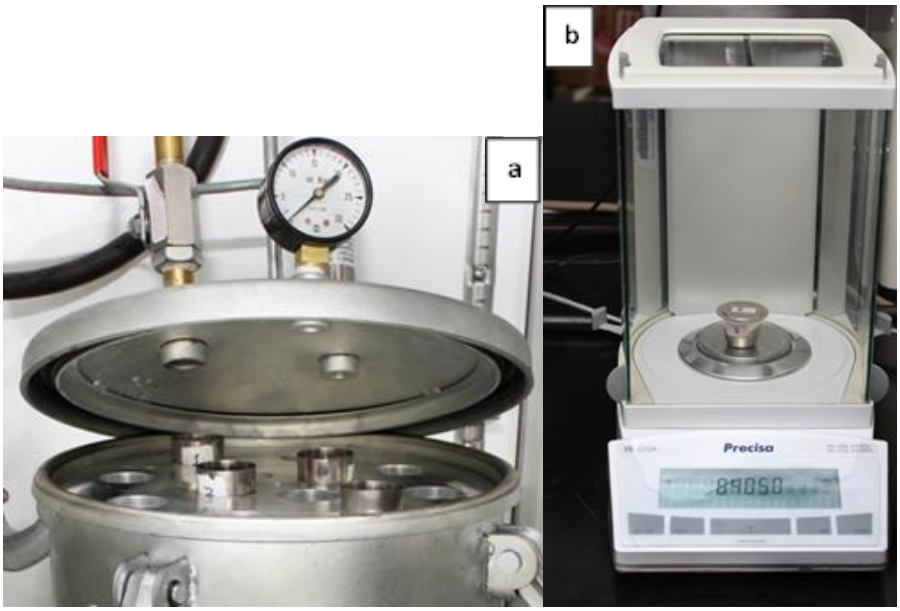

Figure 1. Isopiestic chamber to conduct solubility experiments; a) aluminum block with holes for the nickel crucibles; b) analytical balances weighing crucibles.

Figure 2. Isopiestic chamber to conduct solubility experiments connected to the acquisition system.

As a preliminary step, air is evacuated until pressure reaches around 4.5 kPa (Blanco et al., 2006). After gas is evacuated in a closed vessel, then the volatile component is transported through the vapor phase until the solutions reach equilibrium. This transport of mass observed during the contact of solid phases with solution is due to the chemical potential, which is usually

expressed in terms of activity coefficients. The activity of water in aqueous solutions relates to its fugacity by equation (Rard and Clegg, 1997):

$$a_w(T,p,x) = f_w(T,p,x)/ f^0_w(t,P^0, x^0) \quad \text{Eq 16}$$

Where a_w is the water activity, f_w and f_w^0 are the fugacities of the solution in the system and the pure liquid or solid at 1 atmosphere total pressure at specified temperature conditions, respectively; p and p^o are vapor pressure of the solution in the system and vapor pressure of pure reference, respectively; and *x* is the mole fraction of solution. It is usually assumed that, in ambient temperature and moderate pressure, water vapor behaves ideally and the fugacities can be replaced by partial pressure (Reid et al., 1987).

$$f_w/f_w^o = p_w/p^o_w \quad \text{Eq 17}$$

Where p_w and p_w^0 are the vapor pressures of water in the system and of pure water at the same temperature. Under this assumption:

$$a_w = p_w/p^o_w \quad \text{Eq 18}$$

Hence, the activity of water in any electrolyte solution can be determined by measuring the vapor pressure of water over the solution at known temperature and dividing that value by the value of the vapor pressure of pure water at the same temperature (Garrels and Christ, 1965).

The vapor pressure *p* is converted to water activity a_w according to the equation:

$$\ln a_w = \ln(\frac{p}{p_0}) + B_T\frac{(p - p_0)}{RT} + V_w(p - p^o) \quad \text{Eq 19}$$

Where p^o and *p* are the vapor pressure of pure water and salt solution at temperature T, R= 8.314 $Jol^{-1} K^{-1}$, V_w is the partial molar volume of water in the solution and approximately taken as the value of pure water and B_T is the second virial coefficient taken from literature at various temperatures (Hill, 1990). The uncertainty arising from the approximation for V_w can be negligible, compared with the experimental error of the vapor pressure *p*.

Nonvolatile solute lowers the vapor pressure of a solvent according to Raoult's law:

$$P_{soln} = X_{solv}P^o_{solv} \quad \text{Eq 20}$$

Where P_{soln} = observed vapor pressure of solution, X_{solv} = mole fraction of solvent, and P^o_{solv} = vapor pressure of pure solvent.

So, since the mole fraction is always less than 1, the vapor pressure of the solvent in solution will always be less than the vapor pressure of the pure solvent. It is known that if the vapor pressure of a solution is measured, the molecular weight of the dissolved substance could be calculated. Raoult's Law is defined as:

$$\frac{p_o - p}{p_o} = x = \frac{\frac{g}{m}}{\frac{G}{M}+\frac{g}{m}} \quad \text{Eq 21}$$

Where: x = mol fraction of solute, g = weight of solute present, G = weight of solvent present, m = molecular weight of the dissolved solute, M = molecular weight of the solvent, p_o = vapor pressure of pure solvent, and p= vapor pressure of solvent in the solution.

The molecular weight of the solute can be found as:

$$m = \frac{p_0\, g\, M}{(p_o - p)G} - g\frac{M}{G} \quad \text{Eq 22}$$

Then molality can be calculated as (Where the weight is in grams):

$$\frac{weight\ of\ solute * 1000}{formula\ weight\ of\ solute * weight\ of\ water} \quad \text{Eq 23}$$

Our initial experiments suggested that the direct measurement of vapor pressure is not accurate and that it is better to calculate vapor pressure lowering theoretically via mole fractions according to Raoult's law and then use the calculated mole fraction of each component to compute the partial pressure.

The conditions of isopiestic equilibrium for each of the separate solutions involved in an equilibrium is a_s= constant. The conditions can be rewritten as ln a_s=ln a_{ref}. If two or more solutions of different salts are in isopiestic equilibrium, the osmotic coefficient of a test solution, ϕ_x, is calculated from the reference solution, ϕ_{ref}, from the fundamental equation for isopiestic equilibrium:

$$\phi_s = \frac{v_{ref} m_{ref} \phi_{Rref}}{v_s m_s} \quad \text{Eq 24}$$

The water activities a_w of the reference can be calculated using the following equation:

$$\ln a_w = -0.001\, v_s m_s M_w \phi_{ref} \quad \text{Eq 25}$$

Where v_s is the number of ions formed by the complete dissociation of one molecule of the reference standard, and for the NaCl and KCl, v=2, M_w is molar mass of H_2O, and φ is the practical osmotic coefficient of the reference standard. The Eq. 24 is defined for mixtures, as well as for single-salt solutions (Rard and Platford, 1991). The ratio ($\frac{m_{ref}}{m_s}$) is called the isopiestic ratio. The osmotic coefficient can be measured with 0.1%-0.3% accuracy at molalities down to 0.1mol/kg.

Preliminary testing indicated that 3-5 days is enough to reach equilibrium with moderate and high molalities; up to 7-8 days equilibration is needed at low molalities to allow the large amounts of solvent to be transferred between solutions in different crucibles.

The isopiestic method is a mostly gravimetric method that relies on the assumption that only one volatile component is present. The mass of the empty crucible along with the number of moles of electrolyte in each sample should be known. Therefore, any gains or losses in mass during isopiestic equilibrations are only due to gains or losses of solvent. The observed changes in mass can then be used in the calculation of the solution molalities at isopiestic equilibrium (Rard and Platford, 2000). Metler Toledo analytical balances XS205DU will be used to weigh the sample crucibles and solution samples with readability to about 1 x 10^{-4} g. Sample size will be in the

range of 0.8-2.0 g. Isopiestic references will be weighed as liquid samples prepared from the analytical stock solutions. Samples to study the occurrence of solid–liquid transitions will be prepared as dry solids. Thus, the number of moles of solute added to each crucible will be carefully recorded. After an isopiestic equilibrium is reached, samples will be accurately weighed to calculate the molalities due to solvent weight loss or gain. Experiments will be continued with the reuse of solute samples; more solvent will be added to the standard crucible and the samples will be reequilibrated. This will be repeated a number of times until dry samples will solubilize or sample size becomes too large. To reduce the amount of water in the crucibles, the solutions can be concentrated by absorbing water in an additional crucible with a few drops of concentrated sulfuric acid or a desiccant to have a "sink' for water vapor. The accuracy of results could be checked if the molalities ratios are reproducible after a number of equilibrations with the sequential dilution using the same solution and then concentrated back via stepwise reequilibration.

So, all solutions in the isopiestic chamber that are allowed to exchange solvent until isopiestic equilibrium is reached will have the same solvent activity with a value of $(\sum_i v_i m_i)\phi$.

Initial experiments have started with solutions of NaCl and KCl equilibrated against each other to check if the experimental data correlate with values obtained from literature. The osmotic coefficients for the NaCl reference were taken from Guo et al. (2012) or Rard and Platford (2000). Data for the osmotic coefficient for aqueous KCI at 298.15K was taken from Rard and Platford (2000).

Deliquescence behavior of multicomponent precipitates

The tendency for solutes to deliquesce depends on their solubility and is influenced by the particular character of solute-solvent interactions described according to Raoult's law in vapor-pressure lowering ability. The deliquescence behavior of the multicomponent salts systems studied will improve the understanding of the stability of the U-bearing precipitates in the post-treated vadose zone at specific temperatures. The measurements of the solvent mass and the vapor pressure from the isopiestic apparatus, in conjunction with the deliquescence, relative humidity (RH) and temperatures will help to detect the points where new phases appear or disappear in the multicomponent salts systems. Deliquescence behavior of precipitates will be studied by starting from solid salt mixtures via a progressive increase in the relative humidity. The phase changes will be visible as breaks in the curve, representing the osmotic coefficient of the solution as a function of relative humidity (Gruszkiewicz et al. 2007). In the case of decreasing the relative humidity, it is assumed that the results are reversible with respect to the direction of the changes in relative humidity.

The osmotic coefficient, ϕ, can be calculated as:

$$\phi = 1000 w_s / M_s \sum n_i \, ln a_s \qquad \text{Eq. 26}$$

Where M_s ($g \cdot mol^{-1}$) is the molecular weight of water, a_s is the activity of water, n_i are the numbers of moles for each ion, and w_s (kg) is the mass of water. The value of a_s will be obtained from values calculated for an aqueous reference NaCl or KCl solutions. The stoke solutions will be prepared approximately in the 3-3.5 mol kg^{-1} range. The temperature range of the study is between 5^o C and 50^o C. After each equilibration, the isopiestic chamber will be opened in order to determine the concentrations of the samples by weighing.

The osmotic coefficients of samples can also be calculated from:

$$\phi_x = \phi_{ref} v_{ref} m_{ref} / (v_s m_s) \quad \text{Eq 27}$$

Where *v* is the number of moles of ions produced by one mole of salt (v = 2 for NaCl).

Initial experiments with isopiestic apparatus

The initial stage of the experiments was focused on the evaluation of the experimental procedures to confirm the accuracy of the results obtained by the isopiestic apparatus fabricated in-house. The isopiestic apparatus was kept in the environmental chamber with the temperature set to 25^{o}C. The testing procedures involved two standards, NaCl and KCl, for which solubility parameters such as the osmotic coefficient and water activity were well characterized in literature (Rard and Platford, 2000). Prior to recording measurements, the Labview code used to record the direct vapor pressure measurements was updated to show pressure in inches of mercury (in of Hg) and torr. The code was also modified to indicate when the system is under vacuum after the chamber degassing. The power supply currently being used to power the pressure transducer and the data acquisition system is sensitive to temperature, which apparently affected readings collected from the pressure transducer. So, the power supply was adjusted to provide stable voltages, which helped to improve the accuracy of vapor pressure measurements. However, despite the adjustment, the direct vapor pressure readings of the aqueous solutions were still not accurate enough to be used for the water activity (a_w) calculations according to Eq 18. Similar inaccuracy of the direct measurements for the activity calculations was noted by Gruszkiewicz et al. (2007). They concluded that the relative isopiestic method based on reference solutions was significantly superior to direct pressure measurements. The accuracy of the direct pressure measurements in their experiments was limited by some thermodynamic effects such as temperature and surface tension of the water present inside the transducer.

Our initial testing included three experiments. The first experiment employed a binary system, NaCl - water. At equilibrium, the vapor pressure for the solution was calculated theoretically following Raoult's law. This required computing the mole fractions of each component of a solution that were used to calculate vapor pressure of the solution by multiplying the vapor pressure of pure water at the appropriate temperature (Eq. 20). For our experiments, vapor pressure of pure water at 25^{o}C is 23.8 mm Hg. The results were compared with water activity calculations based on the NaCl osmotic coefficient values reported by Guo et al., 2012.

The experiment included eleven samples placed in the isopiestic chamber. Eight crucibles containing sodium chloride (NaCl) solutions were prepared from high purity NaCl [Puratronic, 99.999% (metal basis), Alfa Aesar] that was dried at 40 ^{o}C prior to the experiment. The masses of NaCl used for sample preparation are presented in Table 1. Each sample was diluted in 700 µl of plasma-grade DIW, reaching initial molalities of NaCl solutions between 1.482 and 4.285 mol kg^{-1}. An additional three crucibles contained only plasma-grade DI water to facilitate vapor exchange in the isopiestic chamber. The samples were weighed three times over an 8-day period to monitor the attainment of equilibrium conditions. The final weights and molalities calculations are presented in Table 1. The osmotic coefficient for each molality was calculated by two different approaches. The first approach was following Eq. 28 as presented in Guo et al. (2012).

$$\phi = a + b\left(\frac{m}{mol\ kg)}\right)^{1/2} + c\left(\frac{m}{mol\ kg)}\right) + d\left(\frac{m}{mol\ kg)}\right)^{3/2} + e\left(\frac{m}{mol\ kg)}\right)^{2} + f\left(\frac{m}{mol\ kg)}\right)^{5/2} + g\left(\frac{m}{mol\ kg)}\right)^{3} + h\left(\frac{m}{mol\ kg)}\right)^{7/2} \quad \text{Eq. 28}$$

Where coefficients a, b, c, d, e, f, g, were obtained from Guo et al. (2012).

The ϕ values calculated from the above equation were in agreement with osmotic coefficients obtained by interpolation of osmotic coefficient data presented in Hamer and Wu (1972). Values obtained from both methods are presented in Table 1.

The osmotic coefficient (ϕ) values derived from Eq. 28 were used to calculate water activity (a_w) quantities for each sample of NaCl using Eq. 25 at molalities after attainment of isopiestic equilibrium in the chamber. The average value of water activity for all samples was calculated as 0.9221. This value was compared to the theoretical water activity of 0.9288 computed using Eq18 via vapor pressure lowering above the solution containing an ionic solute of NaCl at 25^{o}C. The obtained difference in water activities between experimentally determined values and theoretically calculated values was determined to be 0.7223%. This error percentage is small enough to conclude that water activity values are similar for all samples at equilibrium attained in the isopiestic chamber.

Table 1. Osmotic coefficient and water activity for NaCl

Sample	NaCl weight (g)	Water weight (g)	Molality (mol/kg)	ϕ	$\phi*$	a_w
1	0.061	0.6260	1.66745	0.9657	0.9657	0.9436
2	0.0608	0.6295	1.65274	0.9650	0.9649	0.9441
3	0.0609	0.6089	1.71147	0.9680	0.9681	0.9421
4	0.1758	1.0909	2.75760	1.0293	1.0295	0.9028
5	0.1754	1.0465	2.86806	1.0365	1.0366	0.8984
6	0.1754	1.1167	2.68776	1.0249	1.0250	0.9055
7	0.1122	0.8478	2.26463	0.9989	0.9994	0.9217
8	0.1122	0.8168	2.35058	1.0040	1.0043	0.9185
Average						0.9221

ϕ- data obtained from Guo et al, 2012, ϕ^*- obtained from Hamer and Wu, 1972

The second experiment involved a ternary system prepared with samples of two well characterized standard solutions of NaCl and KCl. Both samples were prepared in crucibles and placed in the isopiestic chamber. Salts of NaCl and KCl were dried at 40^{o}C prior to the experiment and then dissolved in 3000 µl of plasma-grade DIW. The initial molalities were 3.1194 and 2.3831 mol kg^{-1} for NaCl and KCl, respectively. Sample weight is shown in (Table 1). The samples were weighed three times during a 20-day period to monitor the attainment of equilibrium conditions. In this experiment, the attainment of equilibrium took more time than previously due to the large amount of water used as a solvent.

The osmotic coefficients and water activities of each standard were calculated against each other and compared for accuracy with literature values. First, the osmotic coefficient for NaCl was calculated according to the Eq. 24 using KCl osmotic coefficient literature data (Hamer and Wu,

1972). For the next stage of the calculations, the osmotic coefficient of the potassium chloride was calculated according to Eq. 24 using values obtained for NaCl as a known reference standard (Guo et al., 2012). Both parameters for a_w were compared to the theoretical value of water activity, 0.8339, computed via Eq18 for the solution vapor pressure.

Table 2. Calculated osmotic coefficient and water activity for NaCl and KCl

Sample	Sample weight (g)	Final water weight (g)	Isopiestic molality (mol/kg)	$\phi_{reference}$	ϕ_{sample}	a_w
NaCl	0.5506	2.9459	4.1257	KCl ref 1.1276	1.1653	0.8457
KCl	0.5344	2.9035	4.2634	NaCl ref -1.1248	1.0885	0.8460

The comparison showed that water activity values in both cases were in excellent agreement, with a maximum difference of 0.03%.

The third experiment involved preparation of 8 samples that included 2 crucibles with standard solutions prepared from high purity sodium chloride (NaCl) salt and six (6) crucibles containing the dried multicomponent precipitate samples. Crucibles with multicomponent samples and standards were weighed at regular time intervals to record changes of water activities (a_w).

The number of moles of each compound was recalculated based on its concentration in 50 mL of stock solution and corrected values are presented in (Table 3).

Table 3. Number of moles of each compound in the 50 mL of solution

	Na_2SiO_3 (100 mM)	$KHCO_3$	$Al(NO_3)_3$ (5 mM)	$CaCl_2$
n of moles	2.37E-04	2.25E-07 (3 mM)	5.00E-06	1.00E-07 (5 mM)
		6.25E-05 (50 mM)		2.00E-07 (10 mM)
$\boldsymbol{v}$	3	2	4	3

Crucibles with multicomponent samples and standards were weighed to monitor the attainment of equilibrium conditions. Every time the chamber was opened and weights of the crucibles were recorded, the osmotic coefficients and water activities were calculated for all samples. The osmotic coefficient, ϕ, for the NaCl was calculated using an average of its molalities according to the equation proposed in Guo et al. (2012); the ϕ for the solute multicomponent samples were calculated as follows:

$$\phi = \frac{v_{NaCl} * m_{NaCl} * \phi_{NaCl}}{\sum v_i m_i} \quad \text{Eq.29}$$

Where v for NaCl is the number of ions formed by the complete dissociation of one molecule of the reference standard (NaCl=2), and ϕ for standard was taken from Guo et al. (2012). In calculations of water activities we assumed that a_w is the same for all samples.

The respective water activities (a_w) were calculated following the equations below:

$$\ln a_{NaCl} = m_{NaCl} * \phi_{NaCl} / \mho$$

$$\ln a_i = m_i * \phi_i / \mho$$

Where, omega (molality of water), $\mho$, is 55.5084 mol/kg.

Table 4 summarizes the recalculated osmotic coefficient ϕ and a_w for standard NaCl and solute multicomponent samples obtained each time the sample was weighed. In our case for the sample composition of Na_2SiO_3+ $Al(NO_3)_3$+ $KHCO_3$ the ∑molality of sample was calculated as (moles Na_2SiO_3*3+ moles $Al(NO_3)_3$*4+ moles $KHCO_3$*2)/(sample water weight at equilibrium). Data were recalculated considering the assumption that water activity values for all samples and standards at isopiestic equilibrium in the chamber are the same.

Table 4. Recalculated osmotic coefficient and water activity values after each weighing

Crucible Number	Sample	Data from weights recorded on April 1st				Data from weights recorded on April 11th				Data from weights recorded on April 29th			
		Water weight at equilibrium (g)	Isopiestic molality (mol/kg)	ϕ	a_w	Water weight at equilibrium (g)	Isopiestic molality (mol/kg)	ϕ	a_w	Water weight at equilibrium (g)	Isopiestic molality (mol/kg)	ϕ	a_w
1	NaCl	0.3888	4.9821	1.1896*	0.80794	0.3704	5.2291	1.209†	0.7965	0.3654	5.3008	1.2148‡	0.7930
2	NaCl	0.3899	4.9695			0.3713	5.2190			0.3659	5.2967		
7	Na_2SiO_3+ $Al(NO_3)_3$+ $KHCO_3$	0.2079	1.1644	3.3670	-	0.2007	1.2061	3.4683		0.1999	1.2109	3.5208	
8		0.2526	1.2047	3.4958	-	0.2438	1.2481	3.6000		0.2408	1.2638	3.6239	
9	Na_2SiO_3+ $Al(NO_3)_3$+ $KHCO_3$ + $CaCl_2$	0.2067	1.1715	3.3464	-	0.2017	1.2005	3.4845		0.2004	1.2084	3.5282	
10		0.2587	1.1768	3.5787	-	0.24850	1.2251	3.6677		0.2467	1.2339	3.7115	
11		0.2075	1.1673	3.3586	-	0.2006	1.2076	3.4639		0.1991	1.2166	3.5042	
12		0.2604	1.1694	3.6012	-	0.2512	1.2123	3.7064		0.2487	1.2246	3.7397	

* calculated using average isopiestic molality of 4.97584 mol/kg
† calculated using average isopiestic molality of 5.22404 mol/kg
‡ calculated using average isopiestic molality of 5.29876 mol/kg

FUTURE WORK

Future work will focus on the deliquescence behavior of U(VI)-free precipitates and U-bearing precipitates created after NH_3 (5% NH_3 in 95% nitrogen) pH manipulation in the synthetic solutions mimicking conditions found in the vadose zone at the Hanford Site 200 Area. Experiments will be conducted using an isopiestic chamber. Two reference solutions, $CaCl_2$ and $LiCl_2$, will be used to obtain osmotic coefficients for the low water activity values. The dry precipitates, composed of Si-Al-Ca- HCO_3, will be prepared to investigate the solid-liquid transitions and determine the activity of water and relative humidity in the multicomponent salt systems. Isopiestic experiments will be conducted at different temperatures up to 50^oC using multicomponent samples prepared with various bicarbonate and calcium ion concentrations.

ACKNOWLEDGEMENTS

Funding for this research was provided by U.S. DOE grant number DE-EM0000598. We truly appreciate Dr. Mirosław Gruszkiewicz from ORNL for the valuable suggestions on these experiments. The isopiestic chamber was fabricated in ARC's machine shop with the support of Amer Awwad and Jairo Crespo.

REFERENCES

Alexander, G. B., W. M. Heston, and R. K. Iler, 1953. The solubility of amorphous silica in water. J . Am. Chem. Soc. 75, p.553-455.

Amado, Eliseo G and Luis H. Blanco, 2004. Osmotic and activity coefficients of aqueous solutions of KCl at temperatures of 283.15, 288.15, 293.15 and 298.15 K. A new isopiestic apparatus. *Fluid Phase Equilibria* 226, 261–265

Christian, S. D., H. E. Affsprung, J. R. Johnson, and J. D. Worley. Control and Measurement of Water Activity. *Journal of the Chemical Society* 40 (1963): 419-21.

Dolejs, D., and C. E. Manning. "Thermodynamic Model for Mineral Solubility in Aqueous Fluids: Theory, Calibration and Application to Model Fluid-flow Systems." *Geofluids* 10 (2010): 20-40. *Univerzita Karlova v Praze Přírodovědecká Fakulta*. Web. 13 June 2012. <http://web.natur.cuni.cz/~ddolejs/pdf/gf010.pdf>.

Elless, M. P., and S. Y. Lee, 1998. Uranium solubility of carbonate rich uranium contaminated soils. *Water, Air, and Soil Pollution,* 107, p.147–162*.*

Felmy, Andrew R., Yuanxian Xia, and Zheming Wang, 2005. The Solubility Product of NaUO2PO4*xH2O Determined in Phosphate and Carbonate Solutions. *Radiochim Acta* 93, p.401-08.

Garrels, RM and Charles L. Christ, 1965. Solutions, minerals and equilibria. Freeman, Cooper &Company, 1736 Stockton Street, San Francisco, California 94133. Science, 450p.

Giammar, Daniel E., and Janet G. Hering, 2002. Equilibrium and Kinetic Aspects of Soddyite Dissolution and Secondary Phase Precipitation in Aqueous Suspension." *Geochimica Et Cosmochimica Acta*. 66,18 p.3235-3245.

Gorman-Lewis, Drew, Peter C. Burns, and Jeremy B. Fein., 2008. Review of Uranyl Mineral Solubility Measurements. *J. Chem. Thermodynamics,* 40, p.335–352

Gorman-Lewis, D., Shvareva, T., Kubatko, K-A., Burns, P. C., Wellman, D., and Bruce Mcnamara, 2009. Thermodynamic Properties of Autunite, Uranyl Hydrogen Phosphate, and Uranyl Orthophosphate from Solubility and Calorimetric Measurements. *Environmental Science and Technology, 43*, 7416–7422

Gruszkiewicz, MS., Palmer, D A., Springer, RD., Wang, P., Anderko, A, 2007. Phase Behavior of Aqueous Na–K–Mg–Ca–Cl–NO3 Mixtures: Isopiestic Measurements and Thermodynamic Modeling. *J Solution Chem*, 36, p. 723–765

Gruszkiewicz , M.S and J.M. Simonson, 2005. Vapor pressures and isopiestic molalities of concentrated $CaCl_2$(aq), $CaBr_2$(aq), and NaCl(aq) to T = 523 K. *J. Chem. Thermodynamics*, 37, p. 906–930

Guo, L., Sun, B., Zeng, D., Yao, Y., Han, H., 2012. Isopiestic Measurement and Solubility Evaluation of the Ternary System LiCl−SrCl2−H2O at 298.15 K. *J. Chem. Eng*. 57, p.817−827. dx.doi.org/10.1021/je201044n

Hamer, WJ and Yung-Chi Wu, 1972. Osmotic coefficients and mean activity coefficients of uni-univalent electrolytes in water at 25^o C. *J. Phys. Chem Ref Data*, vol. 1, 4.

Helgeson, H. C.; Kirkham, D. H.; Flowers, G. C., 1981. Theoretical Prediction of the Thermodynamic Behavior of Aqueous-Electrolytes at High-Pressures and Temperatures: IV. Calculation of Activity-Coefficients, Osmotic Coefficients, and Apparent Molal and Standard and Relative Partial Molal Properties to 600°C and 5 KB. *Am. J. Sci. 281* (10), p.1249–1516.

Hill, P.G., 1990. J. Phys. Chem. Ref. Data, 19, p. 1233–1274.

Holm, J. L., O. J. Kleppa, and Edgar F. Westrum, (1967). Thermodynamics of Polymorphic Transformations in Silica. Thermal Properties from 5 to 1070°K and Pressure-temperature Stability Fields for Coesite and Stishovite. *Geochimica Et Cosmochimica Acta* 31 2289-307.

Iler, R.K., 1979. The chemistry of silica: solubility, polymerization, colloid and surface properties, and biochemistry. John Wiley and Sons, p.886.

Ilton, Eugene S., Chongxuan Liu, Wassana Yantsee, Zheming Wang, Dean A. Moore, Andrew R. Felmy, and John M. Zachara., 2006. The Dissolution of Synthetic Na-boltwoodite in Sodium Carbonate Solutions. *Geochimica Et Cosmochimica Acta* 70, 4836–4849.

Jang, Je-hun, Brian A. Dempsey, and William D. Burgos, 2006. Solubility of Schoepite: Comparison and Selection of Complexation Constants for U (VI). *Water Research* 40, p. 2738-746.

Jones, Loretta, Ruth Chabay, Elizabeth Kean, Elizabeth Rogers, Iris Stovall, and Stanley Smith. "Solubility." *Fundamentals of Chemistry*. Falcon Software, Inc., 200. Web. 11 June 2012. http://www.chem.wisc.edu/deptfiles/genchem/sstutorial/Text11/Tx112/tx112.html

Kohler, Stephan J., Fabien Dufaud, and Eric H. Oelkers, 2003. An Experimental Study of Illite Dissolution Kinetics as a Function of PH from 1.4 to 12.4 and Temperature from 5 to 50°C STEPHAN." *Geochimica Et Cosmochimica Acta* 67.19, p. 3583-594.

Liu, Chongxuan, John M. Zachara, Odeta Qafoku, James P. Mckinley, Steve M. Heald, and Zheming Wang, 2004. Dissolution of Uranyl Microprecipitates in Subsurface Sediments at Hanford Site, USA. *Geochimica Et Cosmochimica Acta* 68.22, p.4519-537.

Mason, CM and Gardner, HM., 1936. Isopiestic method for the determination of molecular weights. *J. Chem. Educ*., 13, 4, p. 188

Perez, Isabel, Ignasi Casas, Maria Martin, and Jordi Bruno, 2000. The Thermodynamics and Kinetics of Uranophane Dissolution in Bicarbonate Test Solutions. *Geochimica Et Cosmochimica Acta* 64.4. p. 603-08.

Prausnitz, J.M., Lichtenthaler, R.N., Azevedo, E.G., 1986. Molecular thermodynamics of fluid-phase equilibria (2nd ed.) Englewood Cliffs, New York, Prentice-Hall.

Rai, Dhanpat, Yuanxian Xia, Linfeng Rao, Nancy J. Hess, Andrew R. Felmy, Dean A. Moore, and David E. McCready, 2005. Solubility of (UO2)3(PO4)2·4H2O in H+-Na+-OH−-H2PO− 4 -HPO2− 4 -PO3− 4 -H2O and Its Comparison to the Analogous PuO2+ 2 System. *Journal of Solution Chemistry* 34, 4. DOI: 10.1007/s10953-005-5216-4

Rard, J and Platford, R, 2000. Experimental method: isopiestic, Chapter 5 in Activity coefficients in the electrolyte solutions edited by K.Pitzer, CRC press, Boca Raton, Florida

Rard, J. A. and Platford, R. F. 1991. Experimental Methods: Isopiestic. In Activity Coefficients in Electrolyte Solutions, 2nd ed.; Pitzer, K. S., Ed.; CRC Press: Boca Raton, FL, Chapter 3.

Rard, J. A., and Clegg, S. L., 1997. Critical Evaluation of the Thermodynamic Properties of Aqueous Calcium Chloride. *J. Chem. Eng. Data*, 42, 819–849.

Rard, Joseph, 1985. Solubility determinations by the isopiestic method and application to aqueous lanthanide nitrate at 25°C. *Journal of Solution Chemistry*, 14, 7, p.457-471.

Reid, R.C., Prausnitz, J.M., and Poling, B.E., 1987. The properties of gases and liquids (4th Ed). New York, McGraw-Hill.

Ticehurst, Martyn D., Richard A. Storey, and Claire Watt. 2002. Application of Slurry Bridging Experiments at Controlled Water Activities to Predict the Solid-state Conversion between Anhydrous and Hydrated Forms Using Theophylline as a Model Drug. *International Journal of Pharmaceutics* 247.1-2, p. 1-10.

Velazquez-Rivera, M., Palmer, D A., Kettler, R M., 2006. Isopiestic measurement of the osmotic coefficients of aqueous $\{xH_2SO_4 + (1-x)Fe_2(SO_4)_3\}$ solutions at 298.15 and 323.15 K., *J Solution Chem*, 35, p.1699–1730.

TASK 1.1.1: CHARACTERIZATION OF NEW URANIUM-BEARING SAMPLES PREPARED TO MINIMIZE NITRATINE IMPACT

INTRODUCTION

Past practices of radioactive waste disposal operations at the DOE Hanford's 200 Area allowed waste discharges to retention trenches, basins and cribs where uranium contaminated water percolated into the vadose zone (VZ). The uranium leakages created a potential source for groundwater contamination and risk to potential receptors through water uptake from contaminated wells or discharges to surface water. This investigation targets uranium contamination in the VZ of the 200 Area that may affect potential discharges to the Colombia River via groundwater migration. Injection of reactive gases (i.e.: NH_3) is an innovative method aiming to reduce uranium mobility in the subsurface without the addition of liquid amendments, which could promote undesired downward contaminant migration. The injection of ammonia gas in the vadose zone prompts the formation of NH_4OH, followed by a subsequent increase in pH. The alkaline conditions can greatly enhance the solubility rates of most Si-containing minerals. The following decrease in pH as the system stabilizes and reaches natural equilibrium will trigger uranium co-precipitation reactions during the recrystallization of minerals.

This subtask investigates the mineralogical and morphological characteristics of precipitates by means of X-ray diffraction (XRD) and scanning electron microscopy with energy dispersive spectroscopy (SEM-EDS) to confirm the identity of the uranium-bearing solid phases. During FIU Year 3, uranium-bearing precipitate samples prepared with the addition of 200 ppm of U(VI) in the mixture solution with and without Ca using "high" (50 mM) and "low" (3 mM) concentrations of bicarbonate were evaluated by means of SEM-EDS and XRD analysis. The majority of samples prepared with 50 mM HCO_3^- exhibited hot spots, showing them in the crystal-like form. EDS analysis of these areas resulted in uranium atomic percentages that regularly exceeded 1% and often reached up to 10%. The powder XRD analysis of the select samples resulted in patterns of well-defined peaks that best corresponded to the diffraction pattern of nitratine ($NaNO_3$). The abundance of sodium ions through the addition of sodium silicate (Na_2SiO_3) in the solution mixture and the adjustment of pH by concentrated nitric acid during sample preparation were the leading cause of the nitratine formation.

This progress report summarizes results on alternative sample preparation methods that attempt to limit the formation of nitratine or help to increase the atomic percentage of U(VI) in the composition of solid phases for the identification of known phases via X-ray diffraction. One set of samples was prepared following the same procedures of sample preparation but the concentration of U(VI) was increased up to 500 ppm. The increase in uranium concentration can help to increase the atomic percentage of U(VI) in the sample composition. Another set of uranium-bearing samples was prepared from silicic acid that replaced the primary sodium contributor, sodium metasilicate ($Na_2SiO_3 \bullet 9H_2O$), with scarcely soluble silicic acid hydrate ($SiO_2 \bullet nH_2O$). The procedures to solubilize colloidal silica hydrate ($SiO_2 \bullet nH_2O$) includes basifying the suspension by sparging ammonia (NH_3) gas to the pH range of 11-12. These experiments can provide the necessary information on U mineral phases that can be created in soil via pH manipulation by the ammonia gas injection method.

MATERIALS & METHODS

SAMPLE PREPARATION

Though the sample preparation methods for these two sets of samples were modified, the general approach remains largely the same as in previously reported studies (Katsenovich et al., 2012; Katsenovich et al., 2014). Stock pore water solutions were prepared for each set using a combination of various salt solutions formulated such that the concentration of the primary components of interest (HCO_3^-, Al^{3+}, and Si) would be within the desired ranges. These concentrations were based on the characterization of vadose zone sediments from borehole 299-E33-45 performed by Serne et al. (2008) at the Hanford 200 Area. The concentrations of the primary constituents of interest in this pore water simulation are given in Table 5.

Table 5. Desired Concentrations of Primary Constituents

[Si]	[Al^{3+}]	[HCO_3^-]	[Ca^{2+}]	[U]
100 mM	5 mM	3 & 50 mM	0, 5, & 10 mM	200 ppm

The first set of samples were prepared in much the same way as described in prior reports (Lagos et al., 2012; Lagos et al., 2014) with the difference being the elevated uranium content. In response to the overwhelming presence of nitratine in earlier samples, the concentration of uranium was doubled in an attempt to bolster the response of the associated uranyl phases in spectroscopic and diffraction analysis. It was hypothesized that the increased uranium in the pore water solution would facilitate an increase in the yield of the crystalline forms spotted by SEM-EDS analysis in prior studies.

This set of elevated uranium samples was comprised of six samples prepared from pore water solutions described in Table 6. These solutions were consistent across the samples, only differentiating in the bicarbonate (HCO_3^-) and calcium (Ca^{2+}) content added. To continue to observe the impact that these two variables have on the uranium phases, sample solutions with combinations of high and low bicarbonate concentrations and a range of calcium concentrations were prepared. The concentrated stock solutions were prepared such that when added into the pore water solutions, the desired concentrations would be reached.

The first step of the sample preparation entailed mixing the appropriate concentrations of $KHCO_3$, Na_2SiO_3, and $Al(NO_3)_3$ in a 50-mL vial to form two stock solutions for the two HCO_3^- concentrations being evaluated. This relatively alkaline solution would then be adjusted to a pH of 8, using concentrated nitric acid, to bring the solution down to a pH that better mimics the natural conditions of the Hanford 200 Area vadose zone (Szecsody et al., 2012). At this point, prior to the addition of the calcium and uranium components, the remediation method is applied by basifying the solution by sparging ammonia (NH_3) gas to the pH range of 11-12. From here, 10-mL aliquots of the 50 mL stock were dispensed into 15-mL sample vials, one for each calcium concentration. Solutions were finished by adding small volumes of the concentrated $CaCl_2$ and $UO_2(NO_3)_2$, minimally effecting the total concentration of the other components in solution. The mixture was allowed to settle and interact over the course of 2 weeks, a period which has shown in prior sample preparations (Lagos et al., 2013), to be a significant enough stay period for crystal formation to occur. The separated supernatant was then decanted and reserved for analysis via KPA while the solid was dried in an oven at 30°C over two weeks. This precipitate was retained for SEM-EDS and XRD analysis.

Table 6. Stock Solutions and Sample Mixtures - 500 ppm U

Stock Solution	Stock Solution Concentration (mM)	Synthetic Pore Water Concentrations (mM)					
		Low bicarbonate w/o calcium	Low bicarbonate w/ calcium		High bicarbonate w/o calcium	High bicarbonate w/ calcium	
$CaCl_2 \cdot 2H_2O$	2500.00	0	5	10	0	5	10
$KHCO_3$	400.00	3			50		
$Na_2SiO_3 \cdot 9H_2O$	422.24	100					
$Al(NO_3)_3$	50.00	5					
$UO_2(NO_3)_2 \cdot 6H_2O$	210.06	2.1006					
5% NH_3 in N_2 (g)	Injected until pH ≈ 11						

The second set of samples were prepared with the intention of minimizing nitratine ($NaNO_3$) in order to lessen the obtrusive peaks that obscure the meager peaks of the less plentiful components of the sample XRD patterns. It was hypothesized that this could be accomplished by minimizing the sodium content in the system by selecting alternatives to the salts used in the pore water solution. These changes are reflected in **Error! Reference source not found.**. The primary sodium contributor, sodium metasilicate ($Na_2SiO_3 \bullet 9H_2O$), was replaced with silicic acid hydrate ($SiO_2 \bullet nH_2O$), a scarcely soluble solid under normal conditions. The primary concern about this course of action, the low solubility of this silicate, was addressed by basifying the suspension. A study by Niibori et al. showed that the solubility of amorphous silica was significantly increased with time and temperature in highly alkaline solutions (2000). The sample preparation steps were modified in order to keep the silicic acid in basic conditions overnight, much longer than the aforementioned Niibori studies, and ensure the silicic acid solid dissolved.

Table 7. Stock Solutions and Sample Mixtures - Reduced Sodium Samples

Stock Solution	Stock Solution Concentration (mM)	Synthetic Pore Water Concentrations (mM)			
		Low bicarbonate w/o calcium	Low bicarbonate w/ calcium	High bicarbonate w/o calcium	High bicarbonate w/ calcium
$CaCl_2 \cdot 2H_2O$	2500.00	0	5	0	5
$NaHCO_3$	400.00	3		50	
$SiO_2 \cdot nH_2O$	422.24	100			
$Al(NO_3)_3$	50.00	5			
$UO_2(NO_3)_2 \cdot 6H_2O$	210.06	2.1006			
5% NH_3 in N_2 (g)	Injected until pH ≈ 11				

Also of note is the change from potassium to sodium bicarbonate. Though the aim was to minimize sodium, the opportunity to further narrow the focus of this study by removing potassium's impact from consideration was taken. The area where potassium played a particularly intrusive part was the EDS analysis of samples, where the near overlap of the peaks for the two elements complicated uranium identification.

Similar to the aforementioned elevated uranium samples, the sodium reduced samples began with preparation of the 50 mL concentrated stock solutions for the bicarbonate, aluminum, and silica contributors to the pore water solution ($NaHCO_3$, $Al(NO_3)_3$, and $SiO_2 \cdot nH_2O$, respectively). The silicic acid solution, prepared assuming 100% dissolution for calculating concentrations, was basified using ammonia gas and left stirring at pH (~11.5) overnight. The ammonia gas

treatment was repeated to compensate for pH elevation while stirring. After the overnight stay, the stock solutions were combined in the appropriate ratios to achieve the desired final concentrations. From this mixed solution, 10-mL aliquots were transferred into four 15-mL sample vials for the four combinations of components being evaluated. Small volumes of concentrated $CaCl_2$ followed by $UO_2(NO_3)_2$ were added to finish the solutions. This mixture was allowed two weeks to settle before decanting and reserving the supernatant for KPA analysis to determine soluble uranium content. The solid precipitate was dried in an oven at 30°C for two weeks and set aside for SEM-EDS and XRD analysis.

Side Study: Open-Air Samples

In parallel with the study samples, a single sample was prepared as an exploratory test of a recently proposed change to the sample preparation methodology. The alterations involved leaving the standing post-treatment solution open to the atmosphere to promote the gas exchange with air that is expected to occur in the system on the field scale. It has been reported that this gas exchange is important for the gradual return to normal vadose zone pH conditions from the extremely alkaline environment created by the ammonia gas injection. These samples were prepared identically to the high-bicarbonate, 10 mM [Ca^{2+}] variant of the aforementioned elevated uranium samples. The open-air (OA) sample is distinguished by the prolonged stay in solution, up to ~3 months, and the exposure to air during that sitting period. The dried products of this sample would then be imaged by SEM-EDS and analyzed by XRD, if warranted.

SEM-EDS Analysis

Scanning electron microscopy and energy dispersive spectroscopy (SEM-EDS) were used to study the surface morphology and composition of the precipitates formed and dried in sample preparation. These analyses were done at the Florida Center for Analytical Electron Microscopy located on the Florida International University Modesto A. Maidique Campus (MMC). The SEM system used was a JOEL-5910-LV with acceleration potentials ranging from 10 to 20 kV. EDS analysis was produced using an EDAX Sapphire detector with UTW Window controlled through Genesis software. Any required gold coating was done with an SPI-Module Control and Sputter unit for 2 minutes to produce a thin layer of gold.

Small specimens were taken from the solid precipitates and mounted to aluminum studs with double-sided carbon tape. These studs were evaluated for alpha emission, in accordance with the guidance of the campus Radiation Safety Officer, prior to transferring for analysis. The specimen were coated with gold to enhance conductivity and analyzed in both standard and backscatter modes. The majority of analysis took place in backscatter electron capture mode, which is preferred for its property of distinguishing the differences in average atomic weight in an area. This was of particular use to this study for identifying areas of elevated uranium content.

XRD Analysis

After taking specimens for SEM analysis, samples, selected based on the detection of uranium by SEM-EDS analysis, were carefully ground by pestle and mortar for powder X-ray diffraction analysis. The samples were used with a custom sample holder designed specifically for holding the small quantities of sample available in this experiment. Analyses were performed on the dried precipitates at 35 kV and 40 mA via a Bruker 5000D XRD instrument. Diffraction patterns were obtained using a copper Cu Kα radiation source (λ=0.154056 nm) with a tungsten filter.

The XRD was programmed to run over a 2-theta (2θ) range from 10° to 75° with a 0.02° step size and 2 second counting per step.

RESULTS AND DISCUSSION

The experimental procedure for evaluating uranium remediation via NH_3 gas injection into a synthetic pore water solution was modified in order to minimize the effect of nitratine on solid phase analysis. It was hypothesized that increasing the uranium concentration or decreasing sodium available to the system would grant the latitude necessary for more accurate identification of the uranium phases produced.

Elevated uranium samples

SEM-EDS analysis of the first set of elevated uranium samples showed an unforeseen lack of the crystal shaped uranium-rich phases produced in prior analysis. Figure 3 shows the crystal-like shapes spotted relatively consistently in prior studies. It was proposed that the increase of uranium available to the system would, in turn, result in an increased yield of these crystalline phases. Unlike the results presented in the FIU Year 3 report (Lagos, et al., 2013), the results of the samples prepared in this study using the same method, save for the dramatic increase in uranium, showed no sign of the crystalline structures expected (Figure 4 & Figure 5).

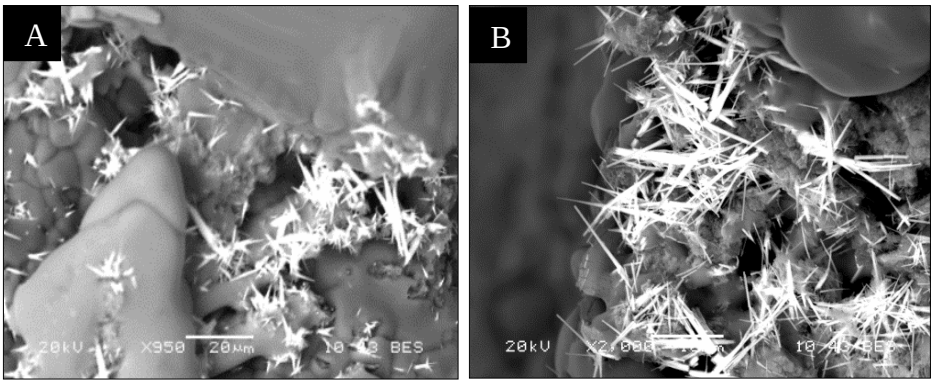

Figure 3. Crystalline uranium phases on the surface of samples prepared using 50 mM of bicarbonate and 200 ppm U after a 2 week stay in solution. With (A) and without (B) 5 mM Ca^{2+}. (Lagos et al, 2013)

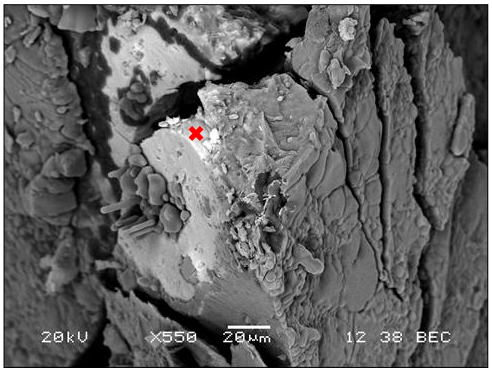

Element	Wt%	At%
CK	13.72	29.97
NK	15.08	28.24
NaK	15.77	18.00
AlK	02.14	02.08
SiK	17.26	16.12
ClK	00.27	00.20
UM	33.20	03.66
KK	02.57	01.72
CaK	00.00	00.00

Figure 4. Uranium phases on the surface of samples prepared using 50 mM of bicarbonate, 5 mM of Ca, and 500 ppm U after a 2 week stay in solution.

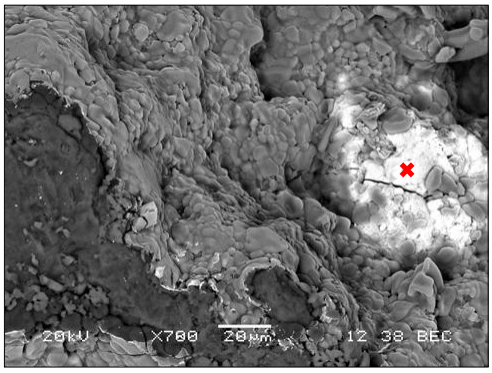

Element	Wt%	At%
CK	11.07	26.67
NK	12.19	25.18
NaK	16.99	21.39
AlK	01.39	01.49
SiK	18.62	19.18
UM	37.73	04.59
KK	02.02	01.49

Figure 5. Uranium phases on the surface of samples prepared using 50 mM of bicarbonate and 500 ppm U (no calcium) after a 2 week stay in solution

Though the expected crystal-like shapes were not present in these samples, X-ray diffraction analysis showed a clear set of peaks, confirming the presence of a repeating crystalline structure in these samples. The diffraction pattern produced for the sample prepared from the low bicarbonate (3 mM) solution containing 5 mM of calcium was a near perfect match for nitratine ($NaNO_3$) with every major peak produced showing a corresponding match when compared to the 2θ and intensity ratios from literature (Figure 6). With no other discernible peaks, it is unlikely that any other crystalline mineral phase was present in any significant proportion to the rest of the sample. The lack of any significant uranium-bearing mineral phases in the XRD pattern is not unexpected considering the SEM-EDS of the sample (Figure 7), which showed the atomic percentage of uranium rarely exceeded 0.5%.

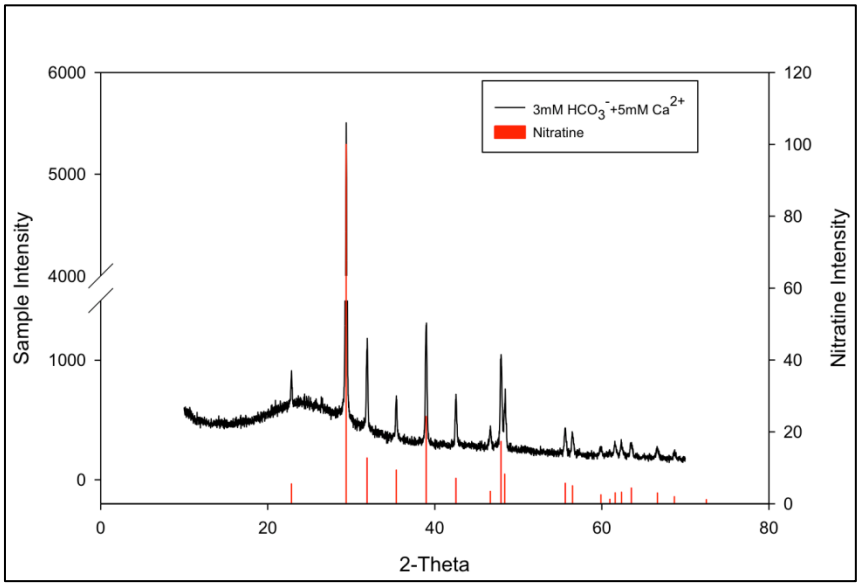

Figure 6. Comparison of the XRD pattern for the low bicarbonate, 5mM Ca^{2+} sample to literature values for nitratine

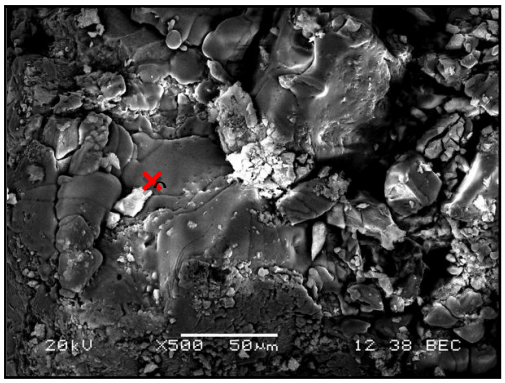

Element	Wt%	At%
CK	10.68	16.36
NK	08.66	11.37
OK	41.46	47.67
NaK	10.43	08.34
AlK	01.21	00.83
SiK	19.55	12.81
ClK	02.97	01.54
UM	03.27	00.25
KK	01.10	00.52
CaK	00.67	00.31

Figure 7. SEM and EDS for the surface of the sample prepared using 3 mM of bicarbonate, 5 mM of Ca^{2+}, and 500 ppm U after a 2 week stay in solution

Much like the aforementioned samples, those precipitates prepared from the 50 mM bicarbonate, 5 mM Ca^{2+} solution produced XRD patterns that strongly suggest a large presence of nitratine. Unlike that same sample, however, the diffraction pattern showed evidence to suggest the presence of another mineral. This result supports the SEM-EDS analysis that distinctly showed a strong presence of a secondary uranium-bearing phase (Figure 4). Comparing those extraneous peaks to patterns for predicted uranium phases, such as andersonite and rutherfordine, showed no significant matches when considering the angle and intensity ratios of the most prominent peaks. XRD analysis of these samples will be repeated because it is possible that the diffraction pattern comparisons could be improved by expanding the 2 θ range to include more of the lower angles found in some of the literature values of predicted phases.

The high and low bicarbonate specimens produced with 10 mM of calcium showed the fewest sites of high uranium content by SEM imaging. The high bicarbonate specimen, in particular, showed no areas of elevated average atomic weight that showed a discernibly intense uranium peak (Figure 8). No site on this sample had an atomic percentage of uranium that exceeded 0.20%. The low bicarbonate, 10 mM calcium, specimen showed a single location with the expected bright areas and elevated uranium content (Figure 9). While there was a markedly high atomic percentage of uranium (8.50%), the area showed a stark lack of the anticipated crystalline structure. Finely detailed secondary electron capture (standard mode) SEM imaging showed no distinguishable difference in the morphology of the areas of high uranium content and the amorphous surroundings.

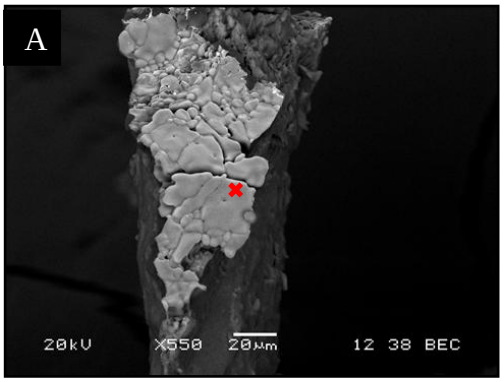

Element	Wt%	At%
CK	16.01	22.20
NK	40.36	47.98
NaK	39.42	28.54
AlK	00.31	00.19
SiK	00.46	00.27
ClK	00.43	00.20
UM	01.85	00.13
KK	00.60	00.26
CaK	00.57	00.24

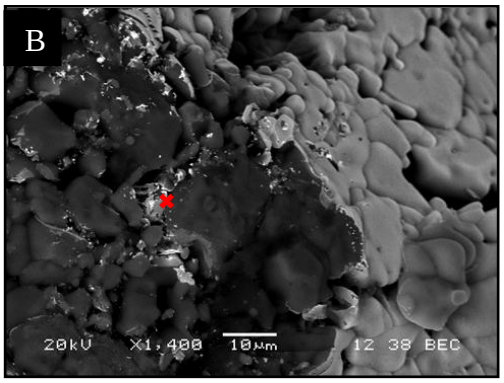

Element	Wt%	At%
CK	20.65	28.42
NK	33.36	39.38
NaK	43.46	31.25
AlK	00.00	00.00
SiK	00.76	00.45
ClK	00.00	00.00
UM	00.68	00.05
KK	00.62	00.26
CaK	00.47	00.19

Figure 8. SEM micrographs and EDS data for two sites on the surface of samples prepared using 50 mM of bicarbonate, 10 mM of Ca^{2+}, and 500 ppm U after a 2 week stay in solution

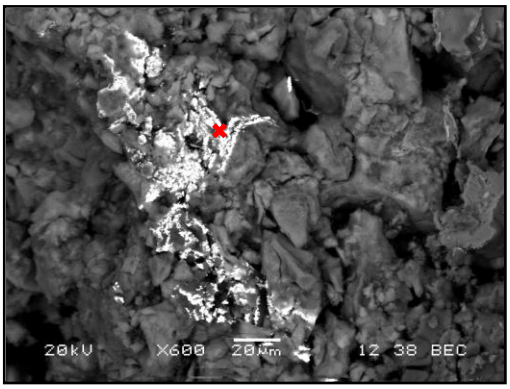

Element	Wt%	At%
CK	03.71	11.56
NK	16.75	44.75
NaK	12.34	20.08
AlK	00.50	00.70
SiK	05.53	07.37
ClK	02.51	02.65
UM	54.05	08.50
KK	03.28	03.14
CaK	01.33	01.25

Figure 9. SEM micrograph and EDS data for the lone uranium-rich site spotted on the surface of the sample prepared using 3 mM of bicarbonate, 10 mM of Ca^{2+}, and 500 ppm U after a 2 week stay in solution

Sodium Reduced Samples

The sodium-reduced samples, prepared with silicic acid supplanting the previous sodium-containing silica source, yielded significantly less precipitate, relative to their sodium metasilicate based counterparts. While this was not completely unexpected, it is possible that it poses a new problem during instrumental analysis. Even considering the replacement of potassium bicarbonate with its sodium analogue, the change from sodium metasilicate to silicic acid represents a 75% reduction in sodium present in the system. If this decrease corresponds with a lessened nitratine impact on XRD analysis, while maintaining, or increasing, the yield of the crystalline uranium phases, characterization should be less problematic.

The SEM-EDS analysis of the precipitates produced from these samples revealed very few uranium-rich sites. Contrary to the bulk of previous samples, the majority of uranium-bearing phases (confirmed by EDS analysis) were found in precipitates prepared using low bicarbonate concentration, though none of those phases appeared to be crystalline based on SEM imaging (Figure 10 & Figure 11). Magnification of these uranium phases showed none of the crystal-like structures that were spotted in previous samples, though further analysis by XRD will be used to determine the presence of any crystalline phases. The SEM of the sodium reduced samples also showed the surface morphology to be much more granular than prior studies. Based on this observation, it could be inferred that the dissolution step did not allow for the complete dissolution of the silicic acid nano-particle starting materials in the sample preparation process. This suggests either gross error in the sample preparation process, or a need to re-evaluate the sample preparation methodology used in these sodium reduced samples. A comparison to untreated silicic acid may be required to confirm that conclusion.

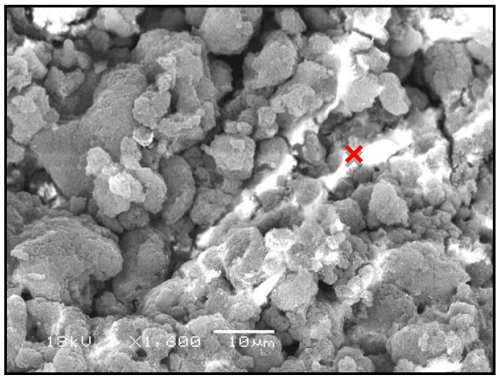

Element	Wt%	At%
CK	17.69	37.10
NK	23.40	42.08
NaK	00.91	01.00
AlK	01.86	01.74
SiK	14.77	13.25
ClK	00.76	00.54
UM	40.61	04.30

Figure 10. SEM-EDS data for uranium-rich site spotted on the surface of the sample prepared using silicic acid, 3 mM of bicarbonate, No Ca^{2+}, and 500 ppm U after a 2 week stay in solution

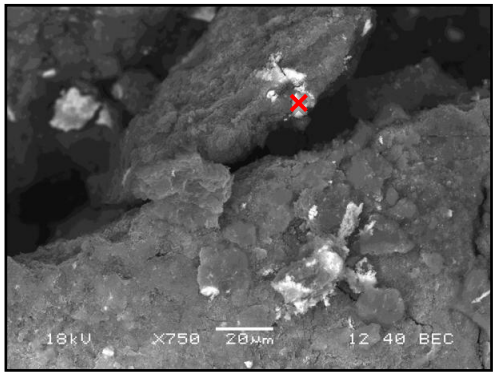

Element	Wt%	At%
CK	15.80	41.80
NK	13.50	30.61
NaK	00.93	01.29
AlK	01.17	01.37
SiK	12.69	14.36
ClK	02.51	02.25
UM	51.59	06.89
CaK	01.82	01.44

Figure 11. SEM-EDS data for uranium-rich site spotted on the surface of the sample prepared using silicic acid, 3 mM of bicarbonate, 5mM of Ca^{2+}, and 500 ppm U after a 2 week stay in solution

The supernatants from these samples were reserved after decanting and will be evaluated by KPA for uranium content. This analysis is important for determining the fraction of the uranium that remained in the liquid phase, rather than the solid precipitate. Based on the dearth of uranium in the solid phase under SEM, it is anticipated that the amount in solution will be significant.

Open-Air Sample

SEM analysis of the open-air test sample showed a considerably dissimilar surface morphology, relative to the similarly prepared samples (Figure 12), which would prove to be primarily made up of potassium after EDS analysis. Upon closer inspection, it was discovered that the OA sample had the same crystal-like uranium-bearing shapes seen in prior studies (Figure 13). EDS analysis confirmed the elevated presence of uranium as well as potassium, which seems to dominate the rest of the sample.

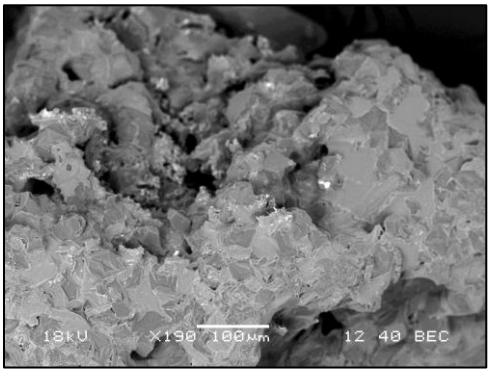

Figure 12. SEM image of the surface of the open-air sample

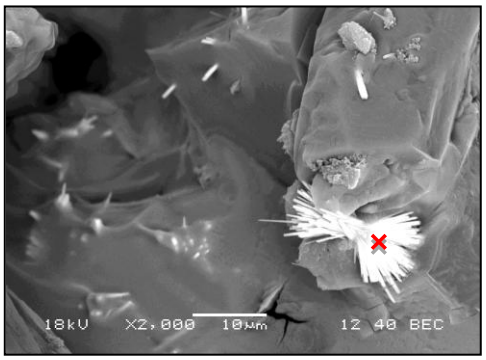

Element	Wt%	At%
CK	01.88	07.98
NK	07.51	27.35
NaK	04.42	09.82
AlK	00.89	01.68
SiK	02.70	04.90
ClK	03.19	04.59
UM	54.96	11.78
KK	24.45	31.91
CaK	00.00	00.00

Figure 13. SEM-EDS data for uranium-rich site on the surface of the open-air sample

The promising SEM-EDS data was supplemented with X-ray diffraction analysis, which confirmed the presence of crystalline phases (Figure 14). Like the other XRD results discussed thus far, comparison of the OA sample diffraction pattern with some of the reference patterns suggested a match for nitratine ($NaNO_3$) with a second potential match for cejkaite ($Na_4(UO_2)(CO_3)_3$), consistent with a determination made with prior XRD analyses (Lagos, et al., 2013).

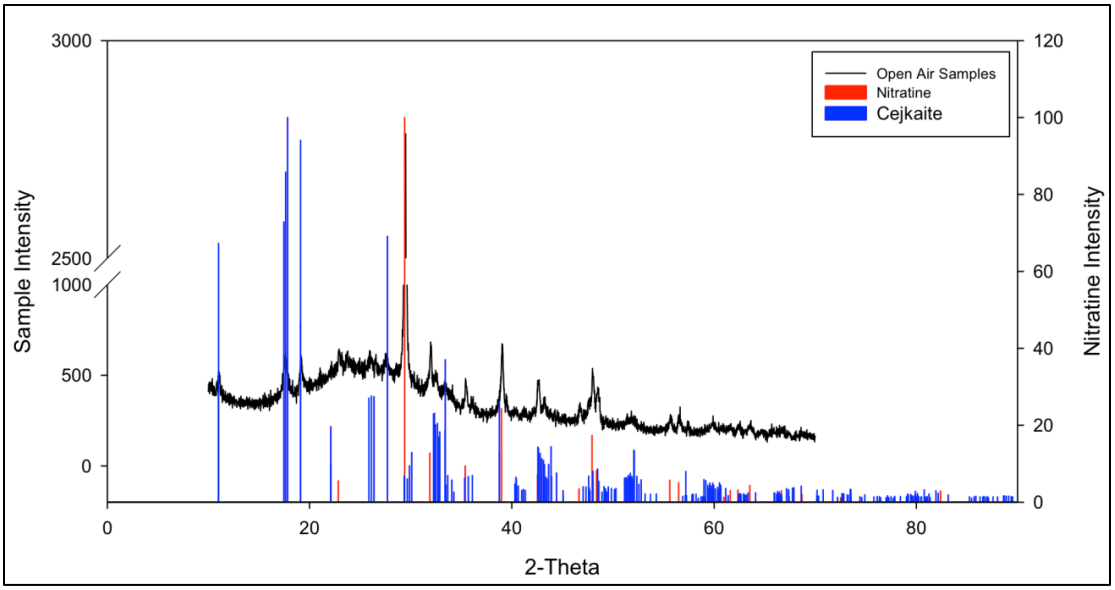

Figure 14. Comparison of the XRD pattern for the open-air sample to patterns for nitratine & cejkaite

It was speculated that the sample preparation for the open-air test sample was flawed due to the fact that the supernatant ended up being evaporated rather than decanted from the sample tube. This would likely result in the precipitation of the otherwise soluble components from the solution, changing the composition of the precipitate. Despite that, this methodology will continue to be modified and investigated as a potential improvement upon the original.

FUTURE WORK

Scanning electron microscopy, particularly in backscatter electron capture mode, allowed for identification of the uranium rich sites in the precipitates produced by the NH_3 gas injection remediation method using a synthetic pore water solution. This method, modified to minimize the interference of nitratine ($NaNO_3$), produced solid uranium phases that differed dramatically from those produced in prior sample preparation and analysis. It is possible that the reason for this is the increased uranium concentration led to the production of a different uranium phase than predicted based on earlier studies, but further study is required to draw that conclusion.

Moving forward, the evaluation of the existing samples will continue with SEM-EDS analysis of the sodium reduced samples and XRD analysis of both sets of samples. Continuing further, more samples will be produced for study and the modified preparation method will be honed to efficiently and effectively generate and characterize the uranium phases.

ACKNOWLEDGEMENTS

Funding for this research was provided by U.S. DOE grant number DE-EM0000598. We would like to acknowledge Thomas Beasley from FIU/FCAEM for his assistance with the SEM/EDS analysis.

REFERENCES

Lagos, L., Katsenovich, P., Gudavalli, R., et al, August 2013. Rapid Deployment of Engineered Solutions for Environmental Problems at Hanford. Year End Technical Report, U.S. Department

of Energy Office of Environmental Management Office of Science and Technology under Grant No. DE-EM0000598.

Lagos, L., Katsenovich, P., Gudavalli, R., et al, June 2012. Rapid Deployment of Engineered Solutions for Environmental Problems at Hanford. Year End Technical Report, U.S. Department of Energy Office of Environmental Management Office of Science and Technology under Grant No. DE-EM0000598.

Niibori, Y., Kunita, M., Tochiyama, O., and Chida, T., 2000. Dissolution Rates of Amorphous Silica in Highly Alkaline Solution, Journal of Nuclear Science and Technology, 37, 4,

Serne RJ, MJ Lindberg, SR Baum, GV Last, RE Clayton, KN Geiszler, GW Gee, VL LeGore, CF Brown, HT Schaef, RD Orr, MM Valenta, DC Lanigan, IV Kutnyakov, TS Vickerman, CW Lindenmeie, 2008. Characterization of Vadose Zone Sediment: Borehole 299-E33-45 Near BX-102 in the B-BX-BY Waste Management Area. 2002. PNNL-14083. Contract DE-AC06-76RL01830.

Katsenovich, Y., Gonzalez, N., Moreno-Pastor, C., Lagos, L., 2012. The Effect of Si and Al Concentration Ratios on the Removal of U(VI) under Hanford Site 200 Area Conditions. In the proceeding of the Waste Management Conference, Feb 26 – March 2, 2012, Phoenix, AZ.

Katsenovich, Y.P., Cardona, C., Lagos, L.E, 2014. The Effect of Ca Ions on the Removal of U(VI) via In-Situ Ammonia Gas Injection at the Hanford Site 200 Area. In the proceeding of the Waste Management Conference, March 2 – 6, 2014, Phoenix, Arizona, USA

Szecsody, J.E., Truex, M.J., Zhong, L., Johnson, T.C., Qafoku, N.P., Williams, M.D., Greenwood, W.J., Wallin, E.L., Bargar, J.D., Faurie, D.K., 2012. Geochemical and Geophysical Changes during Ammonia Gas Treatment of Vadose Zone Sediments for Uranium Remediation. Vadose Zone Journal, 11, 4. doi: 10.2136/vzj2011.0158

TASK 1.2: INVESTIGATION ON MICROBIAL META-AUTUNITE INTERACTIONS - EFFECT OF BICARBONATE

BACKGROUND

Uranium is one of the most abundant actinide elements found in the environment and is a key contaminant of concern at many U.S. Department of Energy sites, serving a leading role in the nation's defense for over 50 years. Uranium contamination of soil and groundwater is of great environmental concern due to the toxicological properties of the uranyl species. The behavior of uranium and its mobility in the subsurface is affected by various factors such as chemistry of the porewater, groundwater and soil minerals, presence of complex-forming ligands, and micro-organisms that thrive under these conditions. Uranium exists in a number of valence states but, under oxidizing conditions, it dominates as a highly soluble and stable uranyl ion, UO_2^{2+}. In neutral or basic pH conditions, uranium undergoes hydrolysis in aqueous solutions and can readily complex with a wide variety of ligands such as carbonate and phosphate. These complexation reactions often result in the formation of mobile aqueous species or precipitation of U-bearing minerals.

Dissolved inorganic carbon present in soil and groundwater is one of the primary factors controlling uranium aqueous speciation. In oxidized conditions at a pH > 4, uranyl ions interact with carbonate creating strong neutral and negative soluble anionic complexes such as $UO_2CO_3^0$, $UO_2(CO_3)_2^{2-}$, and $UO_2(CO_3)_3^{4-}$ that dominate aqueous speciation of U(VI) (Langmuir, 1978). In Ca-rich soil, calcium-uranyl-carbonate complexes, $Ca_2UO_2(CO_3)_3^0(aq)$ and $CaUO_2(CO_3)_3^{2-}$, became the predominant forms of dissolved U(VI) in the circumneutral and alkaline pH conditions [Bernhard et al., 2001; Kalmykov and Choppin, 2000]. These complexes were identified in contaminated pore water at the Hanford Site, Washington State, and have been shown to inhibit the microbial reduction of U(VI) under specific conditions (Bernhard et al., 2001; Brooks et al., 2003).

It is well established that microorganisms can impact processes that govern the fate and transport of contaminants in soils and sediments. According to several studies, *Arthrobacter* sp. are considered to be ubiquitous and predominant members of culturable soil microbial communities; they are found in large numbers in Hanford soil as well as other subsurface environments contaminated with heavy metals and radioactive materials (Balkwill et al., 1997; Boylen, 1973; Van Waasbergen et al., 2000; Crocker et al., 2000; Fredrickson et al., 2004). *Arthrobacter* sp. are aerobic, chemoorganotrophic, Gram-positive bacteria characterized by a rod-to-coccus morphology change as they enter the stationary phase. These microorganisms have an uncanny ability to survive and reproduce in the oligotrophic conditions in the presence of minimal concentrations of organic content (Crocker et al, 2000; Van Waasbergen et al, 2000). It is well established that microorganisms tend to interact with toxic metals and radionuclides in aqueous environments and several literature studies have given insight into the uranium tolerance of these microorganisms (Merroun et al., 2003; Lloyd et al, 2005). In this study, we attempt to demonstrate the effect of hydrogen bicarbonate (known as bicarbonate) on uranium- bacteria interactions by focusing on the bacterial strain *Arhtorbacte*r *oxydans* G968 (Katsenovich et al., 2012a). In a previous assessment, the *Arhtorbacte*r *oxydans* G975 strain was found to be the fastest growing and the most uranium-tolerant strain among the studied microorganisms obtained from the Subsurface Microbial Culture Collection (SMCC) (Katsenovich et al., 2012a). In

contrast with G975, the *Arthrobacter oxydans* G968 strain was found to have low resistance to the U (VI) toxicity. The alteration in surface morphology for G968 with a reduction in cell size and distorted surfaces was noted at 0.5 ppm of U (VI); in comparison, G975 shows signs of cell inhibition at the much higher concentration of 19 ppm of U (VI) (Katsenovich et al., 2012b). Inhibition of bacterial activity was associated with the binding of U(VI) to the cell envelope. The passive binding of uranyl to cell surfaces reduces the fluidity of the cell membrane, limiting nutrient uptake (Bencheikh-Latmani and Leckie, 2003). However, uranyl-carbonate complexes formed in the solution in the presence of bicarbonate do not strongly interact with the negatively charged bacterial surface, which in turn can mitigate U(VI) toxicity on the cells (Bencheikh-Latmani and Leckie, 2003; Katsenovich et.al., 2012b).

Uranium-bacteria interactions were rigorously studied to understand the microbial effects that influence the mobility of U(VI) in groundwater as well as bacterial viability in the presence of U(VI) (Suzuki and Banfield, 2004; Merroun et al, 2005); however, the mitigation effect of bicarbonate on the viability of cells exposed to U(VI) has not yet been evaluated. The main focus of this investigation was to qualitatively and quantitatively characterize changes on the bacteria surface at the nanoscale level after uranium exposure and evaluate the effect of aqueous bicarbonate on U (VI) toxicity of a low uranium tolerant *Arthrobacter* strain, G968, by analyzing changes in adhesion forces and cell dimensions via profile plots. In addition, supplementing AFM analysis, cell viability was assessed by the Live/Dead BacLight Bacterial Viability Kit (Molecular Probes) to quantitatively illustrate how the viability of bacterial cells are affected when exposed to uranium in the presence of varying concentrations of bicarbonate ions.

OBJECTIVES

The main aim for this investigation was to qualitatively and quantitatively characterize changes on the bacteria surface after uranium exposure and evaluate the effect of bicarbonate ions on U (VI) toxicity of a low uranium tolerant *Arthrobacter* strain, G968, by analyzing changes in adhesion forces and cell dimensions via profile plots. In addition, supplementing AFM analysis, cell viability was assessed by the Live/Dead BacLight Bacterial Viability Kit (Molecular Probes) to quantitatively illustrate how bacterial cells are affected when exposed to uranium in the presence of varying concentrations of bicarbonate ions.

MATERIALS AND METHODS

Atomic Force Microscopy (AFM) Analysis on Bacteria Uranium Interactions

Sample Preparation for AFM Imaging

The bacterial cells were grown in a 5% peptone, yeast, tryptone, and glucose (PYTG) liquid culture media, for two days, consisting of 0.25 g/L peptone, 0.25 g/L tryptone, 0.5 g/L yeast extract, 0.5 g/L glucose, 0.6 g/L $MgSO_4.7H_2O$, and 0.07 g/L $CaCl_2.2H_2O$. The media was prepared in deionized water (DIW) (Barnstead NANOpure Diamond Life Science (UV/UF), Thermo Scientific), autoclaved at 121^{o} C and 15 psi for 15 minutes, then allowed to cool before being used. Log 7 cells/mL of the bacterial stock solution was incorporated with uranyl nitrate and synthetic groundwater (SGW) media to create individual samples for analysis. The SGW solution contained 5.22 mg/L of KCl, and 520.58 mg/L of hydroxyethyl piperazineethanesulfonic acid (HEPES). Phosphorus containing organic media is conducive to produce precipitates and was not included to prevent a potential interference with imaging. The

SGW solution was prepared in deionized water, autoclaved at 121^{o} C, 15 psi for 15 minutes, and allowed to cool to about 30^{o} C. Then it was equally distributed between three 250 mL bottles and aseptically separately amended to contain 0 mM, 5 mM and 10 ppm $KHCO_3$. The samples that were analyzed included 5-mL aliquots as described in Table 8.

Table 8. Samples containing varying concentrations of uranium in bicarbonate bearing media for imaging analyses

Concentration of Uranyl Nitrate (ppm)	Concentration of Bicarbonate (mM)
0	0
5	0
5	5
10	0
10	5

The bacterial samples were centrifuged and pellets were washed three times with deionized water from U (VI) and media residuals, and were then immobilized onto the 3-aminopropyltrimethoxysilane coated silicon wafer substrates. A concentrated sample of about 10 µL was dropped onto a silanized silicon wafer. The bacterial cells must be firmly adhered onto a silicon wafer substrate so the sample is immobilized and stabilized during imaging. Samples were air dried until excess moisture was evaporated completely. The substrates were then fixed onto a metallic disc and transferred to an AFM stage for imaging.

Atomic Force Microscopy Instrumentation and Imaging

AFM was conducted employing a PicoScan AFM (former Molecular Imaging Inc. now Agilent Series 4500 SPM, PicoSPM) for all AFM imaging analysis. A low force constant (~ 0.2 N/m) Silicon AFM probe tip (NanoAndMore, USA) was utilized with a resonating frequency of 15 kHz. The mode of operation that was exercised was a contact mode. The detailed specifications of the cantilever are 500 µm in length, 30 µm in width, and 2.7 µm in thickness. The tip shape is rotated and the tip radius is <10 nm. The AFM tip is 20-25 degrees along the cantilever axis; 25-30 degrees from the side and 10 degrees at the apex. In addition, information on the surface topography of cells exposed to U (VI) was obtained while laboratory conditions were at 25ºC and 55% relative humidity. Along with topographical imaging, a quantitative analysis was conducted; cellular dimensions and force spectroscopy were evaluated. To avoid cell dehydration, the AFM analysis was performed within two hours of sample preparation.

Force Spectroscopy

Forces experienced by the cantilever as it approaches the sample from several microns above the surface can provide information about short-range interactions. As the tip approaches the surface, short-range forces, such as Van der Waals forces, can be determined. Once the tip has approached the sample surface, an additional force can be applied to determine viscoelastic properties such as Young's modulus or stiffness for different strain rates or maximum applied forces. Additionally, when the cantilever is retracted away from the surface, adhesion forces or the detach forces can be measured. Adhesion forces are sensitive to modifications in the surface, such as physiological changes on the cellular membrane when exposed to uranium and bicarbonate [da Silva et al, 2011]. The dynamic changes occurring on the bacterial cell

membrane before and after exposure to the various concentrations of uranium were evaluated using force spectroscopy analysis. Thus, a force spectroscopy analysis was conducted to gain a full understanding of interactions at the atomistic level. The forces are determined using force distance (FD) curves that are generated from the array of force curves over the selected region. The average adhesion force was obtained from an average of 256 different FD curves in a 5 μm x 5 μm sample surface. This experimental approach allows for monitoring of forces on the piconewton/nanonewton scale. These FD curves were processed using Scanning Probe Image Processor (SPIP) software by ImageMetrology, Denmark (version 6.2.0) to determine their average adhesion forces.

Roughness Measurements

The surface of the immobilized bacteria on the Si wafer was also investigated using atomic force microscopy operated in contact mode as mentioned above. The AFM instrument is also capable of measuring surface topography at the atomic scale. Roughness measurements were performed on various points over a selected area. The measured roughness depends on the spatial and vertical resolution of the instrument. The average roughness analysis was determined from the average of the absolute values of the profile heights from the mean level.

Cell Viability

Supplementing AFM analysis, cell viability was assessed by the Live/Dead BacLight Bacterial Viability Kit (Molecular Probes, L-7012) to quantitatively illustrate how bacterial cells are affected when exposed to uranium in the presence of varying concentrations of bicarbonate ions. The Live/Dead assay contains SYTO 9 green fluorescent nucleic acid stain and red fluorescent nucleic acid stain, propidium iodide. SYTO 9 generally stains all bacteria in a population, regardless if they are alive or dead; the addition of propidium iodide to the solution causes a reduction of the SYTO 9 stain fluorescence penetrating damaged membranes. Samples used for viability assessment were similar to samples used for AFM imaging: grown in synthetic groundwater media and amended with varying concentrations of bicarbonate ions. Two control samples were created, one by adding 4 mL of SGW media for the live control, and another with 4 mL of 70% isopropyl alcohol (for killed bacteria). The other samples were simply exposed to varying concentrations of uranium and bicarbonate bearing SGW. Samples were then incubated at room temperature overnight. In order to stain the samples, 3 μL of the dye mixture (containing equal parts of SYTO9 and propidium iodide) were added for each mL of the bacterial suspension. The samples were then incubated at room temperature in the dark for 15 minutes. Following which, the samples were washed 3 times with synthetic groundwater to remove the background fluorescence. Five (5) μL of the stained bacterial suspension was then placed on a microscope slide and covered with a coverslip. It was then allowed to dry for one hour in the dark before being visualized under a fluorescence microscope.

Fluorescence Imaging and Counting

Cells were visualized using a fluorescence microscope (Olympus IX81, Olympus America Inc., Miami, FL). The emission/excitation wavelength of SYTO9 and propidium iodide are 485/530 nm and 485/630 nm, respectively. A region of interest encompassing an area of 4.32 μm^2 was taken from images (ImageJ software, NIH, Bethesda, MD), and to calculate the ratio of live cells, the following formula was used (n=4 images) [9]:

$$Ratio\ of\ live\ cells = \frac{number\ of\ live\ cells}{Total\ number\ of\ live\ cells + number\ of\ dead\ cells} \times 100\%$$

Cell Viability Using Plates

To supplement Live/Dead fluorescent assay, a cell viability experiment was performed in parallel using plates. Live/Dead analysis may show that samples are viable; however, it is necessary to illustrate if samples are culturable as well. In preparation for cell density viability experimentation, a new sleeve of PTYG plates were made using 5% PTYG media and 15 g/L agar. Media was prepared in deionized water (DIW), autoclaved at 121^{o} C, 15 psi for 15 minutes, and allowed to cool to about 30^{o} C. The PTYG media was then poured into sterile plates and allowed to harden overnight. Samples used for this analysis were the same samples described in section sample preparation. To account for viable bacteria, thoroughly mixed samples were subsequently diluted and homogeneous aliquots (0.1 mL) of the suspension from each dilution were uniformly spread on the sterile petri dishes. Viable microorganisms were calculated from the number of colony forming units (CFU) found on a specific dilution.

Statistics

Statistical analysis of the results obtained from the cell viability experiments were examined with analysis of variance (ANOVA) statistics. All statistical tests were investigated using a predictive analytical software, Statistical Product and Service Solutions (SPSS) (IBM, Armonk, NY), with significant levels set at $\alpha = 0.05$.

RESULTS AND DISCUSSION

Cell Viability via Live/Dead Assay

The viability of the cells was observed for twenty-four hours after the bacterial cells were exposed to varying concentrations of uranium in bicarbonate-bearing media. It is important to note that Figure 16 and Figure 18 illustrate a clustering of cells resulting in larger green intensity regions which therefore create the possibility of underestimating the number of live cells in samples containing bicarbonate.

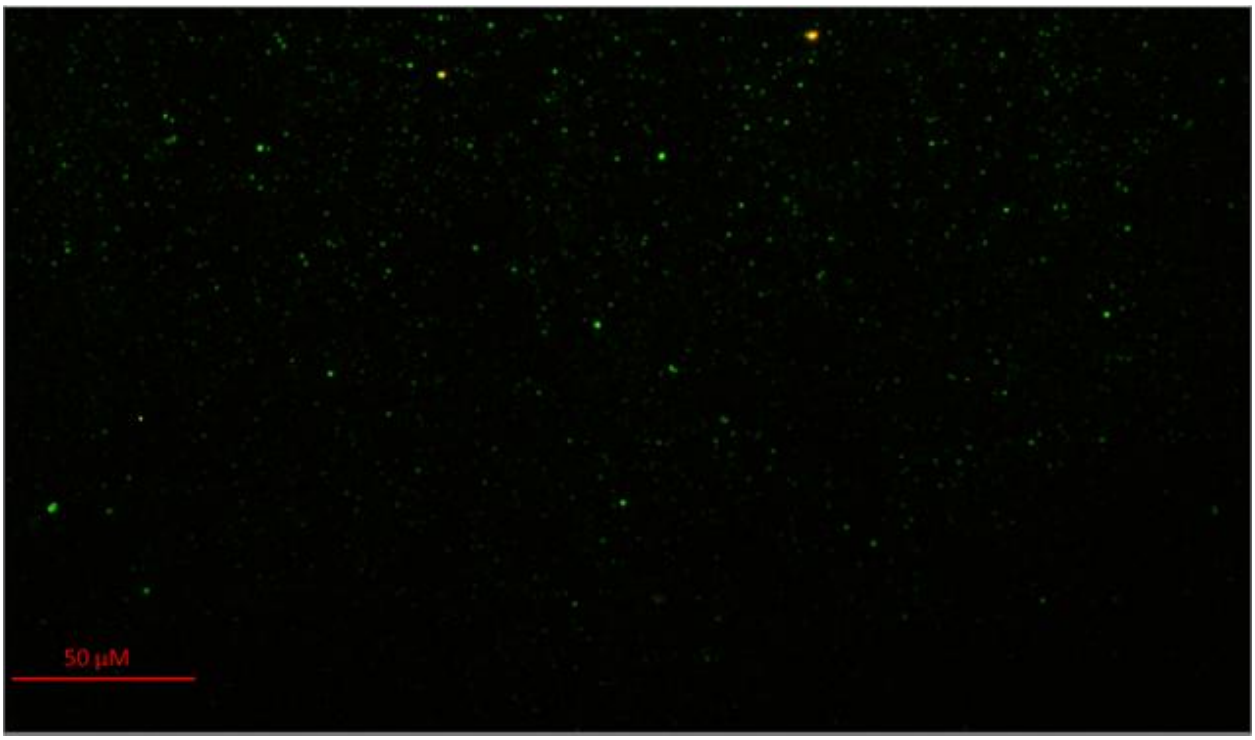

Figure 15. Live/Dead assay of sample containing 5 ppm of U (VI) with no bicarbonate. This sample illustrates a large concentration of live cells (green dots) with scattered dead cells (orange/yellow dots)

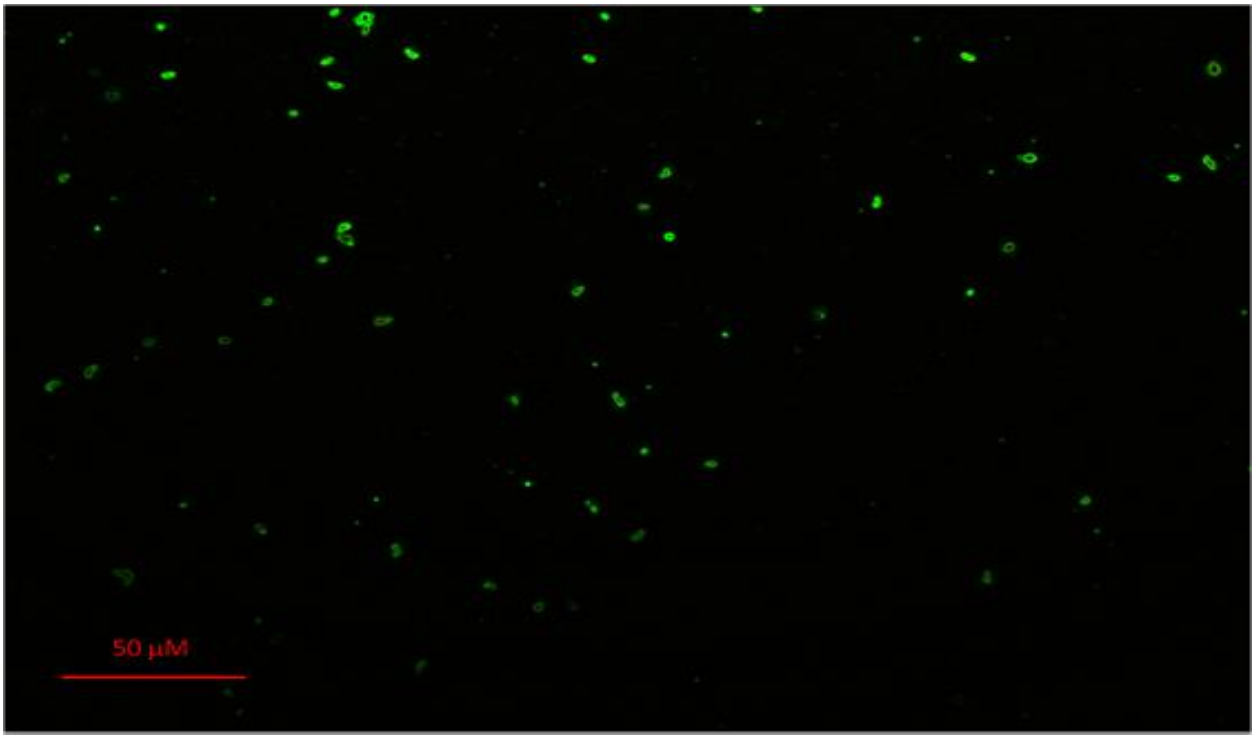

Figure 16. Live/Dead assay of sample containing 5 ppm of U (VI) with 5 mM bicarbonate. This sample illustrates a large concentration of live cells (green dots) with a smaller almost nonexistent concentration of dead cells (orange/yellow dots)

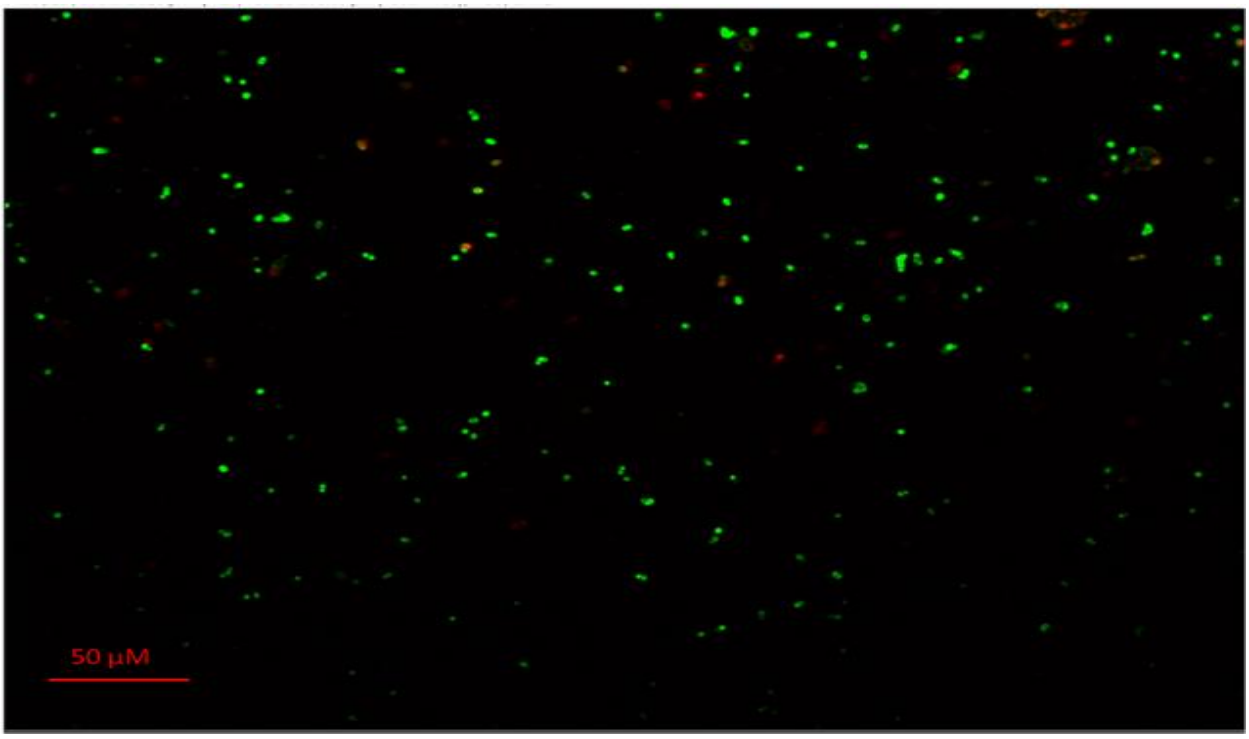

Figure 17 Live/Dead assay of sample containing 10 ppm of U (VI) with no bicarbonate. This sample illustrates a higher concentration of dead cells compared to Error! Reference source not found.

Figure 18 Live/Dead assay of sample containing 10 ppm of U (VI) with 5 mM bicarbonate. This sample illustrates a large concentration of live cells

During viability calculations, no significant difference was observed between the varying concentrations of uranium and bicarbonate. Each sample exhibited a ratio of live cells greater than 95% and when making a comparison between samples that contain 10 ppm of U(VI), the sample containing bicarbonate contained a higher ratio of live cells as noted in Table 9. Statistical analysis indicated a significant difference between the means of cell viability among the different levels of uranium and bicarbonate concentrations ($P < 0.05$).

Table 9. Quantitative Assessment of Percentage Cell Viability in Samples Subjected to Live/Dead Assay (n=4)

Sample Type	Ratio of Live cells (in percentages)
5 ppm U, 0 mM Bicarbonate	98.00 ± 1.02
5 ppm U, 5 mM Bicarbonate	97.51 ± 0.67
10 ppm U, 0 mM Bicarbonate	95.60± 1.22
10 ppm U, 5 mM Bicarbonate	100± 1

Cell Viability via Plates

Although all samples seem viable despite the concentrations of uranium and bicarbonate present, they may be unable to develop into culturable colonies in media. Bacteria enters a state known as the "viable but nonculturable (VBNC) state", first coined by Rita Colwell [Xu, et al, 1982]. Bacteria would enter this state as a feedback response from natural stresses such as starvation or being exposed to deadly substances [Oliver and Bockian, 1999]. These environmental stresses could be lethal if cells do not enter the VBNC state. Plating efficiency was calculated by comparing cell viability in the control media before and after U (VI) exposure, which is determined via counts of colony forming units (CFU). Samples containing 5 ppm U with 0 mM bicarbonate illustrated a G968 plating efficiency of 1.75%; with 5 mM bicarbonate, the efficiency increased to 42%. Similarly, samples containing 10 ppm U with 0 mM bicarbonate had a CFU plating efficiency of 3.25%; with 5 mM bicarbonate, the efficiency increased to 28%. These results illustrate that although the bacterial cells established intact cytoplasmic membranes, resulting in viable cells for the Live/Dead analysis, the cells that are exposed to uranium with no bicarbonate experience a VBNC state. Meaning, the samples containing 5 ppm of U (VI) and 0 mM of bicarbonate, and 10 ppm of U (VI) and 0 mM of bicarbonate keep the integrity of the membrane, showing high levels of viability in the Live/Dead fluorescent assay, but experience low levels of colony growth when plated.

Effect of Uranium on Microbial Surfaces Using Atomic Force Microscopy

AFM was employed to monitor changes at the nanoscale level in cell surface topography and adhesion forces after the cells exposure to various concentrations of uranium. The aim of this task was to present high-resolution AFM images and determine cell dimensions and adhesion forces to illustrate the effect of uranium and bicarbonate on the bacterial surface. The results demonstrated the ability of this method to qualitatively and quantitatively characterize changes on the bacterial surface after U exposure and evaluate the effect of bicarbonate ions on U (VI) toxicity of a less uranium tolerant *Arthrobacter* strain, G968, by analyzing changes in bacterial dimensions via profile plots.

Uranium Effect on the Microbial Cell Surface

Microscopic observation revealed a closer analysis on surface morphology in the presence of varying concentrations of uranium in bicarbonate-bearing or bicarbonate-free solutions. The role

of bicarbonate is qualitatively shown in the images below; the solutions were treated with varying concentrations of uranium, from 0 ppm to 10 ppm. Images revealed changes in bacteria shape and dimensions due to the exposure to uranium.

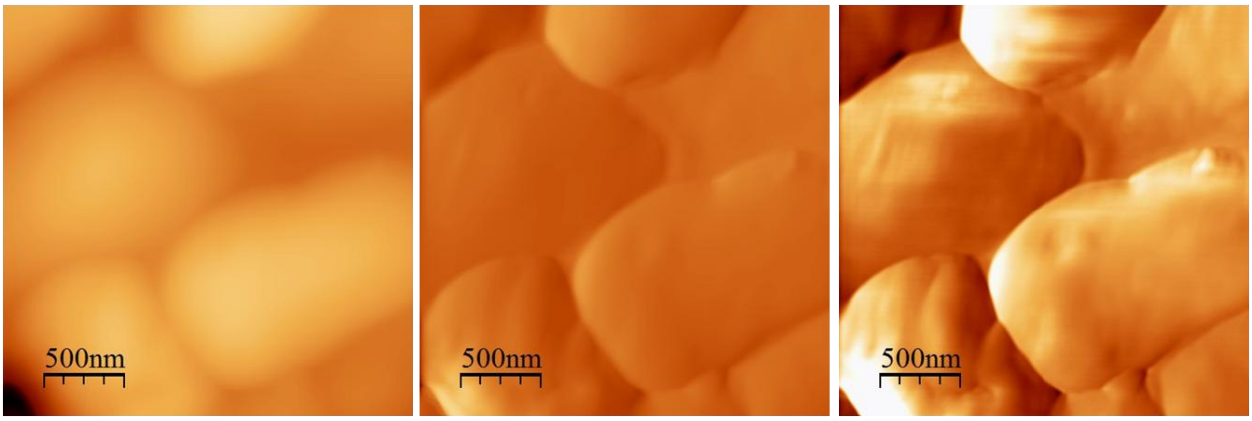

Figure 19. G968 control sample (scan size 2.5 x 2.5 µm^2) illustrating smooth bacterial surface. The topographic image on the left, deflection image in the middle and friction image on the right

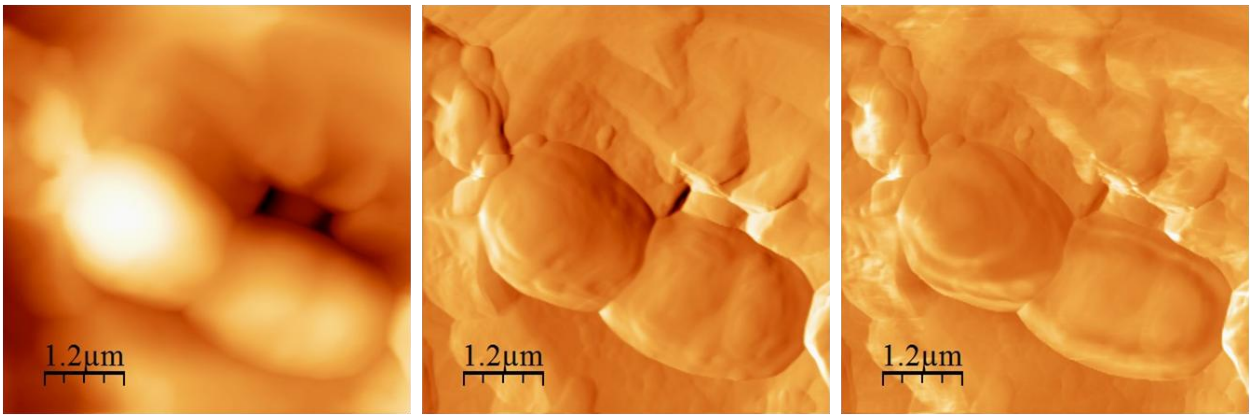

Figure 20. G968 cultured in media amended with 5 ppm U (VI) and 0 mM HCO3 (scan size 6 x 6 µm^2). The topographic image is on the left, deflection in the middle and friction image on the right.

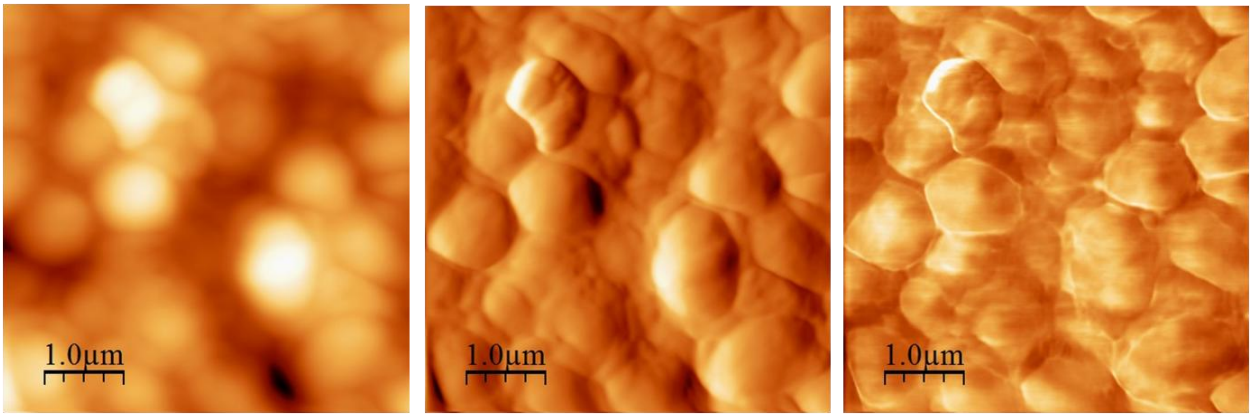

Figure 21. G968 cultured in media containing 5 ppm of U (VI) and 5 mM bicarbonate, (scan size 5 x 5 µm^2). The topographic image is on the left, deflection image in the middle and friction image on the right

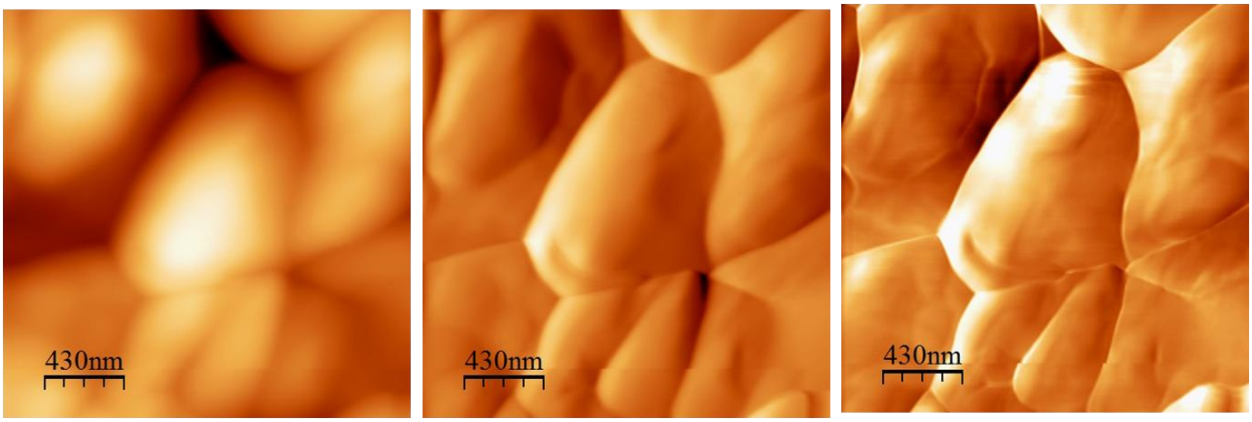

Figure 22. G968 cultured in media amended with 10 ppm U (VI) and 0 mM HCO_3 (scan size 2.1 x 2.1 µm^2). The topography image is on the left, deflection image in the middle and friction image on the right. These images exhibit cells that are slightly deformed indicative of harmful U exposure

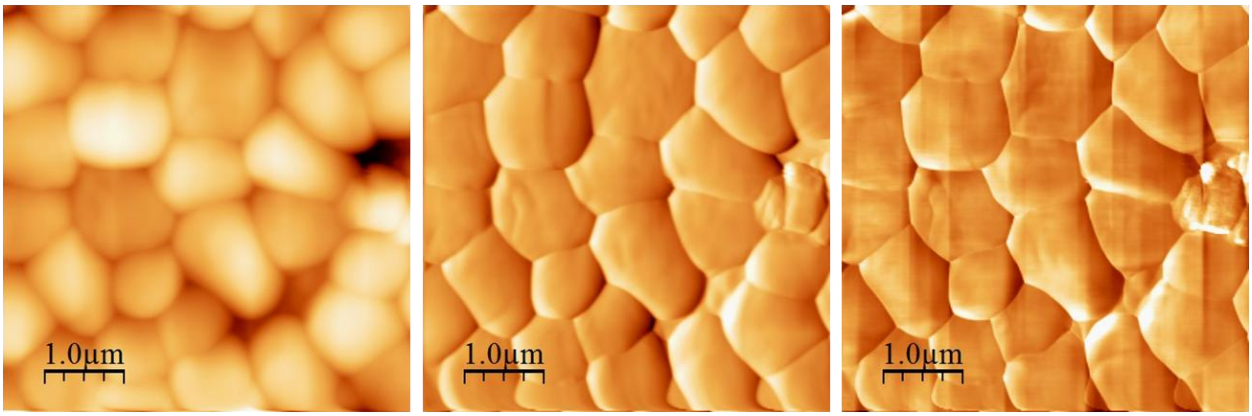

Figure 23. G968 cultured in media amended with 10 ppm U (VI) and 5 mM HCO_3 (scan size 5 x 5 µm2). The topography image is on the left, deflection image in the middle and friction image on the right. These images exhibit no negative effects from uranium exposure on bacterial surface

Force Spectroscopy Analysis

It has been proposed that adhesion forces are sensitive to modifications in the surface [da Silva et al, 2011]; for example, physiological changes occur on the cellular membrane when exposed to toxic environments. So, it was necessary to perform a force spectroscopy analysis to gain a full comprehension of the interaction forces between the tip and the sample surface at the piconewton scale level. The results in Table 10 indicate a significant statistical difference in adhesion force values between control samples and those containing varying concentrations of uranium and bicarbonate ($P < 0.05$).

There is an inverse relationship between the adhesion forces and the concentration of uranium; as the concentration of uranium increases, the adhesion forces will decrease exponentially. Additionally, when bicarbonate is present within the solution, the adhesion forces showed similar values to that of the control sample when no uranium is present. Previous MINTEQ modeling illustrated that the trimetric form of uranium, $(UO_2)_3(OH)^{5+}$, is the most positive species that has the most potential to interact or damage negatively charged cell walls. In the presence of bicarbonate, the solution mostly accumulates the negatively charged uranyl carbonate

$UO_2(CO_3)_3^{-4}$ species, which are not expected to adhere onto the negatively charged bacterial surface [Carvajal et al, 2012].

Table 10 Adhesion forces for *Arthrobacter* sp. G968 (n=3)

Uranium concentration (ppm)	Bicarbonate concentration (mM)	Adhesion (nN)
0	0	11.62 ±1.68
5	0	7.14 ±0.26
5	5	9.14 ± 1.2
10	0	5.54 ± 4.3
10	5	4.88 ± 2.3

Roughness Analysis

Changes in the cells surface roughness in the bacterial strain when exposed to varying concentrations of uranium was analyzed using AFM roughness analysis. Exposure to uranium was conducted 24 hours prior to imaging while the concentrations of uranium ranged from 0 ppm to 10 ppm. Past research has shown some correlation between growing roughness values as the concentration of uranium increased [Kazy et al, 2009]. However, for this particular case, values of roughness were in the range of 23.69 and 41.53 nm, and there was no correlation found with respect to roughness and uranium concentrations. Despite this, however, the data indicates that there is a significant statistical difference in roughness values between control samples and those containing varying concentrations of uranium and bicarbonate (P = 0.006).

Bacteria cells height maps via AFM

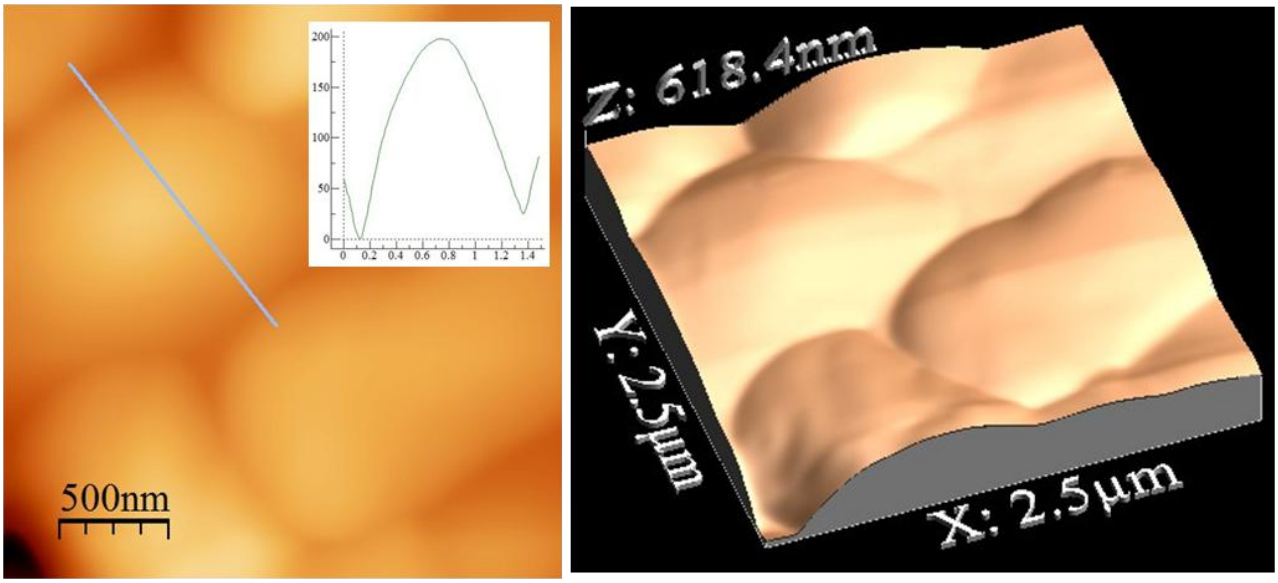

Figure 24. G968 control sample (scan size 2.5 x 2.5 µm2) illustrating a maximum height of 198 nm and length of 1.3 µm. The profile plot is on the left with the 3D topographic image on the right (Z range 618.4 nm)

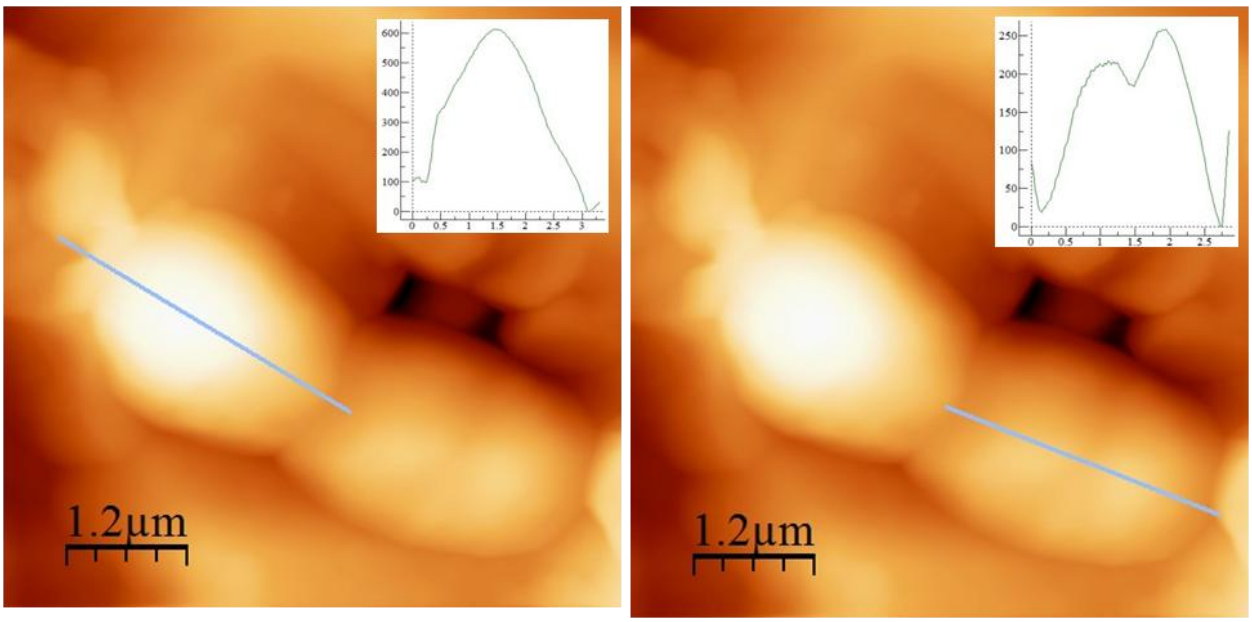

Figure 25. G968 samples amended with 5 ppm U (VI) and no bicarbonate. Profile plot on the left illustrates the height of one cell at 600 nm, while the profile height of the image on the right measure 250 nm

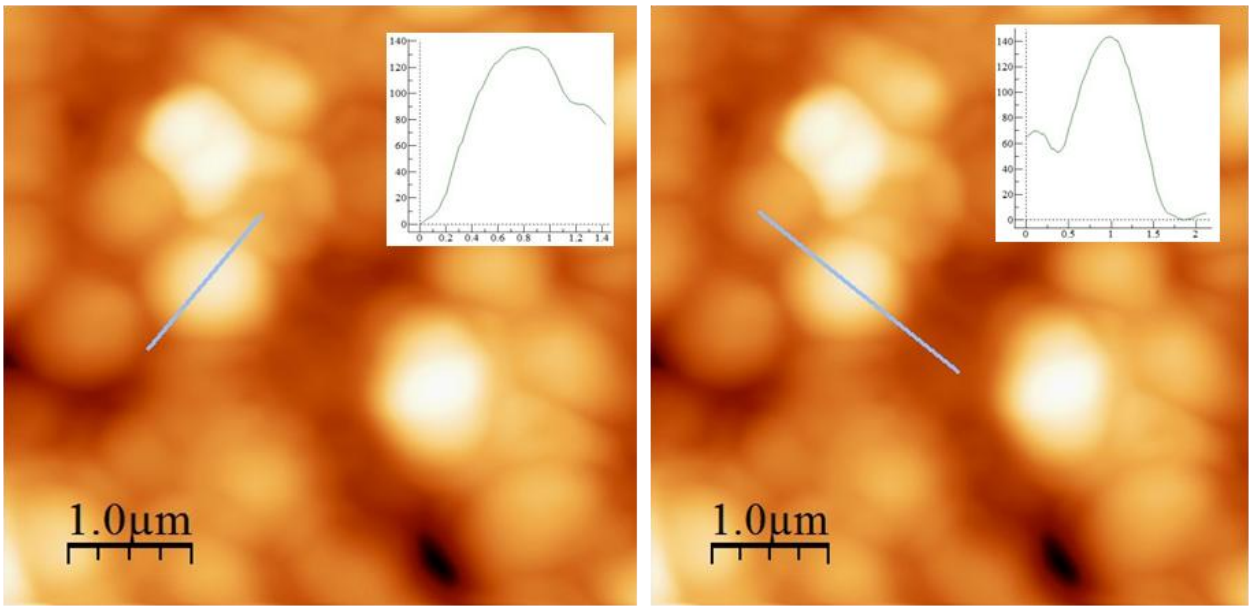

Figure 26. G968 sample amended with 5 ppm U (VI) and 5 mM bicarbonate. The profile heights for this sample ranges from 135 to 140 nm. The effect of uranium could have caused these bacterial cells to shrink revealing rod-to-coccus shape change.

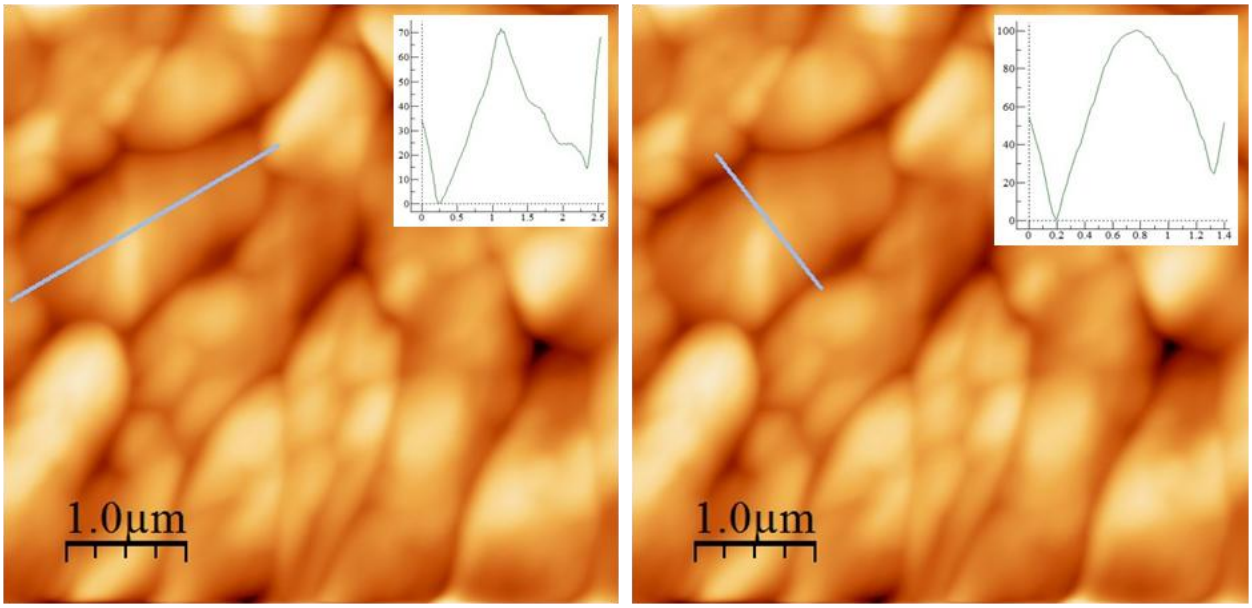

Figure 27. G968 sample amended with 10 ppm U (VI) and 0 mM bicarbonate. The profile heights for this sample ranges from 70-90 nm. Images also show cells deformation

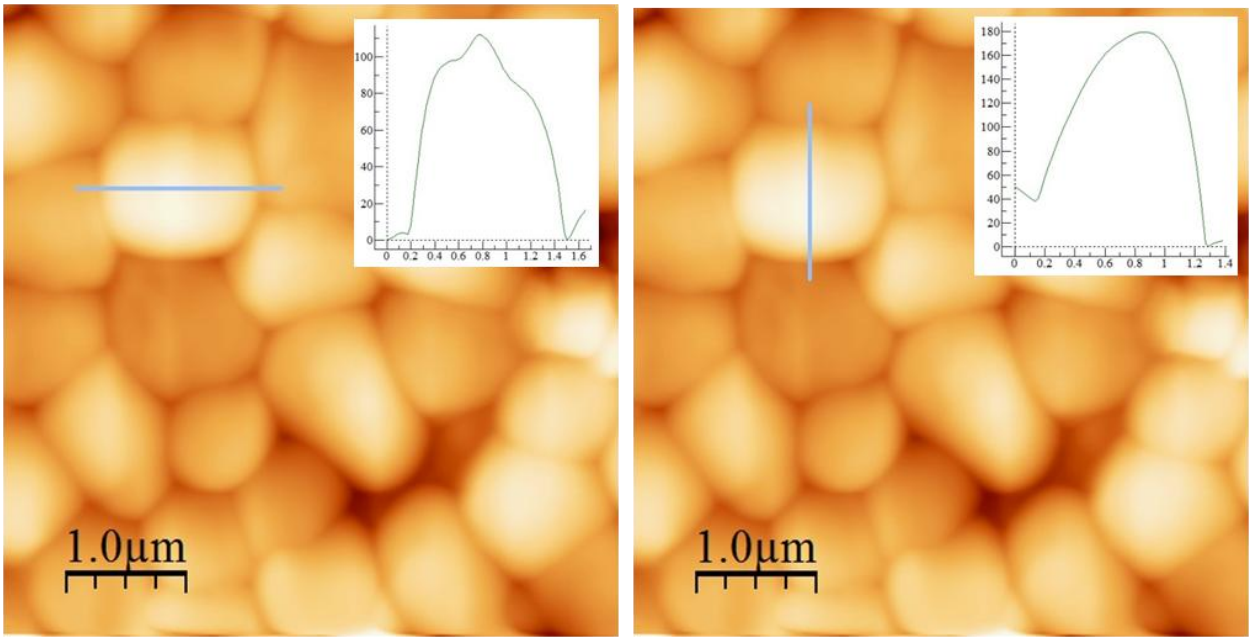

Figure 28. G968 sample amended with 10 ppm of U (VI) and 5 mM of bicarbonate. The profile heights for the above sample range from 110-180 nm, showing lower values than U-free controls but higher values than the profile heights in bicarbonate-free media (Figure 17).

The height of a bacterial cell is a good indication of cell response to U toxicity; U-free control samples exhibit a large profile height. When comparing the cells in samples containing 10 ppm of uranium with and without bicarbonate, the samples containing bicarbonate (Figure 28) have an increased profile height, revealing a smooth surface. When comparing the plating method and Live/Dead analysis with AFM assessment, we find that bacteria samples taken from bicarbonate-free solutions are mostly not viable; their height may be similar to the uranium-free control sample (Figure 24, Figure 25, and Figure 27) but they are not alive. In opposition, samples containing bicarbonate have a reduced height and a smaller cocci-shape cellular size with no

deformed surfaces and look identical to U-free control samples. It might be an indication that the cells are alive and have acclimated to withstand uranium toxicity. *Arthrobacter* species are known for their ability to change size and shape in response to toxicity, from a rod to spherical cocci; in this cocci shape, the bacteria is more resistant to desiccation and starvation [O' Loughlin et al, 1999].

CONCLUSIONS

AFM analysis and Live/Dead fluorescent assay was used to qualitatively and quantitatively illustrate changes in bacterial cells when exposed to uranium in the presence of bicarbonate bearing media. The Live/Dead analysis showed that despite the concentration of uranium and bicarbonate present in the solution, each sample exhibited a ratio of live cells greater than 95%. Although the samples seemed viable, they also showed that they are not culturable. By performing a cell viability assessment via culture plates, results demonstrated that although the bacterial cells maintained the integrity of intact cytoplasmic membranes, resulting in viable cells for the Live/Dead analysis, the cells that are exposed to uranium with no bicarbonate experienced a viable but nonculturable state, that is, exhibited low levels of colonies when plated. Force spectroscopy results demonstrated that as uranium concentration is added to the media, the adhesion force parameter decreases. Furthermore, the height provided from the profile plots revealed that samples containing bicarbonate have a higher profile height, resulting in a smooth surface. Thus, samples exposed to uranium with no bicarbonate are mostly viable via Live/ Dead assay, but exhibited deformed surfaces and a low height profile, which might be an indication that the cells are not alive. In contrast, samples containing bicarbonate have a higher cell profile height and exhibited smaller cellular size after a rod to cocci-shape transition with surface morphology replicating the control samples. This data illustrated how the cells have acclimated to withstand uranium toxicity.

FUTURE WORK

Future work will include finalizing uranium analysis of the samples collected while preparing for AFM imaging to quantify how much uranium adsorb on the cells surface and preparing two manuscripts to submit for potential publication in peer-review journals.

ACKNOWLEDGEMENTS

Funding for this research was provided by U.S. DOE grant number DE-EM0000598. We truly appreciate FIU graduate students Vishal Musaramthota and Rupak Dua for their help with AFM and fluorescence microscope analysis. Fluorescence imaging was conducted at the FIU Biomedical Department. AFM imaging was conducted at the FIU/ARC.

REFERENCES

Balkwill, DL, Reeves RH, Drake GR, Reeves JY, Crocker FH, King MB, Boone DR. Phylogenetic characterization of bacteria in the subsurface microbial culture collection. *FEMS microbiology reviews* 1997; 20: 201-216.

Bernhard G, Geipel G, Reich T, Brendler V, Amayri S, & Nitsche H (2001) Uranyl (VI) carbonate complex formation: validation of the Ca2UO2(CO3)3(aq.) species. *Radiochim. Act,* **89**, 511-518.

Bencheikh-Latmani, R and Leckie, JO., 2003. Association of uranyl with the cell wall of Pseudomonas fluorescens inhibits metabolism. Geochimica et Cosmochimica Acta, Vol. 67, No. 21, pp. 4057–4066.

Brooks SC, Fredrickson JKSLC, Kennedy DW, Zachara JM, Flymale AE, Kelly SD, Kemner KM, Fendorf S. 2003. Inhibition of bacterial U(VI) reduction by calcium. Environ Sci Technol 37:1850–1858.

Boylen, CW. Survival of Arthrobacter crystallopoietes during prolonged periods of extreme desiccation. *Journal of Bacteriology* 1973; 113:33-37.

Carvajal, D, Y Katsenovich, and L Lagos. The effects of aqueous bicarbonate and calcium ions on uranium biosorption by Arthrobacter G975 strain. *Chemical Geology* 2012; 330-331: 51-59.

Crocker, FH, Fredrickson, JK, White DC, Ringelberg, DB and DL Balkwill. Phlogenetic and physiological diversity of Arthrobacter strains isolated from unconsolidated subsurface sediments. *Microbiology* 2000; 146: 1295-1310.

da Silva, L, Ochsner, A and R Adams. *Handbook of adhesion technology.* Springer- Verlag Berlin Heidelberg; 2011

Fredrickson JK, Zachara JM, Balkwill D L, Kennedy D, Li SW, Kostandarithes HM, Daly MJ, Romine MF and Brockman FJ, (2004). Geomicrobiology of high-level nuclear waste-contaminated vadose sediments at the Hanford Site, Washington State. *Appl. Environ. Microbiol*. **70**, 4230.

Kalmykov SN and Choppin GR (2000) Mixed $Ca^{2+}/UO_2^{2+}/CO_3^{2-}$ complex formation at different ionic strengths, *Radiochim. Acta*, **88**, 603.

Katsenovich, YP, Carvajal, DA, Guduru, R and LE Lagos. Assessment of the Resistance of Hanford Site Arthrobacter Isolates to Uranium (VI) Exposure. *Geomicrobiology Journal* 2012a; 30-2: 120-130.

Katsenovich, YP, Carvajal, DA., Wellman, DM and LE Lagos. Enhanced U (VI) release from autunite mineral by aerobic Arthrobacter sp. in the presence of aqueous bicarbonate. *Chemical Geology* 2012b; 308-309: 1-9.

Kazy, S, D'Souza, S.F and P Sar. Uranium and thorium sequestration by a Pseudomonas sp.: Mechanism and chemical characterization. *Journal of Hazardous Materials* 2009; 163: 65-72.

Langmuir, D. Uranium solution- mineral equilibria at low temperatures with application to sedimentary ore deposits. *Geochimica et Cosmochimica Acta* 1978; 42: 547-569.

O' Loughlin, EJ, Sims, GK and SJ Traina. Biodegradation of 2-methyl, 2-ethyl and 2-hydroxypyridine by an Arthrobacter sp. isolated from subsurface sediment. *Biodegradation* 1999; 10: 93-104.

Lloyd RJ, Renshaw CJ. Bioremediation of radioactive waste: radionuclide–microbe interactions in laboratory and field-scale studies, 2005. *Cur. Opi. Biotech.*, 16, p.254–260

Merroun, M. L., G. Geipel, R. Nicolai, K. Heise, and S. Selenska-Pobell. 2003. Complexation of uranium(VI) by three eco-types of *Acidithiobacillus ferrooxidans* studied using time-resolved laser-induced fluorescence spectroscopy and infrared spectroscopy. Biometals 16:331–339.

Merroun ML, Raff J, Rossberg A, Hennig C, Reich T, Selenska-Pobell S. 2005. Complexation of Uranium uranium by Cells cells and S-Layer layer Sheets sheets of Bacillus sphaericus JG-A12. Appl. Environ. Microbiol. 71(9): 5532–5543.

Oliver, JD, and R Bockian. The viable but nonculturable state and cellular resuscitation. *Microbial Biosystems: New Frontiers*, Proceedings of the 8th International Symposium on Microbial Ecology Bell CR, Brylinsky M, Johnson-Green P (eds) Atlantic Canada Society for Microbial Ecology, Halifax, Canada, 1999;723-730.

Van Waasbergen, LG, Balkwill, DL, Crocker, FH, Bjornstad, BN and RV Miller. Genetic diversity among Arthrobacter species collected across a heterogeneous series of terrestrial deep-subsurface sediments as determined on the basis of 16S rRNA and recA gene sequences. *Applied and environmental microbiology* 2000; 66: 3454-3463.

Xu, H.S., Roberts, N, Singleton, F.L., Attwell, R.W and D.J. Grimes. Survival and viability of nonculturable Escherichia coli and Vibrio cholerae in the estuarine and marine environment. *Microb. Ecol.* 1982; 8: 313-323.

Suzuki, Y and J.F. Banfield, 2004. Resistance to, and accumulation of, uranium by bacteria from a uranium- contaminated site. Geomicrobiology Journal, 21,2, pp. 113-121.

TASK 2.1: FIU'S SUPPORT FOR GROUNDWATER REMEDIATION AT SRS F/H AREA

INTRODUCTION

The Savannah River Site (SRS) was one of the major producers of plutonium for the U.S. nuclear program during the Cold War. Since then, it has become a hazardous waste management facility responsible for nuclear storage and remediation of contaminated soil and groundwater from radionuclides. From its days of production, between 1955 and 1988, the F/H Area Seepage Basins located in the center of SRS received approximately 1.8 billion gallons of acidic waste solutions containing radionuclides and dissolved metals. This has created a contaminated groundwater plume with an acidic pH between 3- 5.5, polluted with a variety of radionuclides and chemicals from the F-Area separation facilities. The acidic nature of the basin waste solutions contributed to the mobility of several constituents of concern (COCs) associated with the F-Area groundwater plume. These COCs consist of tritium, uranium-238, iodine-129, and strontium-90. The COCs in the H-Area are tritium, strontium-90 and mercury. The primary focus of this investigation is uranium (VI) or U(VI), which is a key contaminant of concern in the basin's groundwater.

To remove contaminates from polluted groundwater, a pump-and-treat and re-inject systems were implemented. Downgrade groundwater within the system would be pumped up to a water treatment facility and then re-injected upgrade within the aquifer. The pump-and-treat water treatment unit designed and built in 1997 to remove metals and radionuclides eventually became less effective, prompting research for new remedial alternatives. The pump-and-treat system was discontinued and in 2004 a funnel-and-gate process was implemented to carry out injections of sodium hydroxide solution directly into the gates of the F-Area groundwater to raise pH levels. The purpose was to create a treatment zone in which the acidic nature of the contaminated sediments could be reversed, thereby producing a more negative net charge on the surface of sediment particles and enhancing adsorption of cationic contaminants. Monitoring data indicated that injection of the base helped to decrease concentrations of Sr and U; however, the concentration of iodine was unaffected by this treatment. A solution with high carbonate alkalinity was initially used to overcome the surface acidic conditions and natural partitions of the groundwater system. This system of remediation would require a systematic re-injection of a base to maintain the neutral pH of the treatment zone. However, the continuous use of high concentrations of a carbonate solution to raise pH creates a concern of re-mobilization of uranium previously adsorbed within the treatment zone. In the presence of bicarbonate ions, U(VI) easily forms highly soluble aqueous uranyl-carbonate complexes.

To avoid uranium remobilization issues at the F/H areas of the SRS site, FIU-ARC was conducting an investigation to replace the carbonate base with a sodium silicate and evaluate whether these solutions have sufficient alkalinity to correct the acidic nature of the aquifer sediments. To get an answer for this question requires determining if a silica solution with an inherent pH$\leq$10 has sufficient alkalinity to restore the pH of the treatment zone, and whether silica solutions can be injected into the subsurface without clogging the aquifer permeability. The necessity of the silicate solution to have a pH $\leq$10 was derived from the regulatory constraints of injecting solutions of high pH values into subsurface systems. In addition to this, the research

was extended to investigate if U(VI) is bound to colloidal silica and if any synergy exists between humic acid (HA) and colloidal Si that would influence the removal of uranium.

Humic substances (HS) are a major component of soil organic matter and are known for their abilities to influence the migration behavior and fate of heavy metals. HS are ubiquitous polyfunctional organic macromolecules formed by the chemico-microbiological decomposition of biomass. HS have abilities to interact with both metal ions and organic substances and, based on their solubility, they are usually divided into three fractions (Choppin, et al., 1992). Humin represents a fraction which is insoluble at all pH values. HA represents a fraction of the humic substances, which is soluble at pH values greater than 3.5, and the fulvic acid fraction is soluble at all pH values.

Studies showed that HA function as an important ion exchange and metal-complexing ligand carrying a large number of functional groups with high complexing capacity that can greatly affect the mobility behavior of actinides in natural systems (Davis, 1982; Choppin, 1998; Plancque et al., 2001). Previous studies suggested that the retention of U(VI) via sorption in the presence of HA is a complex process due to HA abilities to form organic coatings by sorbing on the surface of oxides and minerals, hence modifying the sorption behavior of metal ions (Davis, 1984; Zachara et al., 1994; Labonne-Wall et al., 1997; Perminova et al, 2002). It is generally considered that the sorption of metal ions on the mineral surfaces in the presence of HA is enhanced at low pH and reduced at high pH (Ivanov et al., 2012). It has also been demonstrated that the sorption is strongly dependent on the concentration of HA/FA (Chen and Wang, 2007). HSs are known have a strong influence on the sorption and speciation of lanthanides and actinides in natural aqueous systems (Tan et al., 2008). The U(VI) sorption onto kaolinite is influenced by the pH, U(VI) concentration, presence of inorganic carbon species and naturally occurring HA. It has also been shown that U(VI) prefers to be adsorbed onto kaolinite as a uranyl-humate complex (Krepelova et al., 2007).

This task investigates if there are any synergistic interactions between U(VI) ions, humic acid and colloidal silica under oxidized conditions and studies the influence of HA and Si on the sorption of U(VI) onto sediments collected from the F/H Area. The experiments also evaluate the effects of different environmental variables such as pH, presence of U(VI) and varying concentrations of HA and Si on the removal behavior of U(VI) in the multi-component batch systems.

Thus far, we have created an experimental matrix involving colloidal silica, humic acid, and collected natural sediments from the F/H Area, determined the desired concentrations and ratios of our constituents and simulated the uranium adsorption process in the pH range from 3 to 8.

METHODOLOGY

The experiments were designed to study the removal behavior of U(VI) in the multi-component batch systems in the pH range between 3 and 8; so, the effect of pH on the adsorption mechanism could be evaluated. Several background sediment samples were collected at SRS from the well FSB 91C and brought back to FIU-ARC by the DOE Fellow Valentina Padilla after the completion of her summer 2013 internship at SRS. Six samples were retrieved at the following depths: 65, 80, 90, 95, 100 and 105 feet, respectively (Figure 29). A 10-g soil sample from each zip-loc bag was accurately weighed to prepare a 60-gram soil mixture. After mixing

the soil thoroughly, it was used for the preparation of soil-bearing batches at the soil to water ratio of 1:20.

Figure 29. Core samples shipped to FIU

Batches 1-3 were prepared without sediments. Batch 1 included 3.5 mM of silica and U(VI) to analyze the adsorption capabilities of colloidal Si. Batch 2 was combined with Si, 10 ppm HA and U(VI) to explore the synergy effect between silica and humic acid on the removal of U(VI). Batch 3 explored the capabilities of HA at a concentration of 10 ppm on the U(VI) removal. Batches 4-7 were prepared with sediments. In Batch 4, we analyzed the soil adsorption properties to remove U(VI) in the presence of colloidal Si. Batch 5 reproduced the results of all constituents such as Si, HA, and sediments to observe if there is any synergy between HA and Si to enhance the U(VI) sorption in the presence of sediments. The results of these sediment samples were compared to batch 6, which was looking at sediment sorption in the presence of 10 ppm HA, and no Si, and batch 7, containing sediments alone. The experimental matrix was set up as follows:

- Batch 1: Si (3.5 mM) +U (VI) (0.5ppm) (no sediments and HA).
- Batch 2: Si (3.5 mM) +U (VI) (0.5ppm) + HA (10 ppm), (no sediments)
- Batch 3: U (VI) (0.5 ppm) + HA (10ppm) (no Si and sediments).
- Batch 4: Sediments+ Si (3.5 mM) +U (VI) (0.5 ppm) (no HA)
- Batch 5: Sediments+ Si (3.5 mM) +U (VI) (0.5 ppm) + HA
- Batch 6: Sediments +U (VI) (0.5 ppm) + HA, (no Si)
- Batch 7: Sediments+ U (VI) (0.5 ppm), (no Si and HA)

All samples were prepared in 50-mL conical tubes in triplicate. All control and experimental tubes were vortexed and then kept on the shaker at 100 rpm and room temperature.

Fumed colloidal silica, silicon (IV) oxide 99%, and humic acid sodium salt (50-60% as humic acid) were obtained from Fisher Scientific. Stocks of HA and Si were prepared in deionized water (DIW) at 1000 ppm and 2000 ppm, respectively. A commercial 1000 ppm uranyl nitrate stock solution in 2% nitric acid (Fisher Scientific) was used as a source of U(VI). The resulting sample mixtures were spiked with uranium to yield a concentration within a solution matrix of 0.5 ppm. The pH of the mixture was then adjusted to the required value using 0.01 M of HCl or 0.1 M NaOH. Control samples were prepared in DIW amended with U(VI) at a concentration of 0.5 ppm U(VI) to test for U(VI) losses from the solutions due to sorption to the tube walls and

caps. All volumes of solutions were tracked to have initially 40 mL of the total volume in the sample tube; then the sample volume was reduce to 20 mL in an effort to minimize the amount of liquid radioactive waste (Table 11).

Table 11. Constituencies used for the sample preparation according to the experimental matrix

Batch #	Constituents					
	SiO_2 mL	Humic Acid (HA) mL	Mass of Sediments Mg	Uranium U(VI) mL	DIW Volume mL	Total Volume mL
1	2.24	-	-	0.01	17.75	20
2	2.24	2.00	-	0.01	15.75	20
3	-	2.00	-	0.01	17.99	20
4	2.24	-	400	0.01	17.75	20
5	2.24	2.00	400	0.01	15.75	20
6	-	2.00	400	0.01	17.99	20
7	-	-	400	0.01	19.99	20

Figure 30 presents the experimental set up kept under the fume hood where sample preparation using silica, humic acid, DI water, and adjustments of pH after the U(VI) injections were conducted.

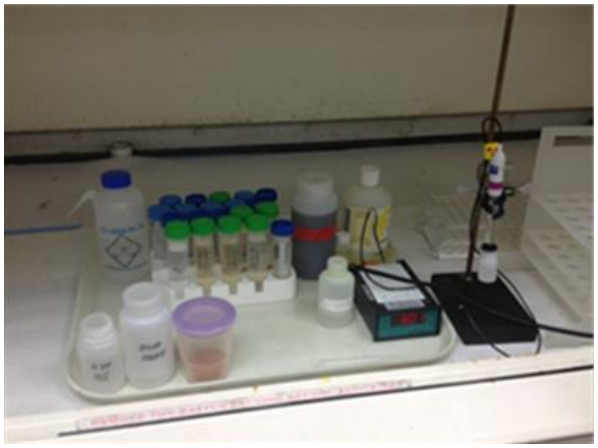

Figure 30. Experimental set up

Samples were shaken for 24 h at 100 rpm and then centrifuged at 2700 rpm at a temperature of 22 degrees Celsius for 30 min (Figure 31). In addition, samples of Batch 1containing colloidal silica with no sediment were filtered using a 0.45µm syringe filter. For analysis with the KPA for U(VI) and ICP-OES for Si and Fe analysis, an aliquot was extracted from the supernatant of each test tube and diluted with 1% nitric acid between 5 to 10 times. In total, each set consisted of 25 samples including controls for testing of uranium and silica concentrations.

Figure 31. Conical tubes on the shaker at 100 RPM and centrifuge to separate supernatant

RESULTS AND DISCUSSION

pH3

Triplicates of pH 3 samples were prepared using 1% HNO_3 with 1:10 dilution ratio and were analyzed for U(VI) via KPA instrument. Uranium removal was calculated from the KPA results and data are presented in Table 12. As data suggested, the percent removal of U(VI) at pH 3 was very small ranging between 8.04-23.6% for all batches. At this pH, the uranyl cations are the major existing U(VI)- bearing species in the solution. Filtered and unfiltered samples showed similar results for uranium sorption; so, at pH 3, sorption of U(VI) on Si colloids was found to be negligible. The presence of HA and sediments increased U(VI) sorption from the solution and, in samples amended with HA, the average U(VI) sorption efficiency increased from 8.04 to 23.6%. Literature data suggests the lack of any detectable U-Si interactions at low pH, which supports the conclusion that adsorption of the uranyl ion onto Si at low pH occurs predominantly through an outer-sphere mechanism (Sylwester et al., 2000).

Table 12. Analytical results for the set of pH 3

Sample-Description, pH 3	U(VI) Avg Removal, %	Std.	Si Avg Removal, %	Std Deviation	Fe, ppm
Batch 1	8.45	1.79	91.28	0.69	No soil
Batch 2	16.63	2.05	87.68	0.45	No soil
Batch 3	15.62	1.90	No Si	NA	No soil
Batch 4	12.73	2.17	92.71	0.73	0.007-0.18
Batch 5	22.43	0.24	89.26	0.69	0.23-0.32
Batch 6	23.58	0.14	No Si	NA	0.21-0.43
Batch 7	19.85	5.76	No Si	NA	0.09-0.28
Batch 1 Filtered	8.04	0.94	98.34	0.03	0

pH4

At pH 4, the removal of U in non-sediment samples was higher than found at pH 3, but still relatively low in comparison with most of the other batches at higher pH. Samples with HA produced only 13.29% of U removal; compared to its counterpart of filtered Batch 1 composed of Si alone with U removal of 45.37%. The mixture of Si and HA produced 22.33% of U

removal. The presence of sediments in the samples seemed to enhance the adsorption of U(VI), showing an average U removal for the Batch 6 of 82.28± 0.61%, the highest for the pH4 set. It was also noticed that Batch 5, composed of sediments and HA, did indeed enhance the U(VI) adsorption compared to no-Si and HA Batch 7 from 45.83% to 78.10% (Table 13).

Table 13. Analytical results for the set of pH 4

Sample-Description, pH 4	U(VI) Avg. Removal, %	Std. Deviation	Si Avg. Removal, %	Std. Deviation	Fe, ppm
Batch 1	45.37	18.50	94.84	3.08	No Soil
Batch 2	22.33	1.65	84.97	2.06	No Soil
Batch 3	13.29	1.40	No Si	NA	No Soil
Batch 4	53.42	1.47	95.45	1.61	0.1-0.2
Batch 5	82.28	0.61	86.10	7.24	0.2-1.3
Batch 6	78.10	1.34	No Si	NA	0.2-0.6
Batch 7	45.83	3.02	No Si	NA	0.1-0.3

pH5

Non-sediment samples of Batch 1 far exceeded the counterpart's Batches 2 and 3, and in comparison with pH 3 and 4, the trend with colloidal silica alone seems to be greater than those combined with Si and HA. The sediment samples of Batch 4 and Batch 7 had the highest U(VI) removal at 88.66±0.39% and 88.81±3.34%, respectively, compared to other sediment-bearing batches (Table 14).

It was noted that the percentage of sorbed U(VI) was greatly increased in filtered samples of Batch 1, from 81.88±1.98% to 92.80±0.76%. The addition of HA slightly reduced U(VI) adsorption in sediment-bearing and non-sediment samples. Thus far, the trend of U(VI) removal in non-sediment samples seems to indicate that silica has a stronger effect on U(VI) removal compared to HA. Results obtained for Batch 6, which was third in ranking on U(VI) sorption efficiency, suggested that the presence of HA at a pH 4-5 slightly hinders sediment sorption. It is interesting to note that higher Si removal always correlated with higher U(VI) removal (Table 14). Sorption efficiency was increased drastically from pH 4 to 5. According to the literature, adsorption of the uranyl onto the silica surface at near-neutral pH appears to occur via an inner-sphere, bidentate complexation with the surface (Sylwester et al., 2000).

Table 14. Analytical results for the set of pH 5

Sample-Description, pH 5	U(VI) Avg. Removal, %	Std. Deviation	Si Avg. Removal, %	Std. Deviation	Fe, ppm
Batch 1/ Filtered	81.88/ 92.80	1.98/0.76	94.43	0.87	No soil
Batch 2	18.40	2.30	64.90	12.41	No soil
Batch 3	9.29	5.43	No Si	NA	No soil
Batch 4	88.66	0.39	80.39	2.14	0.01-0.02
Batch 5	83.21	1.44	84.33	5.26	0.09-0.11
Batch 6	86.05	2.47	No Si	NA	0.19-0.24
Batch 7	88.81	3.34	No Si	NA	0.1

pH6

Non-sediment samples of Batch 1, composed of Si and U(VI), showed a higher uranium removal of 82.19± 3.44% compared to HA-bearing samples of Batches 2 and 3, which exhibited U(VI) removal at 59.84±4.37% and 55.72±11.79%, respectively. Data for the filtered samples of Batch 1 are indicative of increasingly higher U(VI) removal capabilities, possibly due to U(VI) adsorption on Si colloids trapped on the filter (Table 15).

Even though the results of Batch 4 showed a U(VI) removal of 92.62±4.3%, it looks like silica slightly reduced the effect of U(VI) sorption on sediments as compared to its sample counterparts in Batches 7 and 6. Sediment-bearing Batches 4 and 5 were less effective, showing 92.62±4.3% and 92.1±2.28%, respectively, for U(VI) removal. Overall, values for U(VI) removal at pH 6 exceeded the relative efficiency found at pH 4 and 5. The synergistic effect of humic acid and silica is greater in the presence of sediment than without sediment; however, HA was found to reduce sediment sorption when Batches 5 and 7 are compared.

Table 15. Analytical results for the set of pH 6

Sample-Description, pH 6	U(VI) Avg. Removal, %	Std. Deviation	Si Avg. Removal, %	Std. Deviation	Fe, ppm
Batch 1/ Filtered	82.19/98.8	3.44/0.05	78.63/96.43	3.36/0.48	No soil
Batch 2	62.29	1.56	83.22	2.43	No soil
Batch 3	60.99	10.56	No Si	NA	No soil
Batch 4	92.62	4.3	96.66	2.55	0.013
Batch 5	92.10	2.28	92.68	5.80	0.66-0.84
Batch 6	94.53	0.05	No Si	NA	0.82-1.05
Batch 7	99.08	0.30	No Si	NA	0

pH 7

At pH7, Batch 1 exhibited the highest uranium removal with an average of 67.53±10.28% among non-sediments samples (Batches 1-3). With the addition of humic acid (Batch 2), the removal of uranium averaged ~50% which was slightly higher than with the addition of HA alone (Table 16.).

Table 16. Analytical results for the set of pH 7

Sample-Description, pH 7	U(VI) Avg. Removal, %	Std. Deviation	Si Avg Removal, %	Std. Deviation	Fe, ppm
Batch 1/Filtered	73.47/NR	0.15/NR	52.28	1.19	No soil
Batch 2	54.03	3.70	58.12	3.24	No soil
Batch 3	47.33	0.23	No Si	NA	No soil
Batch 4	98.06	1.45	92.04	2.83	0.003-0.03
Batch 5	85.47	2.19	81.25	3.7	0.86-1.4
Batch 6	85.70	2.19	No Si	NA	0.7-1.5
Batch 7	98.64	0.98	No Si	NA	0

Two of the filtered Batch 1 samples need to be reprocessed, which leaves the results of our filtered Batch 1 inconclusive at this time. Similar to samples prepared with pH 6, the

performance of Batch7 (sediments only) surpassed other sediment-bearing batches. At pH 7, the average U(VI) removal of 98.64± 0.98% was observed for Batch 7. As it pertains to the sediment batches, a similar value of 98.06±1.45% U(VI) removal was obtained for Batch 4. This indicates that silica-bearing sediment samples seem to have a trend of being above 90% in U(VI) removal. The removal efficiencies of HA-amended sediment samples in Batches 5 and 6 dropped in comparison to previous pH levels.

Analyzing these results, we can determine that sediment samples out-performed those samples without sediment. Of the sediment batches, we can determine that at pH 7, and trending with pH 6, the sediment sorption capabilities are strongest without the addition of Si and HA. However, we must note that sediment in the presence of colloidal silica still possesses notable sorption properties.

pH8

At pH 8, all U(VI) removal results were in the range between 94-99.9%. For non-sediment samples, Batch 1 proved most effective, both filtered and unfiltered, with values of 96.48± 1.44% and 99.96±0.07% for U(VI) removal, respectively (Table 17).

Table 17. Analytical results for the set of pH 8

Sample-Description, pH 8	U(VI) Avg Removal, %	Std. Deviation	Si Avg Removal, %	Std. Deviation	Fe, ppm
Batch 1/Filtered	96.48/99.96	1.44/0.07	83.23	0.23	No soil
Batch 2	96.34	0.55	38.05	5.26	No soil
Batch 3	94.05	0.68	No Si	NA	No soil
Batch 4	99.45	0.24	83.32	4.94	0.05-0.17
Batch 5	98.07	0.33	80.35	3.02	1.01-1.63
Batch 6	98.21	0.64	No Si	NA	0.98-1.83
Batch 7	99.93	0.07	No Si	NA	0

At pH 8, Batch 2 with no sediment, humic acid and silica had a removal percentage found to be 96.34±0.55%. This trend for Batch 2 has shown up at every pH level from 4-8. The results after sample processing for Si and Fe are presented in Table 16 and Table 17. The higher removal of Si always correlated with the higher removal percentage of U(VI).

Thus far, the two best results for U(VI) removal were gathered from Batches 7, 4 and filtered samples from Batch1 at each respective pH value. At higher pH values, the sediment samples performed best alone; however, sediments amended with colloidal silica maintained increasingly higher levels of U removal. In respect to overall performance, the sediment-bearing batches typically exceeded the performance of non-sediment batches. In terms of HA, sorption results of sediment samples tend to coincide with other literature found. Krepelova et al. (2007) states that HA enhances the U(VI) sediment uptake in the acidic pH range compared to the system without HA and reduces the U(VI) sorption to sediment in the near-neutral pH range. The uranium removal in filtered samples of Batch 1exhibited higher values compared to unfiltered samples, justifying that not all colloidal Si was removed from the supernatant solution after sample centrifugation. Comparison of the results might also require filtering of all the samples and then processing via KPA. A graphical representation of U (VI) removal for pH 3 to 8 is presented in Figure 32.

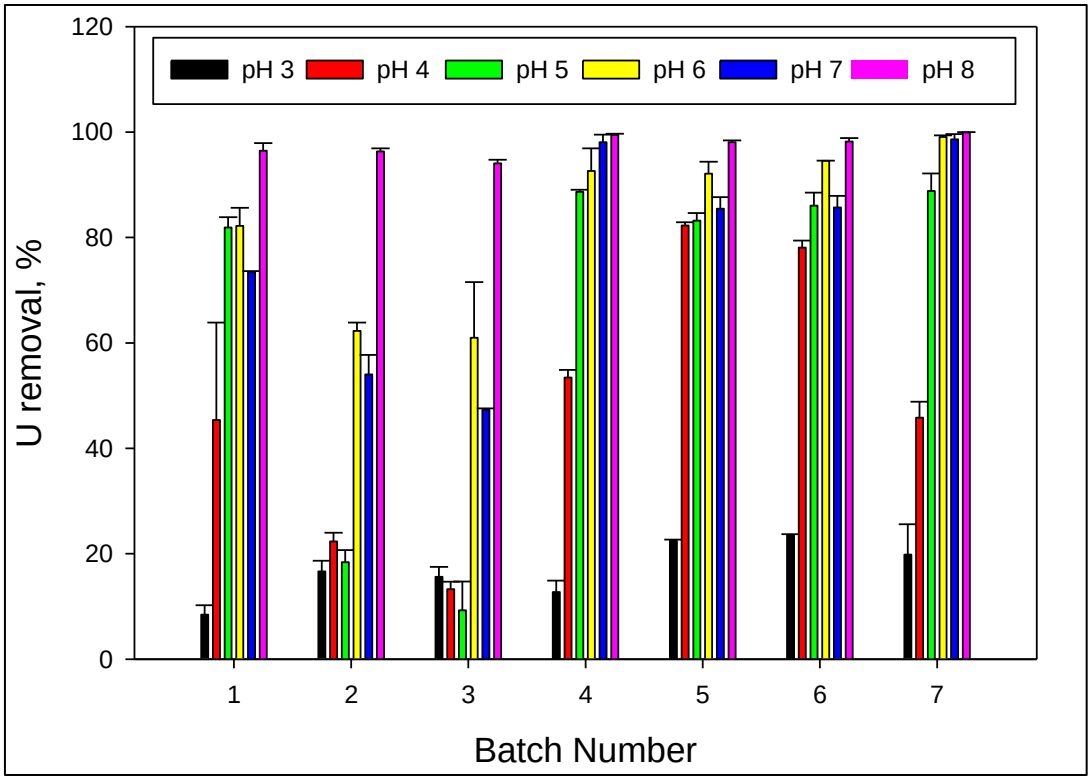

Figure 32. U(VI) adsorption for all batches at pH 3-8

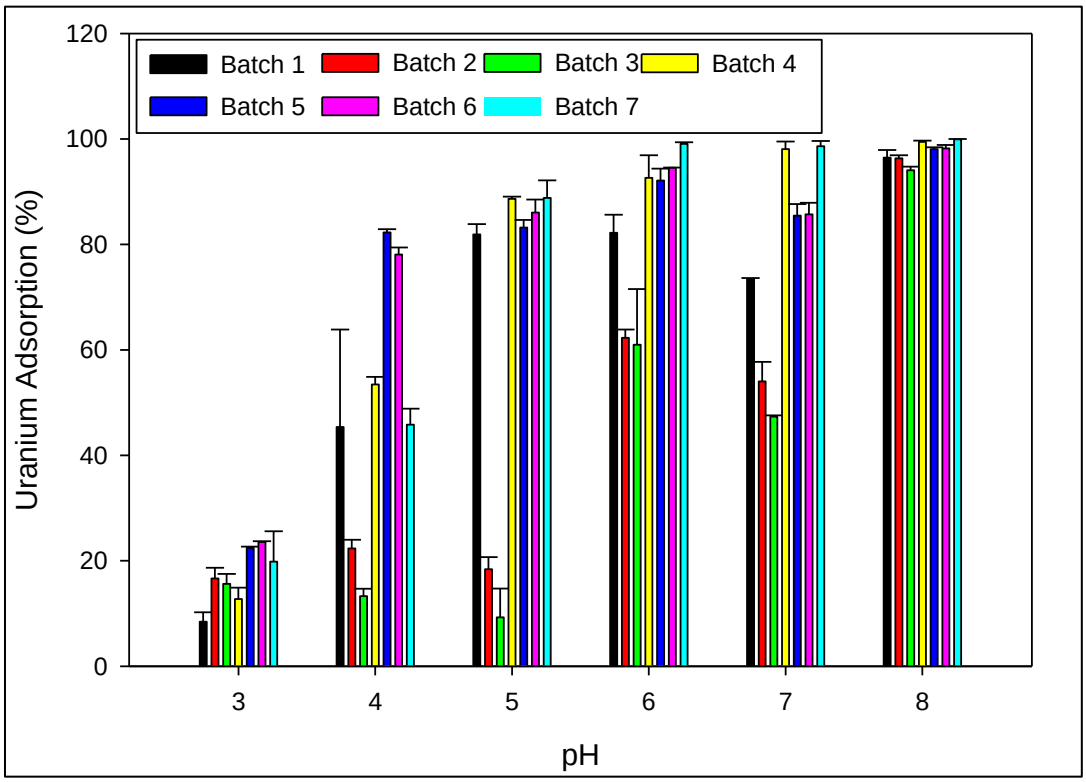

Figure 33. U(VI) adsorption for all batches at pH 3 to 8

The sorption of U(VI) onto sediments is influenced by the pH and the presence of HA. The effect of silica, HA and sediment on uranium adsorption is better explained when considering a change

in uranyl speciation as a function of pH. As pH increases, the simple uranyl cation is transformed to mononuclear and polynuclear hydrolyzed uranyl species (Table 8). As pH is increased to 8, a chemical change from positively charged species to negatively charged species takes place with the formation of a negative polynuclear $(UO_2)_3(OH)_8^{2-}$ and $UO_2(OH)_3^-$ complexes. According to Iler (1979), at pH below 4.5, silica particles bear very little surface charge, thus, limiting the adsorption of positively charged polynuclear hydroxo-uranyl cations. In the presence of HA, the uranyl uptake by Si particles and sediments is modified. At low pH 3, the addition of HA slightly enhances U(VI) sorption compared to the HA-free samples. This result correlates to other studies found that in the acidic pH the addition of HA slightly enhances U(VI) sorption relative to the HA-free system (Murphy et al., 1999; Schmeide et al., 2000; Ivanov et al., 2012). Conversely, in the pH range of 4 to 7, the sorption of U(VI) on Si was reduced in the presence of HA in comparison to the system without HA. This seems reasonable considering the low percent reduction of uranium in the presence of HA due to the formation of uranyl-humate complexes.

Table 18 change in uranyl species with change in pH

pH	3	4	5	6	7	8
Uranyl Species	UO_2^{2+}	UO_2^{2+} $(UO_2)_2(OH)_2^{2+}$	$(UO_2)_3(OH)_5^+$ UO_2OH^+	$(UO_2)_3(OH)_5^+$ UO_2OH^+	$(UO_2)_3(OH)_5^+$ $(UO_2)_3(OH)_7^+$	$(UO_2)_3(OH)_8^{2-}$ $UO_2(OH)_3^-$

As the pH of the solution is increased, the surface charge of silica decreases, resulting in increased adsorption of hydroxo-uranyl cations. The sorption of uranium onto silica colloids might be due to the surface complexation process that can occur on the outer sphere and inner sphere of the electric double layer of the surface (Iler, 1979). During the adsorption process, the silica surface gradually becomes covered with adsorbed cations which finally coat the whole surface. Koopal et al. (1998) reported that HA could be rapidly and strongly absorbed on to the silica surface, thus limiting the adsorbing surface available for uranium; Batch1 and Batch 2 data shown in Figure 4 and Figure 5 is in agreement with the literature data.

FUTURE WORK

Future work will focus on the preparation of the sets with an increase of up to 50 mg/L concentration for HA. In addition, batch sorption experiments will include a series of reactors prepared with HA and U(VI) in the pH range adjusted between 4 and 9. These experiments will provide information on the amount of HA_{sorb} vs. $HA_{dissolved}$ and C/C_o of U(VI) at each pH condition, where C_o and C are the initial and residual concentrations of U(VI) in the solution composition, respectively. The sediments' surface composition will be analyzed via scanning electron microscopy and energy-dispersive-spectrometry (SEM-EDS). The quantitative measurements of the surface composition will show the distribution of elements throughout the sample. The distribution of carbon might suggest if HA polymerized and precipitated on the surface or between sediment particles. The SEM-EDS analysis will also reveal surface topography and provide information of any correlation between elements across the surface. In addition, efforts will be made to conduct U(VI) speciation modeling to make more accurate predictions of subsurface processes.

ACKNOWLEDGEMENTS

Funding for this research was provided by U.S. DOE contract DE-EM0000598. We truly appreciate Dr. Miles Denham and Dr. Brian Looney from the SRNL for their valuable input and support of this research.

REFERENCES

Chen, C., and X. Wang, 2007. Sorption of Th (IV) to silica as a function of pH, humic/fulvic acid, ionic strength, electrolyte type. *Applied Radiation and Isotopes* 65, 155-163.

Choppin, G.R., 1992. The role of natural organics in radionuclide migration in natural aquifer systems. *Radiochim. Acta* 58/59, 113.

Choppin, G.R., 1998. Humics and radionuclide migration. Radiochim. Acta 44/45, 23-28.

Davis, J.A., 1982. Adsorption of natural dissolved organic matter at the oxide/water interface. *Geochim. Cosmochim. Acta* 46, 2381-2393.

Davis, J.A., 1984. Complexation of trace metals by adsorbed natural organic matter. *Geochim. Cosmochim. Acta* 48, 679-691.

Dong, W., Tokunaga, T. K., Davis, JA., Wan, J., 2011. Uranium(VI) Adsorption and Surface Complexation Modeling onto Background Sediments from the F-Area Savannah River Site. *Environmental Science & Technology*

Fairhurst, A. J.; Warwick, P.; Richardson, S. 1995. The influence of humic acid on the sorption of europium onto inorganic colloids as a function of pH. *Colloids Surf.*, A, 99, 187-199.

Ivanov, P., Griffiths, T., Bryan, N.D., Bozhikov, G. and S. Dmitriev, 2012. The effect of humic acid on uranyl sorption onto bentonite at trace uranium levels. *J. Environ. Monit.,* 14, 2968 - 2975.

Krepelova, A., Brendler, V., Sachs, S., Baumann, N., Bernhard, G., 2007. U(VI)-Kaolinite Surface Complexation in Absence and Presence of Humic Acid Studied by TRLFS. Environ. Sci. Technol. 2007, 41, 6142-6147.

Labonne-Wall, N., Moulin, V., Vilarem, J.P., 1997. Retention properties of humic substances onto amorphous silica: consequences for the sorption of cations. *Radiochim. Acta,* 79, 37-49.

Murphy, R. J., Lenhart J. J. and B. D. Honeyman, The sorption of Th(IV) and U(VI) to hematite in the presence of natural organic matter, Colloids Surf., A, 1999, 157, 47.

Perminova, I.V, Hatfield, K., Hertkorn, N., 2002. Use of humic substances to remediate polluted environments: from theory to practice. In the proceedings of the NATO Advance Research Workshop, Springer, P.O Box 17, 3300 AA Dordrech, The Netherland.

Plancque, G., Amekraz, B., Moulin, V., Toulhoat, P., Moulin, C., 2001. Molecular structure of fulvic acids by electrospray with quadrupole time-of-flight mass spectrometry. *Rapid Commun. Mass Spectrom.* 15, 827-835.

Shmeide, K., Pompe, S., Bubner, M., Bernhard G. and H. Nitsche, 2000. Uranium(VI) sorption onto phyllite and selected minerals in the presence of humic acid, Radiochim. Acta, 88, 723

Sylwester, ER., Hudson, EA., Allen, PG, 2000. The structure of uranium (VI) sorption complexes on silica, alumina, and montmorillonite. Geochimica et Cosmochimica Acta, Vol. 64, No. 14, pp. 2431-2438.

Wang, X. K.; Dong, W. M.; Dai, X. X.; Wang, A. X.; Du, J. Z.; Tao, Z. Y. 2000, Sorption and desorption of Eu and Yb on alumina: mechanisms and effect of fulvic acid. Appl. Radiat. Isot. 52, 165-173.

Zachara, J.M., Resch, C.T., Smith, S.C., 1994. Influence of humic substances on Co^{2+} sorption by a subsurface mineral separate and its mineralogical components. *Geochim. Cosmochim. Acta* 58, 553-566.

Liao Jiali, Wen Wei, LI Bing, Yang Yuanyou, Zhang Dong, Kang Houjun, Yang Yong, Jin Jiannan, Liu Ning, 2013. Interaction between uranium and humic acid (II): complexation, precipitation and migration behavior of U(VI) in the presence of humic substances. Nuclear Science and Techniques 24, 030301

L.K. Koopal, Y. Yang, A.J. Minnaard, P.L.M. Theunissen, W.H. Van Riemsdijk, 1998. Chemical immobilisation of humic acid on silica. Colloids and Surfaces A: Physicochemical and Engineering Aspects 141, 385-395.

TASK 2.2: MONITORING OF U (VI) BIOREDUCTION AFTER ARCADIS DEMONSTRATION AT F-AREA

INTRODUCTION

In 2010, ARCADIS demonstrated the *in situ* injections of a carbohydrate substrate, molasses, to create reactive zones for metal and radionuclide remediation via the Enhanced Anaerobic Reductive Precipitation (EARP) process. The addition of the molasses substrate solution to groundwater produces anaerobic conditions conducive to the reductive precipitation of uranium. An important aspect of any *in situ* remediation of metal and radionuclide contamination is the longevity of contaminant immobilization. Regulators and stakeholders will approve leaving contaminants in the subsurface only if they are assured that contaminants will remain sequestered for long periods of time. This is particularly true when the remediation strategy relies on changing the geochemical conditions in a direction that is opposite of their natural evolution. Bioreduction of metals/radionuclides in an aerobic aquifer is an example of this. A microcosm study, prepared with SRS sediments, augmenting the solution mixture with molasses, was designed as a tool to provide evidence of the capabilities of this technology. The objective of the microcosm experiment is to replicate the treatment performed by ARCADIS at SRS and investigate the mineralogical changes that occur in the soil due to the addition of molasses. Specifically, the study aims to determine whether forms of reduced iron such as siderite and pyrite would arise in the reducing zone and if any mineralogical changes occurred in sediments during the re-oxidation period. These experiments will also explain the types of reactions that might occur in the anaerobic aquifer. An understanding of the technology will be useful to determining if it is a viable option for remediation.

BACKGROUND

The initial microcosm study was set up during a summer internship conducted by DOE Fellow Valentina Padilla at the Savannah River Site. The study included the setup of two centrifuge tubes with perforated holes in the caps. The tubes were connected through the holes with a long thin plastic conduit (Figure 34). The sample contained 20 mL of sediments from the F-area that was amended with 0.014 g of $NaNO_3$ and 7 g of molasses (20% w/w). The samples were kept over a period of 30 days, and experimental observations suggested that the microcosm study did not yield successful results, showing no signs of activity from anaerobic microorganisms. Several factors are believed to have contributed to these results: the growth of the anaerobic bacteria was too slow or perhaps the air present inside the tubes was significantly slowing the process. Another reason could be that the experimental tubes were not completely sealed off, leaving the possibility of oxygen entering the system. This could suppress anaerobic bacteria that probably were not present in any significant quantity in the sediment samples collected from the oxygenated aquifer. The details of these experiments are presented in the internship report “SRS In-Situ Bioremediation Techniques and F-area Post Molasses Injection Analysis” that can be found on the DOE Fellows website under the section for internship reports (http://fellows.fiu.edu/InternshipReports.asp).

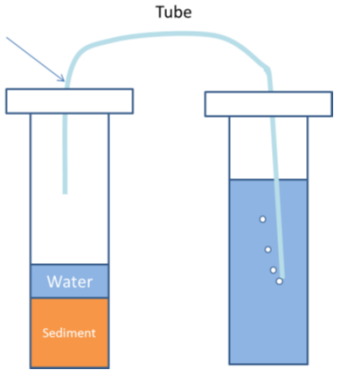

Figure 34: Set up of microcosm study performed at SRS

During the design of the microcosm experiment that was performed at FIU, there were several precautions taken to prevent any of the same issues from happening. The setup of the experiment was modified to include an anaerobic chamber filled with the nitrogen gas; this ensured that no oxygen could enter the samples. The anaerobic process is very slow; so, to speed up the molasses fermentation process, some samples were inoculated with anaerobic bacteria. Bacterial samples for inoculations were collected from the South Miami wastewater treatment plant anaerobic digester. We discuss bacteria inoculation in greater detail in the methodology section.

Several background core samples were collected from a well near to the molasses injection site and shipped back to FIU-ARC to continue with the microcosm study. The core samples were collected from the well FSB 91C, the closest well to the molasses injection site from which core samples were available (Figure 35). Six samples were retrieved at the following depths: 65, 80, 90, 95, 100 and 105 feet, respectively (Figure 36).

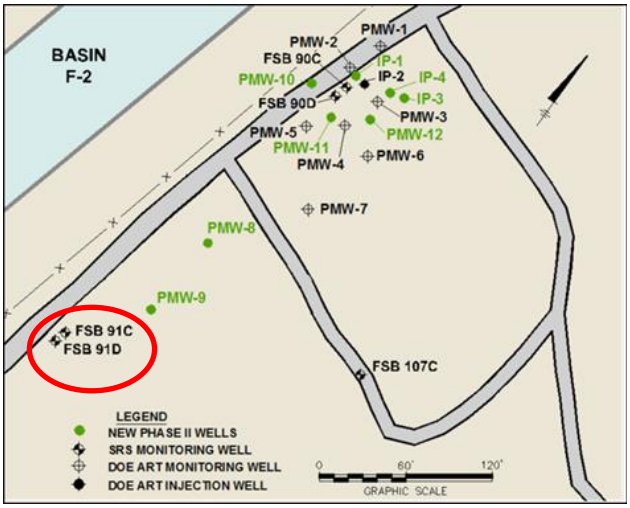

Figure 35: F-Area depicting well FSB 91C where sediment samples were collected

Figure 36: Core samples shipped to FIU

METHODOLOGY

Background samples collected from SRS were analyzed via X-ray diffraction (XRD) method to get baseline information on sediment mineralogy before their treatment with molasses. The fine and coarse fractions were separated via sieving for a second round of XRD analysis to evaluate

only the fine fractions of the sediment. Samples were sieved through the following sieves: No. 170, No. 200, No. 230 and No. 270. This yielded fine fractions of sediment of less than 0.06 mm in size.

X-ray diffraction analyses were performed on the dried precipitates at 35 kV and 40 mA via a Bruker 5000D XRD instrument. Diffraction patterns were obtained using a copper Cu Kα radiation source (λ=0.154056 nm) with a tungsten filter. The XRD was programmed to run over a 2-theta (2θ) range from 10° to 90° with a 0.02° step size and 3 second counting per step. Since the high intensity peaks for many clay solid phases are in the range of 2-theta from 5 to 10, the XRD analysis was repeated to run from a 2-theta range from 2.5^{o} to 90^{o}. The sample was packed into the small recess of a plastic sample holder that was designed specifically for the small amount available.

To create favorable conditions to grow anaerobic bacteria, the molasses was diluted with a basal medium. The basal medium (modified from Freedman and Gossett, 1989) consisted of (in g L^{-1} deionized water) $NaHCO_3$ 1.5, NH_4Cl 0.2, K_2HPO_4 $3H_2O$ 0.1, KH_2PO_4 0.055, resazurin 0.001 as a redox indicator, Na_2S $9H_2O$ 0.039 as a sulfur source and reductant, and $MgCl_2$ $6H_2O$ 0.1. In addition, 5 mL L^{-1} trace metal solution were added. The trace metal solution contained (in g L^{-1}) $FeCl_2$ $4H_2O$ 0.005, $MnCl_2$ $4H_2O$ 0.005, $CoCl_2$ $6H_2O$ 0.001, H_3BO_3 0.0006, $ZnCl_2$ 0.0001, $NiCl_2$ $6H_2O$ 0.0001, Na_2MoO_4 $2H_2O$ 0.0001, and $CaCl_2$ $2H_2O$ 0.002. The basal medium was used to stimulate the growth of anaerobic bacteria and when mixed with molasses accelerate the soil transition from aerobic to anaerobic conditions. The media components were autoclaved and then aseptically mixed in a 1L glass bottle. The prepared basal medium was then used for molasses dilution to minimize the potential of changing the bacterial population existing in the soil. The salts were measured using an analytical balance (Precisa XB220A) and then mixed with deionized water (DIW) (Barnstead Diamond Water Purification System).

A Vinyl Anaerobic Airlock chamber made from flexible PVC vinyl (Figure 37) from COY Lab Products was used to ensure an anaerobic environment.

Figure 37 Anaerobic glove box

To establish anaerobic conditions in the glove box, it was vacuumed and purged several times with pure nitrogen gas according to the procedures provided by the manufacturer, Coy Lab

Products. The process was repeated three (3) times before injecting mixed gas containing 95% nitrogen and 5% hydrogen.

Literature review was performed to determine the dilution factor for molasses addition. Both molasses injection technologies and molasses microcosm experiment literature indicated that maximum bacterial growth occurs at a small molasses concentration of 5-10% [4]. A 5% (by weight) molasses concentration was used in order to not overload the sample with molasses and prevent slowing down the reaction time [2], with the intention of later additions if necessary.

Samples were prepared in 50 mL polypropylene tubes with sediment that occupied a volume of 10 mL and 10 mL of the 5% diluted molasses solution. The diluted molasses solution was composed of 9.5mL of basal medium and 0.5 mL of molasses (using 1.42 g/mL density for the molasses, which is equivalent to 0.7 g of molasses). For accuracy in the preparation of the diluted molasses, it was prepared in quantities of 400 mL at a time (20 mL or 28.4 g of molasses and 380 mL of basal medium) and then distributed between sample vials. The pH of the solution composed of molasses diluted with basal medium without having had any contact with the sediment samples was measured as 7.6.

Two batches and control samples were prepared for this experiment. Each sample represented one of the depths where the samples were taken (65, 80, 90, 95, 100, and 105 ft). The first batch consisted of three subsets, all prepared at the same time and following the same procedure. There was a total of 36 samples prepared, each set consisted of 12 (one for each depth and its duplicate). The original approach was to sacrifice whole set at different time intervals; however, only the first set has been used by taking a small quantity of sample at the time of 1 and 6 weeks, respectively. So, instead of sacrificing the entire sample, a small subportion of each sample was placed to dry at different time intervals. pH measurements were taken before placing the samples to dry. The other two sets have been saved for long term analysis in case sampling needs to be continued.

A second batch of samples was prepared in similar manner as the first batch, but to create anaerobic conditions and ensure the presence of anaerobic bacteria, samples were inoculated with anaerobic sludge collected from the Miami-Dade South wastewater treatment plant anaerobic digester. The initial pH of the soil suspension was measured before placing them inside the anaerobic glove box. After a week, an additional 1 mL of diluted molasses was added to all samples. The composition of this diluted molasses, however, was different from the original solution. It consisted of 0.7 grams of molasses per samples, which is equivalent to the originally added amount of 0.5 mL diluted with 0.5 mL of basal medium for easier pipetting. For efficiency, 15 mL of this diluted molasses was made in advance, containing a total of 8.5 g of molasses and 6 mL of basal medium. After manual mixing, 1mL of solution was added to each sample. Just like the first batch, the pH measurements (Table 19) were taken and a small quantity of wet solids was taken out and set to dry after 1 and 6 weeks for further analysis via XRD.

A control set of samples was prepared in a similar manner as the other batches of samples. They contained enough sediment to fill 10 mL of volume and basal medium only (no molasses). The pH of the basal medium was 8.55. The initial pH was measured before placing the samples in the anaerobic chamber and then re-measured again after 2 weeks.

To test the re-oxidation process of both batches of samples, they were sacrificed at 6 weeks. The pH was measured and each sample was separated into three subsets. The goal was to examine how the samples would react at different levels of oxygenated environments. Three environments have been created for this purpose. The first was created in the anaerobic glove box with no oxygen, the second environment was made in another anaerobic glove box in which the oxygen levels have been allowed to reach 1963 ppm (~2000ppm), and the third one was a laboratory work bench at atmospheric conditions. The solids from each sample were scooped out with a spatula and placed in their respective environments. After 3 weeks of keeping samples in the respective environments, samples were sieved through a 0.355-mm mesh (0.014 in), placed in 5 mL round bottom tubes and carefully sealed to prevent air from entering while transferring the tubes to the XRD facilities. The results of the XRD analysis were compared with the results of the respective background samples. The supernatant solutions tested the remainder liquid from the samples for iron content. To reduce the high turbidity of the samples, the remainder liquids were transferred inside the chamber into 15-mL high clarity polypropylene conical tubes, sealed and then centrifuged at 4000 rpm for 5 min. The samples, after the centrifugation process, were returned to the anaerobic chamber and carefully filtered using a 13 mm HPLC syringe filter with 0.45 µm membrane. Filtered liquids were diluted 10 times with 1% HNO_3 and analyzed via ICP-OES for concentrations of iron and silica in the aqueous-phase.

RESULTS AND DISCUSSION

Observations

Batch 1

Most of the samples from the first batch depicted bacterial growth after few weeks of treatment inside the anaerobic changer. The black-colored bacterial growth was observed on top of the solution and on walls of the container. It was not investigated, but the black powdery appearance of the bacteria that started growing in circular patches on the top of the solution suggested most likely fungal growth and not the anaerobic microorganisms expected. There was also no sign of sediment color change due to the presence of ferrous sulfide as a visible black precipitate in the growth medium (Figure 38) or increase in turbidity indicative of bacterial growth.

Figure 38: Examples of fungal growth on the top of the solution

The pH measurements were taken after a week and six weeks (Table 19). The decline in pH values form a descending trend that could be explained by the solution reaction with the acidic

soil, or by the organic acid production via the molasses fermentation process. Batch 1 sample's pH values were compared with the control samples (Table 19).

Batch 2

During the first couple of days, significant bubble formation was observed in all the molasses-bearing samples inoculated with anaerobic sludge; this bubbling is one of the characteristics of the molasses fermentation process suggesting establishment of anaerobic conditions. However, after several days, gas bubble formation decreased significantly. To sustain bacterial growth, the samples were augmented with molasses again; however, the molasses addition stimulated only a little bubble formation compared to the first time. Otherwise, there have been no other growths observed in the samples.

The pH of the second batch of samples was measured initially, after one week and after six weeks. Similar to the first batch, there was a descending trend observed in the pH values for all samples. The pH of the diluted fresh molasses solution was measured as 7.6; this close to neutral value is important because of the high acidity of the sediment samples. It was noted that after the addition of the diluted molasses to the acidic sediment, the pH of the soil suspension was measured as an average of 6.00. This change was partly due to the neutralization of the acidic soil samples with the more neutral molasses. After a week, the pH level dropped to a value of about 4.00. After the initial decrease, the pH stabilized and after six weeks was averaging 3.87 (Table 19).

Table 19. pH measurements

Depth		65'	80'	90'	95'	100'	105'	Ave
Batch 1	Week 1	5.53	5.21	4.65	4.29	4.89	4.54	4.85
	Week 6	4.28	4.26	4.10	4.63	4.38	4.36	4.34
Batch 2 (Amended with bacteria)	Initial	6.27	4.33	6.59	7.12	5.17	6.53	6.00
	Week 1	3.79	3.81	4.09	4.2	3.89	4.22	4.00
	Week 6	3.75	3.90	3.81	3.81	4.07	3.85	3.87
Control	Initial	6.89	5.76	6.74	7.52	6.43	7.13	6.75
	2 weeks	7.85	5.65	8.06	8.56	7.88	8.46	7.74

Control samples

The pH values of the molasses-free control samples taken at the beginning of the experiment and after 2 weeks showed an ascending trend in all but one samples (depth 80' in which the pH stayed almost unchanged) (Table 19). These results were in opposition to the batches augmented with molasses. Soil in control samples was diluted with basal medium and resulting soil suspension exhibited more neutral pH values due to some buffering effect of carbonate compound present in the medium. Thus, the pH decrease in the batch experiments augmented with molasses was mostly due to organic acids produced by the molasses fermentation process. Since these control samples were molasses-free, there was no drop in the pH due to accumulation of the organic acids originating from the fermentation process (Table 19).

XRD analysis

XRD analysis on background samples

XRD analysis was performed on the background samples following the procedure described in methodology section. Figure 39 depicts the results at depths 65 ft, 80 ft, 90 ft and 100 ft. The results for a depth of 65 ft showed three peaks with high intensity that occurred at 2-theta values of about 21, 27 and 77. There are also some rather high intensity peaks between 2-theta values of 40 to 55, and then again at 2-theta values of 81 and 84 that have moderate intensities that were not present at any other depth. At a depth of 80 ft there are two peaks of significance with high intensities at 2-theta values of 26 and 61. There are also minor peaks with low intensities occurring at 2- theta values of 50, 68, and 80. For 90 ft there is only one peak of high intensity occurring at a 2-theta value of 26. This peak is also observed on the results for 100 ft. At this depth, there were also other moderate intensity peaks at about 2- theta values of 21, 43, and 61.

Efforts in the interpretation of the XRD results of the background samples on the mineralogy of soil minerals have been made and quartz was the most likely match for all the samples. Figure 6 shows the comparison of the samples (depicted in black) and quartz minerals (depicted in red). About 80% of all major peaks are matched in all the samples, although the intensity rations are sometimes off. This could be because those peaks belong to some other mineral also present in the sample but in smaller quantities. Other minerals are being explored as possible matches as well to identify what minor minerals could be present in the samples. In these experiments, the most common occurring minor minerals at the Savannah River Site such as mullite, kaolinite, goethite and muscovite have not been a match. So, samples were dry sieved by hand via 0.355 mm sieve to remove course sand particles and reanalyzed.

XRD analysis on sieved background samples

The sieved background samples have been re-analyzed and the solid phases have been identified. The results, however, are identical to the un-sieved background samples (Figure 40). The data for 65 ft also showed three peaks with high intensity that occurred at 2-theta values of about 21, 27 and 77. The moderate peaks, present only at this depth, between 2-theta values of 40 to 55 and then again at 2 theta values of 81 and 84, are present as well. The results at a depth of 80 ft showed two peaks of high intensities at 2-theta values of 26 and 61. The minor peaks with low intensities occurring at 2-theta values of 50, 68, and 80 are also present. For 90 ft., the main high intensity peak occurring at 2-theta value of 26 is still present. Just like before, this peak is also observed on the results for 100 ft. At this depth, there are also other moderate intensity peaks at about 2 theta values of 21, 43, and 61.

XRD Results (1 week)

The XRD patterns were plotted using sigma plot software and then compared with known mineral XRD patterns (Figure 41 and Figure 42). Even though the samples were sieved, the most likely match is still quartz. There is, however, a potential match for one of the samples from batch 1 at a depth of 90 feet with montmorillonite, a clay mineral, Figure 43. The matching peak occurred at a 2-theta value of 5.89.

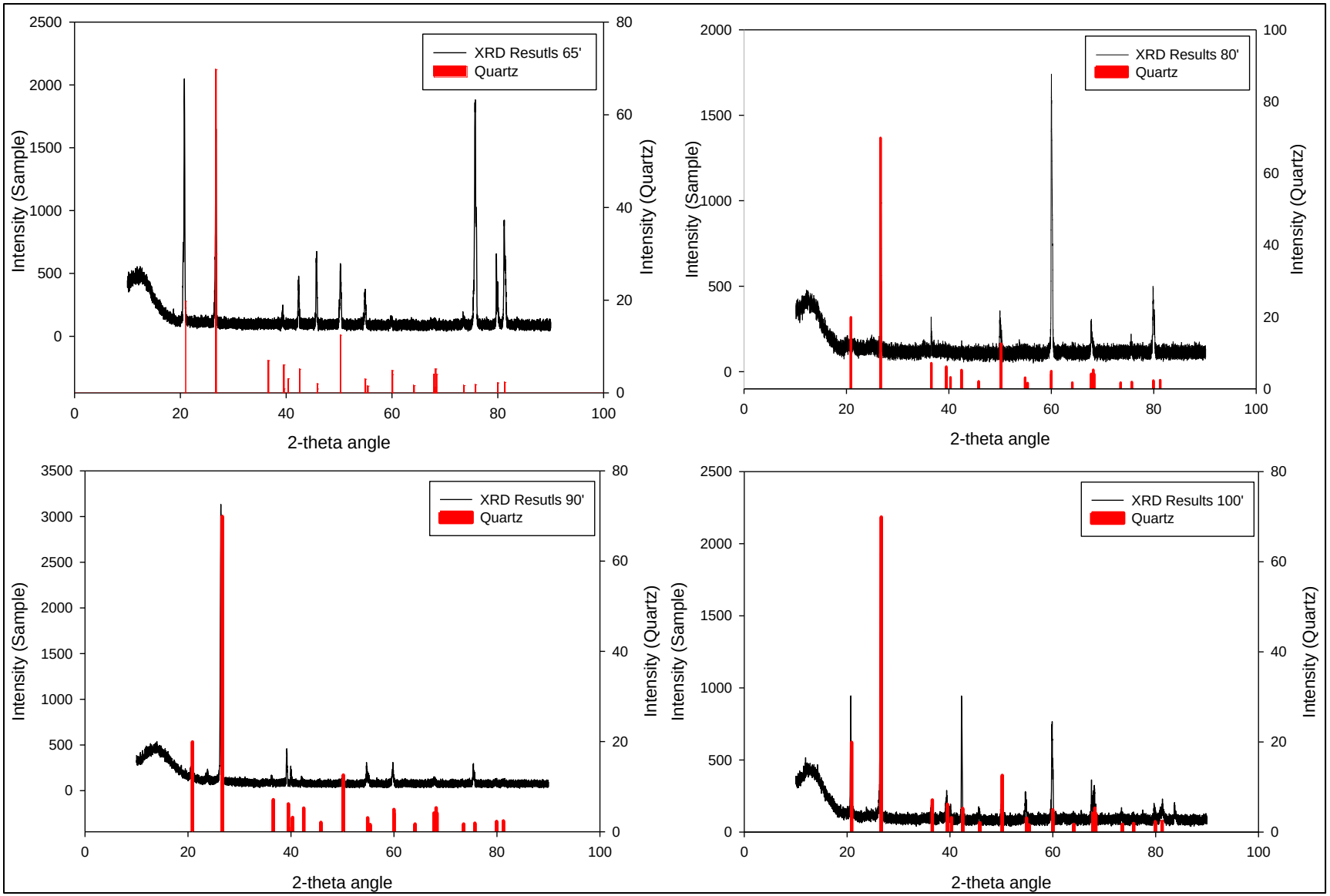

Figure 39. XRD patterns of un-sieved background samples

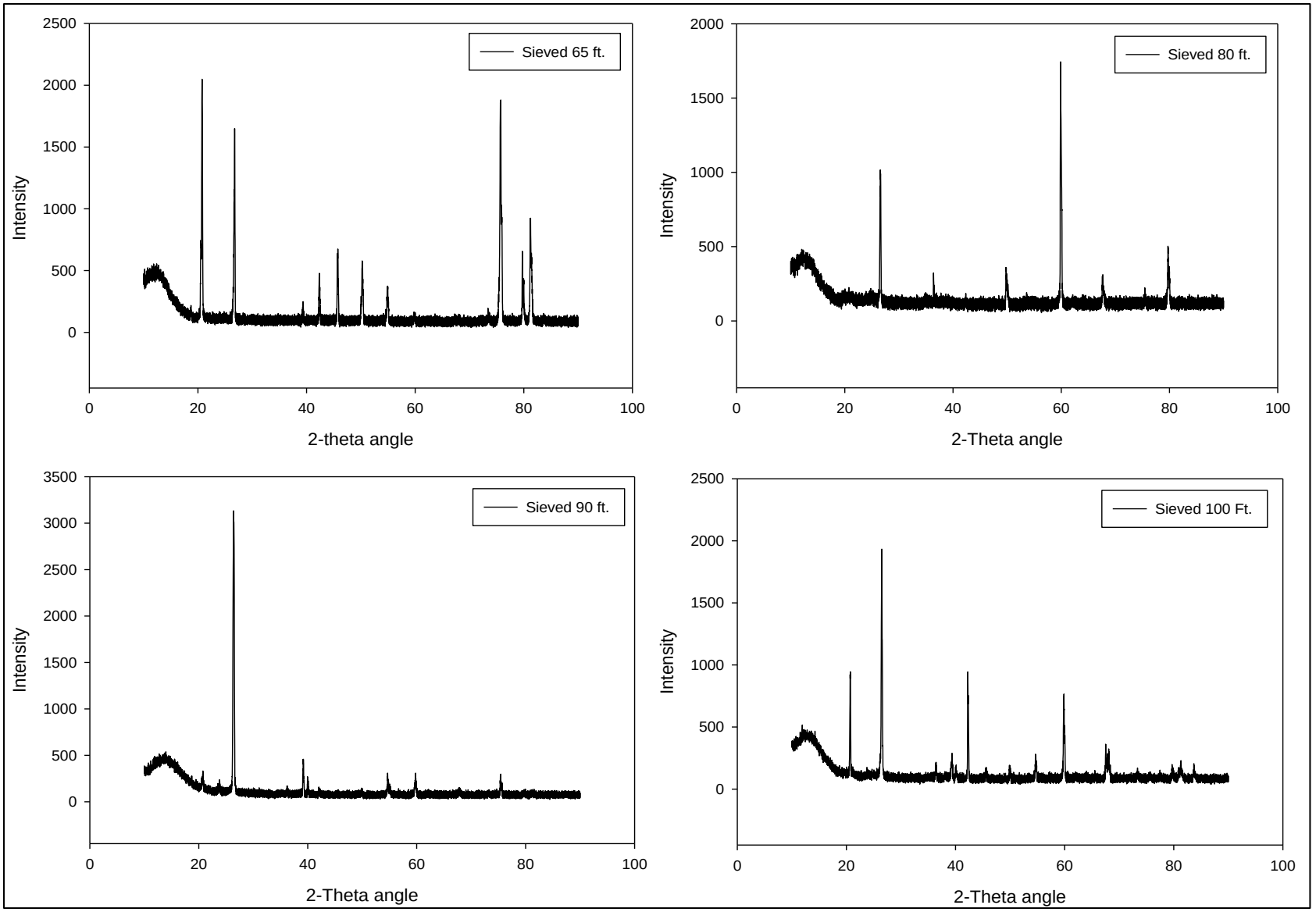

Figure 40 XRD patterns of sieved background samples

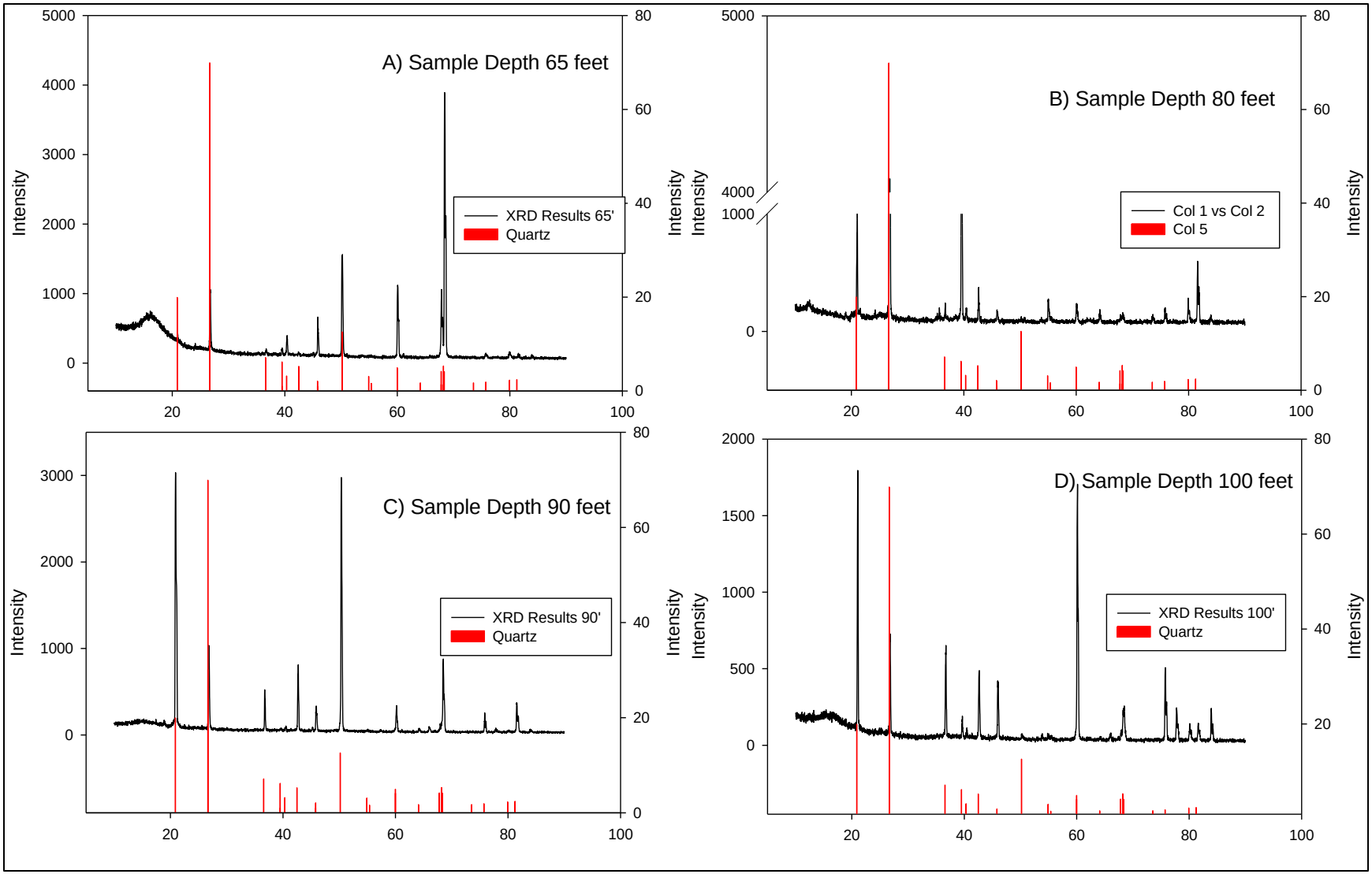

Figure 41 Batch 1 XRD data comparison with quartz (1 week)

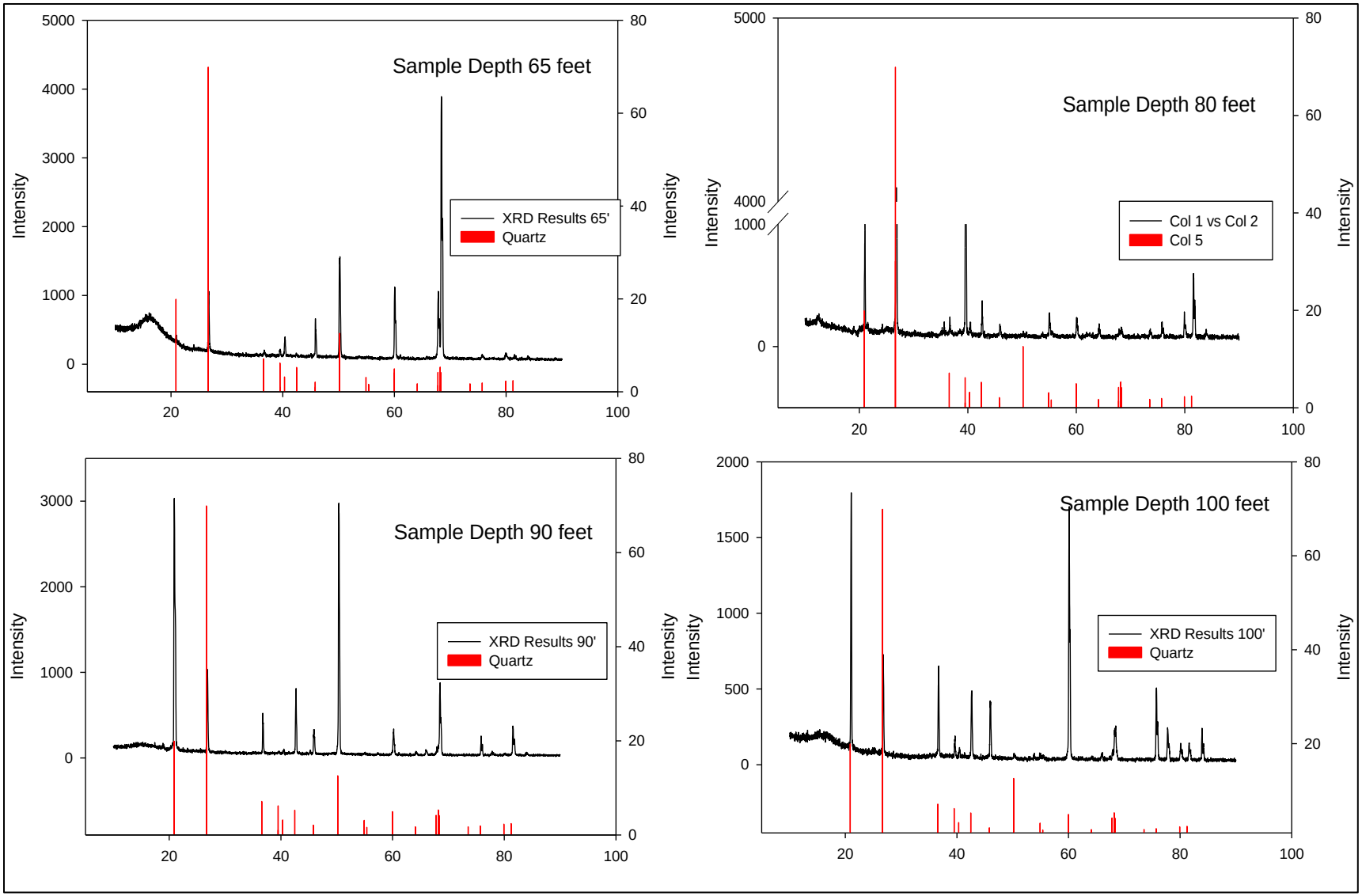

Figure 42 Batch 2 XRD data comparison with quartz (1 week)

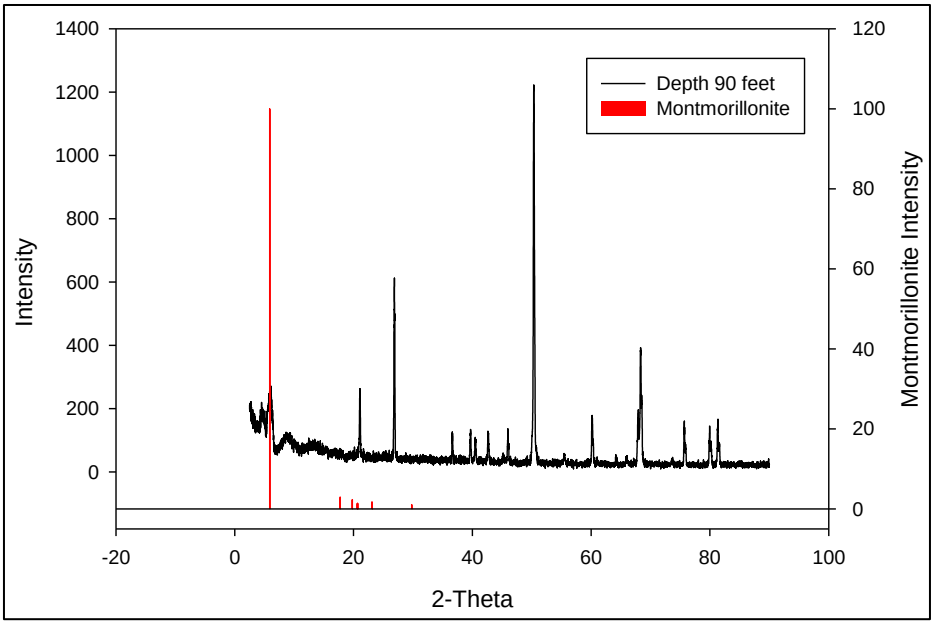

Figure 43 Batch 1 90' sample XRD pattern comparison with Montmorillonite (1 week)

XRD Results Re-oxygenation Period (6 weeks)

The final testing stage of the microcosm experiment of molasses treated samples by testing the re-oxygenated period of the samples. Each of the samples was sacrificed after 6 weeks of treatment and divided into three different environments. The three environments consisted of the regular anaerobic chamber with no oxygen, a smaller chamber with a low oxygen content of 2000 ppm, and the work bench where they were exposed to atmospheric oxygen levels. In each environment there are four different depths (65, 80, 90, and 100 feet) for each batch. After the samples were dried for 3 weeks in their respective environments, they were sieved and transported for X-ray diffraction analysis. The same process was also repeated with the control molasses-free samples kept in basal media; however, only 3 of the control samples were selected for analysis (one from each environment at a depth of 90 feet). There are 27 samples in total that were analyzed using the X-ray diffraction process described in the methodology section. Each of the sieved samples was packed into the small recess of a plastic sample holder that was designed specifically for the small amount available to conduct XRD analysis. The results were plotted using sigma plot software (Figure 44 - Figure 49).

After analyzing the XRD data, it was clear that for each environment (no oxygen, low oxygen and atmospheric oxygen) the only match was quartz and montmorillonite clay. The most intense peaks for each of the samples corresponding to quartz occurred near the 2-theta values of 27 and 21. There is a slight peak at the 2-theta value of about 5.89, which would indicate the presence of montmorillonite (a clay mineral), though it is of low intensity which is most probably caused by the lower percentage of clay in the sample compared to quartz. The intensities for all the samples vary, though the 2-theta peaks stay consistent. This variance could be due to the inconsistencies in the size of the sample crystals which would lead to difference intensities being observed.

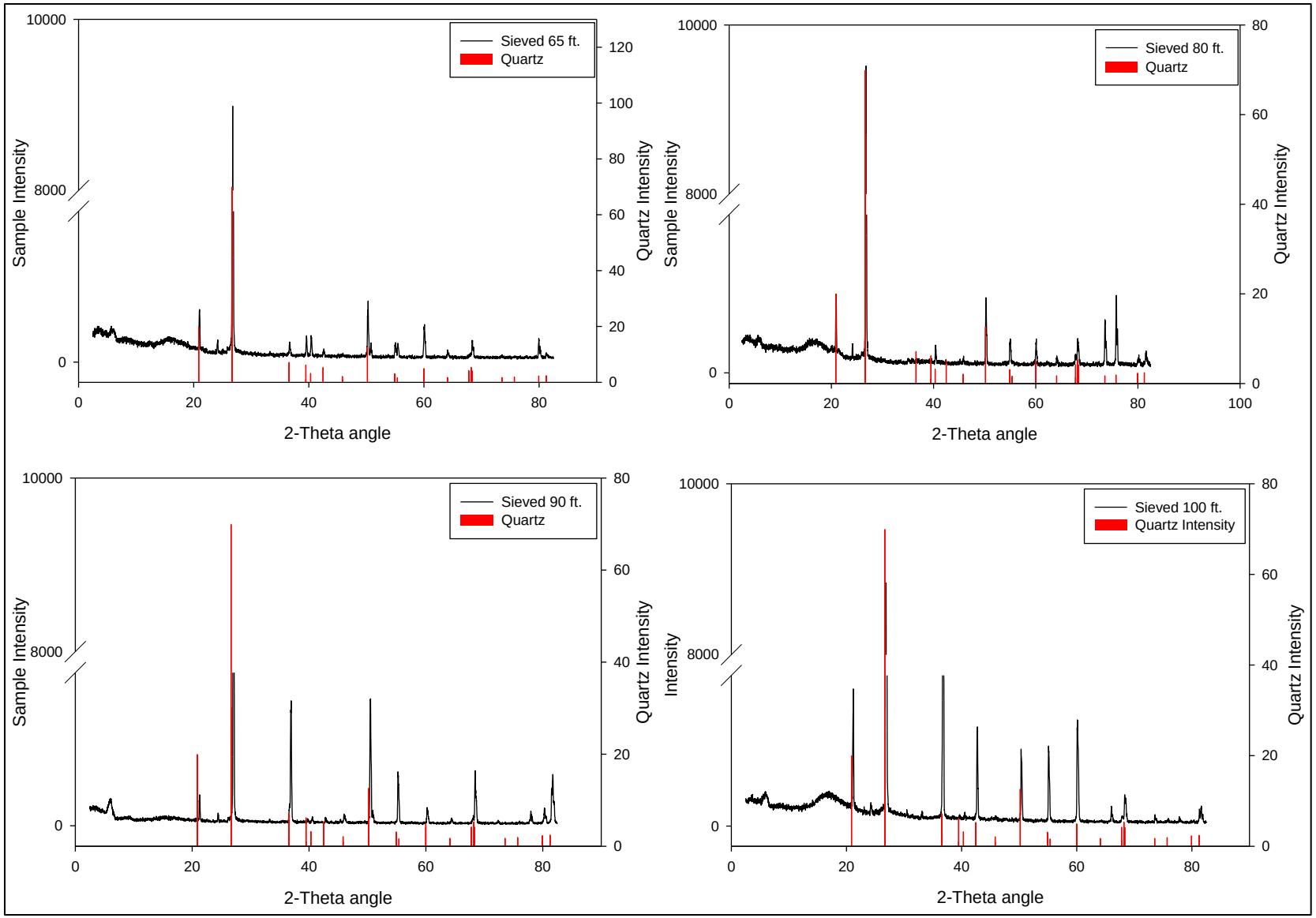

Figure 44 XRD patterns for 6-weeks samples of batch 1, kept in the anaerobic chamber

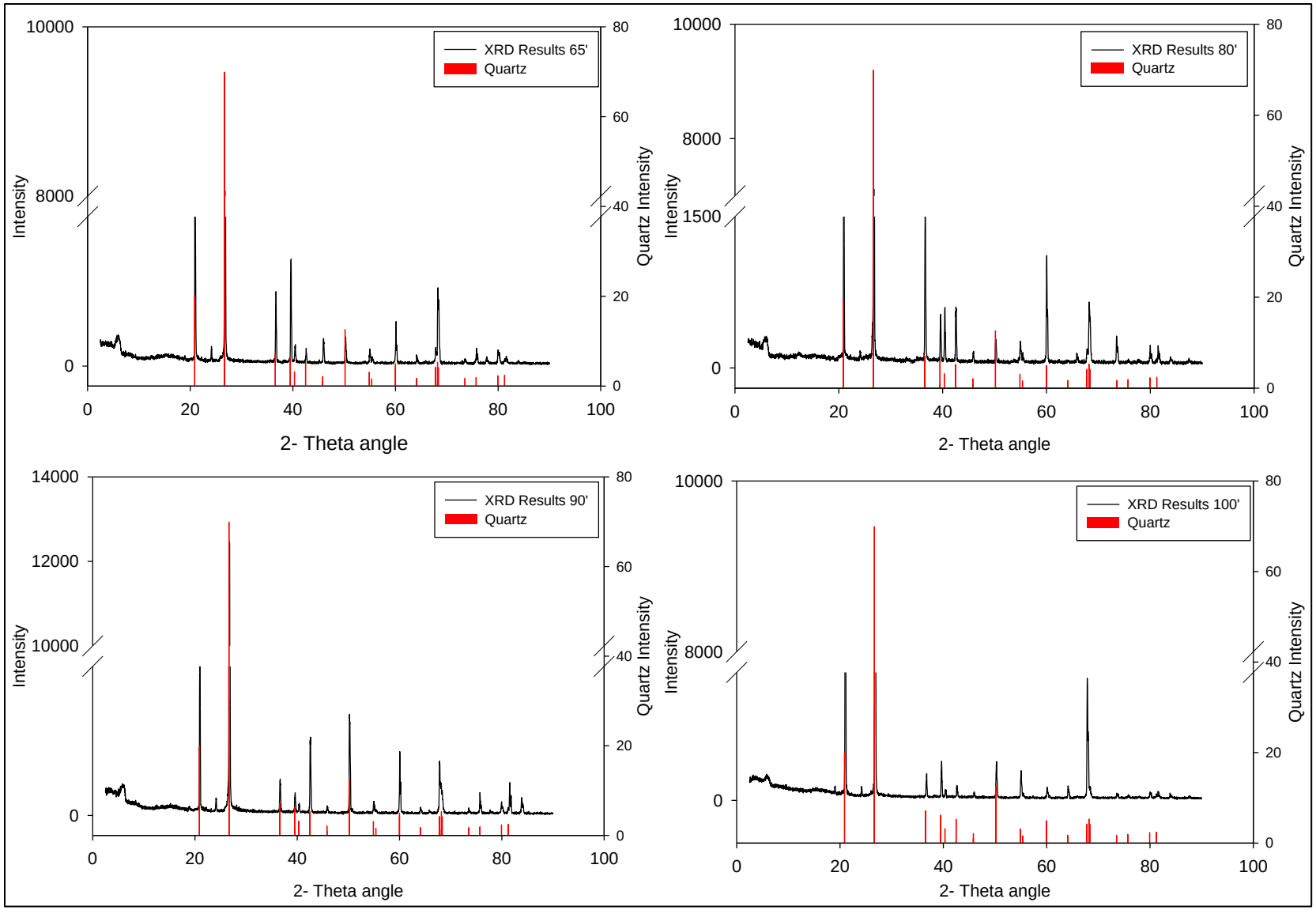

Figure 45 XRD patterns for augmented with bacteria 6-weeks samples of batch 2, kept in the anaerobic chamber

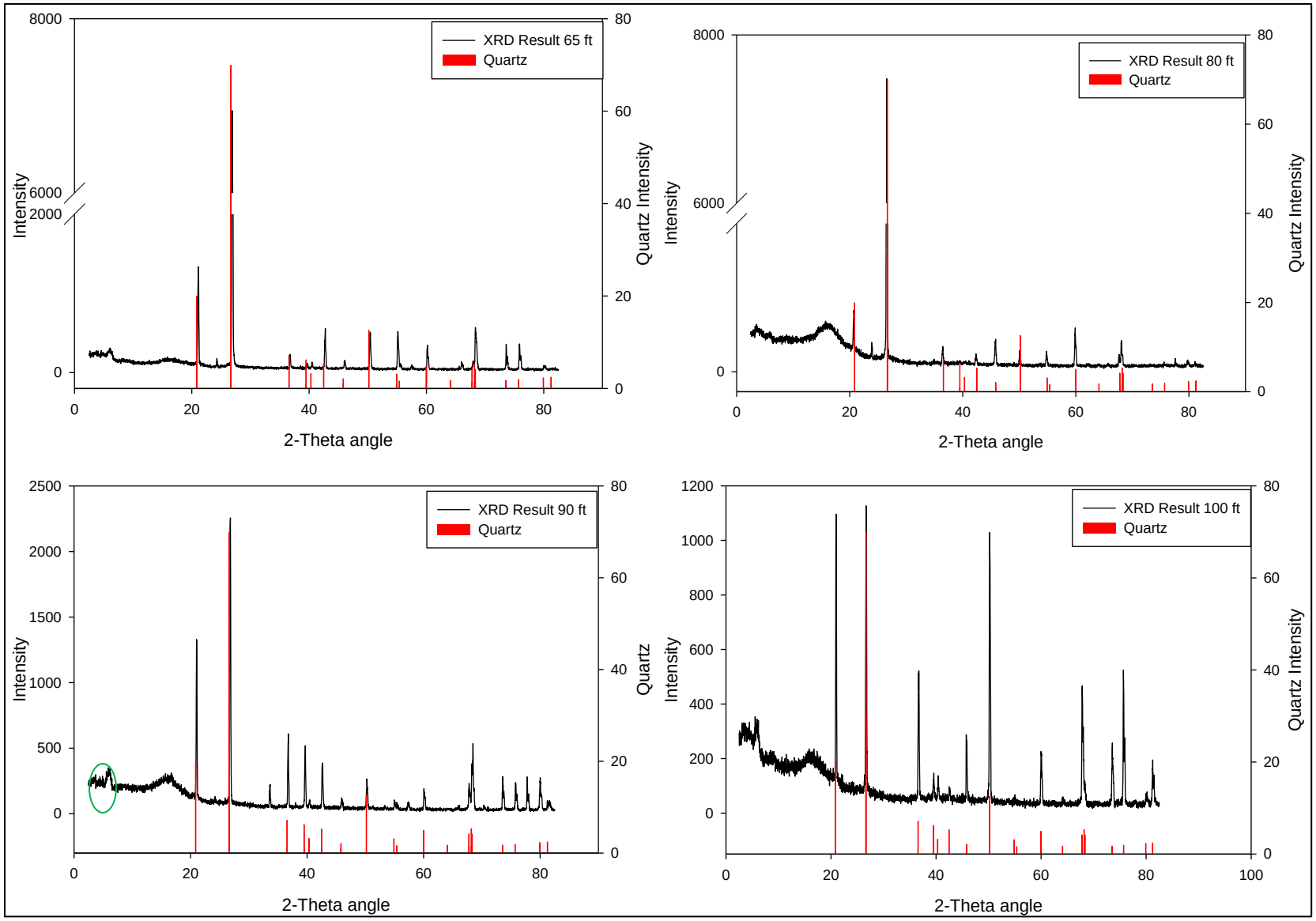

Figure 46 XRD patterns for 6-weeks samples of batch 1kept for 3 weeks in the chamber at low oxygen concentrations

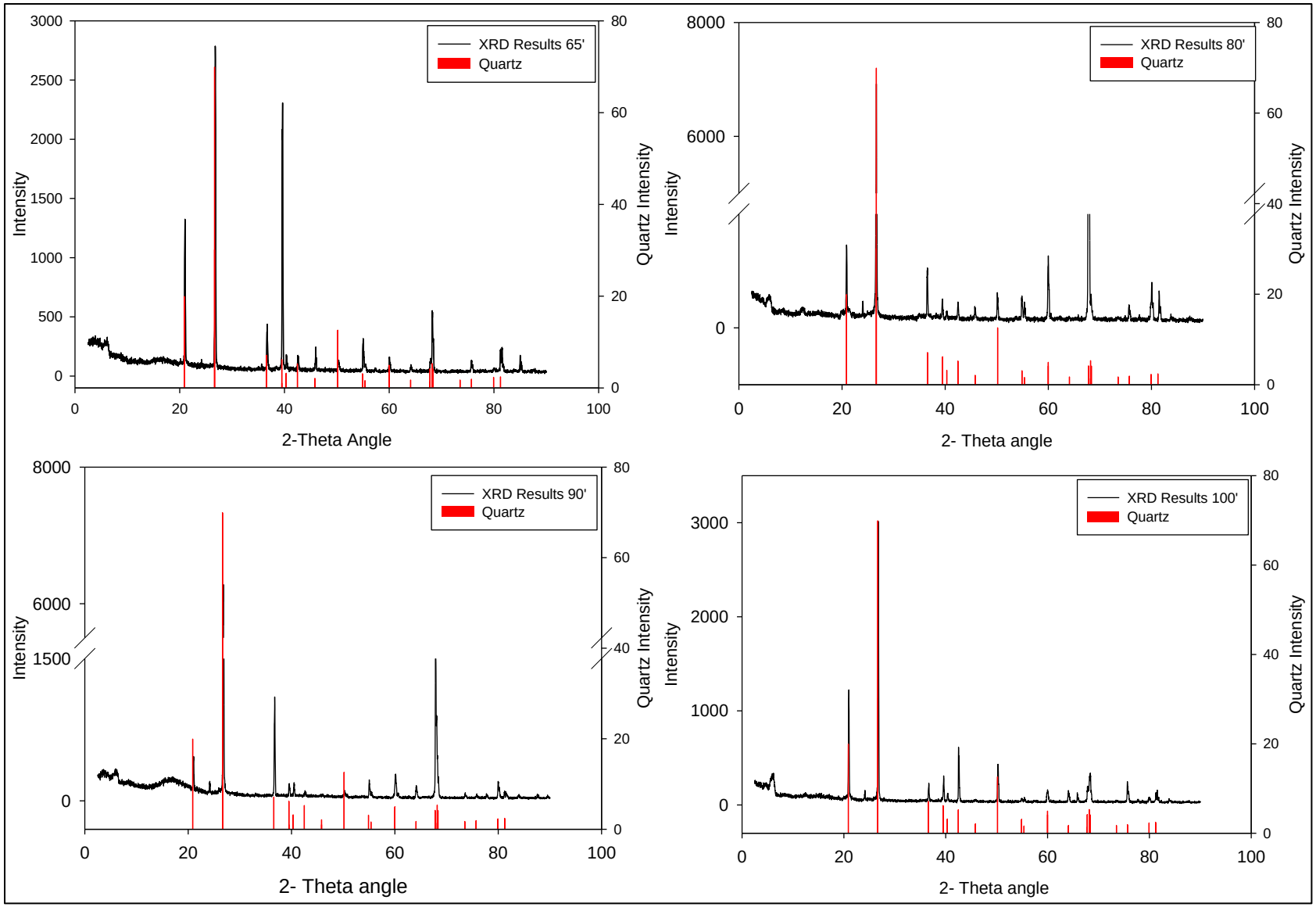

Figure 47 XRD patterns for 6-weeks samples of batch 2 kept in the chamber at low oxygen concentration

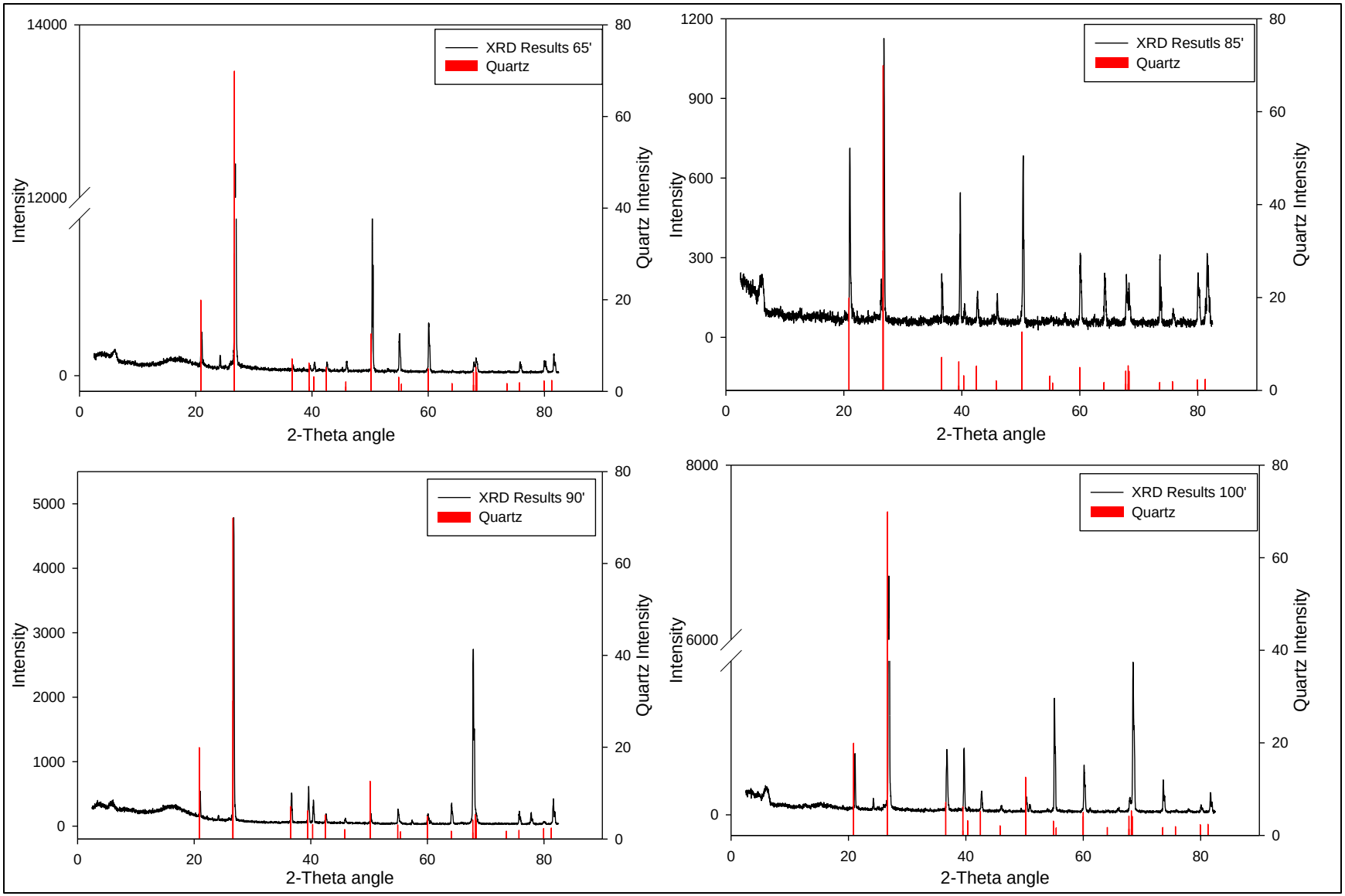

Figure 48 XRD patterns for 6-weeks samples of batch 1 kept on the bench at atmospheric oxygen

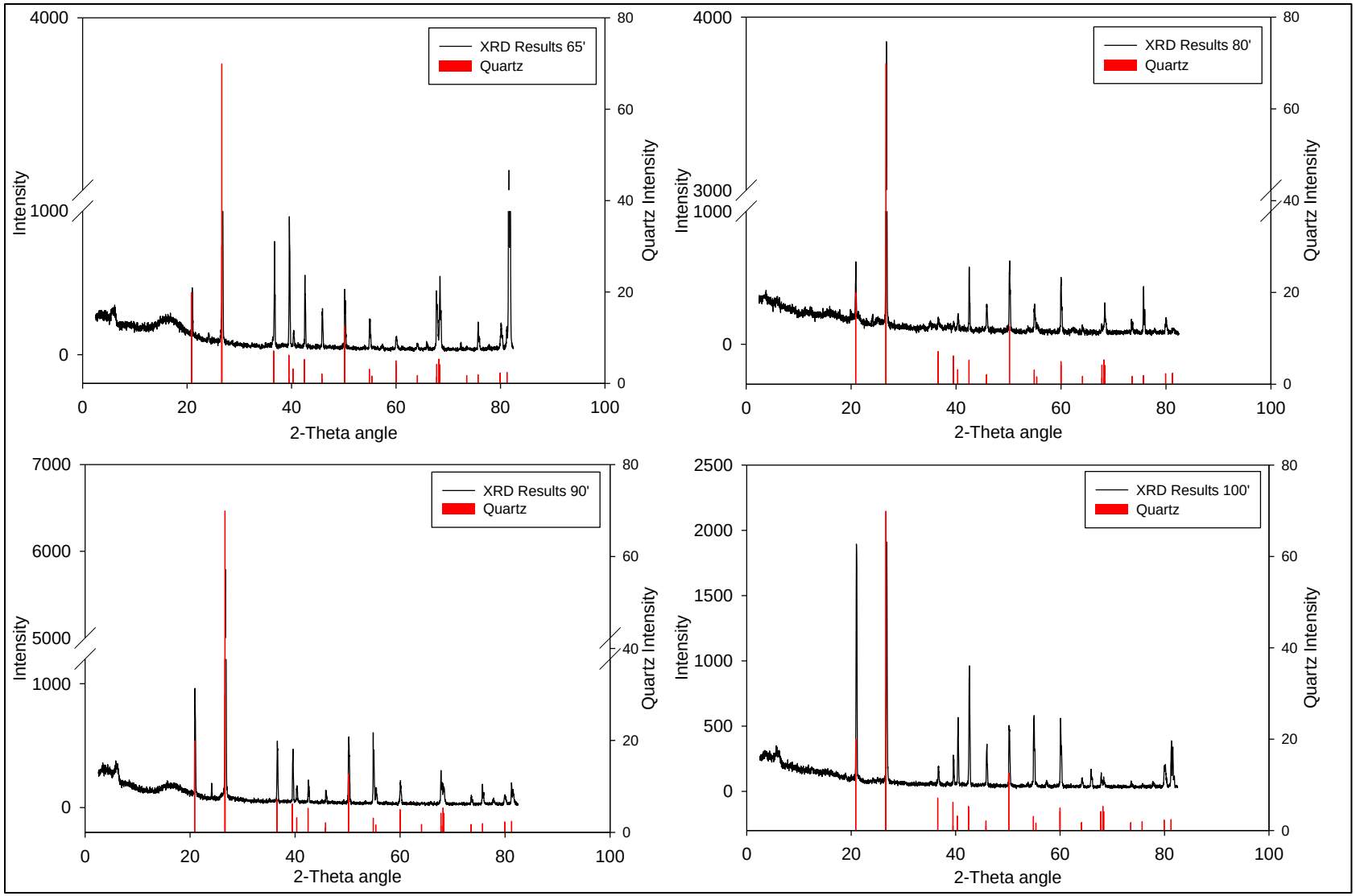

Figure 49. XRD patterns for 6-weeks samples of batch 2 kept on the bench at atmospheric oxygen

Analysis provided only a match for quartz and montmorillonite. SRS sediments are very rich in iron and, with the creation of anaerobic conditions, the formation of siderite (FeCO3) and pyrite (FeS) solid phases were expected. According to the XRD library, the maximum intensity for siderite should be observed at 2-theta 31.98-33.78^{o} while the maximum intensity for pyrite should be at 2-theta 31.25^{o} and 68% intensity at 53.61^{o}. None of the XRD patterns in both batches exhibited distinctive matches with either of these peaks, thus showing no sign of these solid phases in the soil samples composition. Various factors could have led to this result; such as the lack of sulfate in the soil, which could further reduce to sulfide in the anaerobic conditions leading to precipitation of ferrous sulfide. In addition to soil acidity, after the molasses microbial fermentation process, the resulting pH averaged in the 3.87-4 range (Table 20). At this acidic pH, the majority of the inorganic carbon within the system will be present in the form of carbonic acid and CO_2, thus limiting the amount of a carbonate, CO_3^{2-}. So, lack of sulfate and the soil acidity hinder the formation of ferrous iron minerals. The formation of ferrous iron minerals would be expected at more neutral pH conditions. Though, since no precipitation of ferrous iron to form siderite $FeCO_3$ occurred, there is a big possibility that ferrous iron will remain in the soluble form and eventually will be flushed out from the remediation zone with groundwater or re-oxidized to ferric iron with the return of aerobic conditions.

ICP RESULTS

The remainder liquid in all the samples (Batch 1, Batch 2 and control) was separated from the rest of the sample. The liquids were centrifuged in tubes at 4000 rpm for 5 min and afterwards the supernatant was filtered through 0.45 mm filters. Then, filtered liquids were analyzed via ICP-OES for iron content.

The liquid phases of the samples were diluted by a factor of 10 in nitric acid (1%) in preparation for the ICP-OES analysis. The results showed a much higher concentration of iron in the molasses- treated samples compared to the control samples treated only with basal medium. Because the concentrations obtained were outside the calibration range, the samples were re-diluted by a factor of 200 and re-tested through ICP-OES for more accurate results.

Table 20 below shows the results of iron concentrations from the ICP-OES analysis. The concentrations of the control, batch 1 and batch 2 vary significantly. The control samples have the lowest iron concentration with an average of 92.42 ppb. Batches 1 and 2 have higher Fe concentrations with an average of 39,572 ppm and 75,810 ppb respectively. With a concentration of iron almost double of batch 1, the results suggest that the inoculation with bacterial culture collected from the waste water treatment plant anaerobic digester led to higher concentrations of ferrous iron in the batch 2 liquid samples. Possibly, in the presence of iron reducing bacteria, molasses was biodegraded with ferric iron as a terminal electron acceptor, resulting in the production of reduced soluble ferrous iron in a concentration higher compared to batch 1 samples.

Table 20 Iron concentrations in the supernatant solutions

Description	Fe concentration, ppb						
	65'	80'	90'	95'	100'	105'	Average
Control	3.49	N/A	390.9	16.59	27.61	23.52	92.42
Batch 1	15751	N/A	32250	28940	15020	105900	39572
Batch 2	119400	20390	56010	96010	105700	57350	75810

CONCLUSION

Through the experiments conducted with varying environments, of no oxygen, low oxygen and atmospheric oxygen levels, quartz and montmollironite (a clay mineral) were determined to be the best match within the soil samples. The formation of siderite and pyrite was expected when the conditions were reduced to anaerobic by the addition of molasses; however, XRD analysis didn't confirm the presence of these solid phases. The low pH and the fact that were may have not been enough sulfide or bicarbonate/carbonate ions to form ferrous carbonate or ferrous sulfide complexes could be major factors for the obtained results.

FUTURE WORK

Future work possibilities consist of creating a new batch of samples following the same procedures as previous batches but with the addition of a sulfate salt. In the new batch, larger soil samples will be sieved via lower mesh size to obtain clay fractions. The ICP data was clear in showing that ferrous iron is present within the system though the XRD results didn't demonstrate the presence of ferrous iron soil phases. In anaerobic conditions, in which sulfate-reducing bacteria thrive, ferrous iron creates precipitates with sulfide, which is reduced via microbial reduction from sulfate. The microbial reduction of sulfate produces hydrogen sulfide and releases HCO_3^-, resulting in an increase in alkalinity and pH. By the addition of a sulfate salt, it is expected that in the anaerobic conditions sulfate will be reduced to sulfide and bind to ferrous iron in order to create black precipitates of pyrite. These black precipitates might not be visible to the naked eye but could be detected by the XRD analysis. It is also expected that the increase in pH will cause the aqueous phase to become saturated with respect to $FeCO_3$.

ACKNOWLEDGEMENTS

Funding for this research was provided by U.S. DOE grant number DE-EM0000598. We truly appreciate Dr. Miles Denham and Dr. Brian Looney from the SRNL for valuable inputs and support of this research. XRD analyses were conducted at FIU AMERI facilities.

REFERENCES

1. Nyer, Evan., Lenzo, Frank., and Burdick, Jeffery. "*In Situ Reactive Zones: Dehalogenation of Chlorinated Hydrocarbons.*" Ground Water Monitoring & Remediation. 18 (1998): 68-72. Online library Wiley. http://dx.doi.org/10.1111/j.1745-6592.1998.tb00616.x. 1 Dec 2013

2. Wu et al.: Geophysical monitoring and reactive transport modeling of ureolytically-driven calcium carbonate precipitation. Geochemical Transactions 2011 12:7.

3. Harvey F. et al.: "*Arsenic Mobility and Groundwater Extraction in Bangladesh*." Science. 298 no. 5598. (2002): 1602-1606. Science. http://www.sciencemag.org/content/298/5598/1602.full. 5 Dec. 2013

4. S. Labana et al. "*A microcosm study on bioremediation of p-nitrophenol-contaminated soil using Arthrobacter protphormiae RKJ100.*" Applied Microbiology and Biotechnology. 68. 3 (2005): 417-424. Springer Link. http://link.springer.com/article/10.1007/s00253-005-1926-1#page-2. 2 Dec 2013.

5. Christopher C. Lutes. (2003). *In-situ chemical stabilization of metals and radionuclides through enhanced anaerobic reductive precipitation*. doi:10.2172/820029

6. Lutes, C., Frizzel, A., Molnaa, B,. and Palmer, P. (2004). *In-Situ Substrate Addition to Create Reactive Zones for Treatment of Chlorinated Aliphatic Hydrocarbons: Vandenberg Air Force Base.* Air Force Center for Environmental Excellence (AFCEE). Brooks AFB, Texas. Contract # 41624-99-C-8032

7. Moore, D and Reynolds Jr, R. (1989) *X-Ray Diffractions and the Identification and Analysis of Clay Minerals.* New York, New York: Oxford University Press, Inc.

APPENDICES

The following documents are available at the DOE Research website for the Cooperative Agreement between the U.S. Department of Energy Office of Environmental Management and the Applied Research Center at Florida International University: http://doeresearch.fiu.edu

1. P2 APPENDIX I - YR4 - Project Technical Plan
2. P2 APPENDIX II - YR4 - Factsheets
3. P2 APPENDIX III - YR4 - Conference Proceedings
4. P2 APPENDIX IV – YR4 - Research Review
5. P2 APPENDIX V - YR4 - Thesis (DOE Fellow Paola Sepulveda Medina)